

FRAGILITY BASED ASSESSMENT OF LOW-RISE AND MID-RISE
REINFORCED CONCRETE FRAME BUILDINGS IN TURKEY USING
DÜZCE DAMAGE DATABASE

A THESIS SUBMITTED TO
THE GRADUATE SCHOOL OF NATURAL AND APPLIED SCIENCES
OF
MIDDLE EAST TECHNICAL UNIVERSITY

BY

AHSEN ÖZÜN

IN PARTIAL FULFILLMENT OF THE REQUIREMENTS
FOR
THE DEGREE OF MASTER OF SCIENCE
IN
CIVIL ENGINEERING

MAY 2007

Approval of the Graduate School of Natural and Applied Sciences

Prof. Dr. Canan ÖZGEN
Director

I certify that this thesis satisfies all the requirements as a thesis for the degree of Master of Science.

Prof. Dr. Güney ÖZCEBE
Head of Department

This is to certify that we have read this thesis and that in our opinion it is fully adequate, in scope and quality, as a thesis for the degree of Master of Science.

Asst. Prof. Dr. Murat Altuğ ERBERİK
Supervisor

Examining Committee Members

Prof. Dr. Haluk Sucuoğlu (METU, CE) _____

Asst. Prof. Dr. Murat Altuğ Erberik (METU, CE) _____

Assoc. Prof. Dr. Sinan Dede Akkar (METU, CE) _____

Assoc. Prof. Dr. Ahmet Yakut (METU, CE) _____

Assoc. Prof. Dr. Tolga Yılmaz (METU, ES) _____

I hereby declare that all information in this document has been obtained and presented in accordance with academic rules and ethical conduct. I also declare that, as required by these rules and conduct, I have fully cited and referenced all material and results that are not original to this work.

Name, Last name: Ahsen, Özün

Signature :

ABSTRACT

FRAGILITY BASED ASSESSMENT OF LOW-RISE AND MID-RISE REINFORCED CONCRETE FRAME BUILDINGS IN TURKEY USING DÜZCE DAMAGE DATABASE

Özün, Ahsen

M.S., Department of Civil Engineering

Supervisor: Asst. Prof. Dr. Murat Altuğ Erberik

May 2007, 93 pages

In this study, the seismic fragility assessment of low-rise and mid-rise reinforced concrete frame buildings which constitute approximately 75 % of the total building stock in Turkey is investigated to quantify the earthquake risk. The inventory used in this study is selected from Düzce damage database which was compiled after the devastating 1999 earthquakes in the Marmara region. These buildings are not designed according to the current code regulations and the supervision in the construction phase is not adequate.

The building database is divided into sub-classes according to the height and absence of infilled walls. Each building in the database is represented by an equivalent single degree of freedom system with three structural parameters: period, strength, and post-elastic stiffness ratio. The ground motion records are selected from different parts of the world covering a wide range of characteristics. The capacity of the structure is represented for each sub-class by the limit states. Hence, a set of fragility curves for low- and mid-rise reinforced concrete structures are developed by making use of the building characteristics in the database. The generated fragility curve set is referred as “reference” since it forms the basis of a

parametric study. A parametric study is conducted to examine the influence of post-elastic stiffness ratio, simulation and sampling techniques, sample size, limit state definition and degrading behavior on the final fragility curves. Estimated damage distribution after two consecutive major earthquakes is compared with the actual field data in order to investigate the validity of the generated fragility curves.

Keywords: Fragility, low-rise and mid-rise reinforced concrete buildings, parametric study, ground motion characteristics, Düzce damage database.

ÖZ

DÜZCE VERİTABANI KULLANILARAK TÜRKİYE’DEKİ AZ VE ORTA KATLI BETONARME BİNALARIN HASARGÖREBİLİRLİK AÇISINDAN DEĞERLENDİRİLMESİ

Özün, Ahsen

Yüksek Lisans, İnşaat Mühendisliği Bölümü

Tez Yöneticisi: Yrd. Doç. Dr. Murat Altuğ Erberik

Mayıs 2007, 93 sayfa

Bu çalışmada, Türkiye’deki mevcut bina stokunun yaklaşık %75’ini oluşturan ve az ve orta katlı betonarme çerçeveli binaların deprem riskinin tahmini için hasar görebilirlik açısından değerlendirilmesi incelenmiştir. Bina envanteri, 1999 Marmara depremleri sonrası oluşturulan Düzce veritabanı kullanılarak çıkarılmıştır. Son depremlerden etkilenmiş olan bu binalar mevcut yönetmelik şartlarına göre tasarlanmamış olup, inşaat aşamasındaki denetim de uygun değildir.

Bina veritabanı, yükseklik ve dolgu duvarların olup olmamasına göre alt sınıflara ayrılmıştır. Veritabanındaki yapısal parametreler (periyot, dayanım ve elastik ötesi rijitlik katsayısı oranları) her bina için eşdeğer tek serbestlik dereceli sistem olarak tanımlanmıştır. Deprem kayıtları geniş bir alana yayılmış olup dünyanın farklı bölgelerinden seçilmiştir. Her bir alt sınıf için yapısal kapasite hasar sınırları tanımlanmıştır. Sonuç olarak bina karakterleri göz önünde bulundurularak az ve orta katlı binalar için kırılma eğrileri oluşturulmuştur. Oluşturulan kırılma eğrileri parametrik çalışmanın temelini oluşturacağı için referans eğrileri olarak adlandırılmıştır. Son kırılma eğrileri üzerinde elastik ötesi rijitlik katsayısı oranlarının, örnekleme metodlarının, örnek boyutunun, sınır durum tanımının ve

indirgenme davranışının etkilerini gözlemek amacıyla parametrik çalışma gerçekleştirilmiştir. Elde edilen kırılma eğrilerinin geçerliliğini kanıtlamak amacıyla iki büyük deprem sonrası tahmin edilen hasar dağılımı, gerçek hasar ile karşılaştırılmıştır.

Anahtar Sözcükler: Kırılma, az ve orta katlı betonarme binalar, parametrik çalışma, yer hareketi özellikleri, Düzce veritabanı.

To Ozan,

ACKNOWLEDGMENTS

This study was conducted under the supervision of Asst. Prof. Dr. Murat Altuğ Erberik. I would like to express my deepest appreciation for his invaluable guidance, extensive support, advices, criticisms, patience, and encouragements throughout this study.

I would like to thank to my family for their support, encouragement and endless love.

I also would like to thank to my colleagues for their invaluable friendship, tolerance and moral support during the study.

TABLE OF CONTENTS

PLAGIARISM.....	iii
ABSTRACT.....	iv
ÖZ.....	vi
ACKNOWLEDGMENTS.....	ix
TABLE OF CONTENTS.....	x
LIST OF TABLES.....	xii
LIST OF FIGURES.....	xiii
CHAPTER	
1 INTRODUCTION.....	1
1.1 GENERAL.....	1
1.2 LITERATURE SURVEY.....	2
1.3 OBJECTIVE AND SCOPE.....	12
2 DÜZCE DAMAGE DATABASE.....	14
2.1 OBJECTIVE AND SCOPE.....	14
2.2 STATISTICAL CHARACTERISTICS OF DUZCE DAMAGE DATABASE.....	16
2.2.1 SDOF IDEALIZATION FROM PLANAR BUILDING MODELS.....	17
2.2.2 STATISTICAL OUTCOMES FOR EACH SUBCLASS.....	23
3 GENERATION OF REFERENCE FRAGILITY CURVES.....	30
3.1 METHODOLOGY.....	30

3.2	INPUT DATA FOR STRUCTURAL SIMULATIONS	32
3.3	GROUND MOTION DATA SET	34
3.4	RESPONSE STATISTICS	45
3.5	LIMIT STATES.....	47
3.6	GENERATION OF FRAGILITY CURVES.....	50
4	PARAMETRIC STUDY BASED ON FRAGILITY CURVES	56
4.1	INTRODUCTION	56
4.2	INFLUENCE OF POST-ELASTIC STIFFNESS RATIO	56
4.3	INFLUENCE OF SAMPLING TECHNIQUES.....	60
4.4	INFLUENCE OF SAMPLING SIZE	62
4.5	INFLUENCE OF LIMIT STATE DEFINITION	66
4.6	INFLUENCE OF DETERIORATING BEHAVIOUR	68
5	DAMAGE ESTIMATION STUDY	74
5.1	GENERAL.....	74
6	SUMMARY AND CONCLUSIONS.....	82
6.1	SUMMARY	82
6.2	CONCLUSIONS	84
6.3	RECOMMENDATIONS FOR FUTURE STUDY	86
	REFERENCES.....	87

LIST OF TABLES

Table 2.1 General properties of the selected buildings from Düzce damage database.....	16
Table 2.2 PF and α values for for building sub-classes :LR-BR and MR-BR.....	20
Table 2.3 PF and α values for for building sub-classes :LR-BR and MR-BR.....	21
Table 2.4 SDOF parameters for the subclass LR-BR	23
Table 2.5 SDOF parameters for the subclass LR-INF	24
Table 2.6 SDOF parameters for the sub-class MR-BR.....	25
Table 2.7 SDOF parameters for the sub-class MR-INF.....	26
Table 2.8 Main statistical descriptors of each sub-class of buildings after idealization	27
Table 3.1 Ground Motion Characteristics	35
Table 3.2 Statistical Properties of Ground Motion Data Set.....	44
Table 3.3 Limit state definitions for sub-classes of buildings.....	50

LIST OF FIGURES

Figure 1.1 Fragility Curves of RC Frames (Singhal and Kremidjian [6]);	6
Figure 1.2 HAZUS Fragility Curves; a) Low-rise Unreinforced Masonry Buildings (URM-L), b) Mid-rise Concrete Moment Frame (C1M-M) (HAZUS [2]).....	8
Figure 1.3 Fragility curves of mid-rise RC flat-slab structures (Erberik and Elnashai [10])	9
Figure 1.4 Fragility curves of building subclass a) MRF3-P, b) MRF9-P (Ay [13])	11
Figure 2.1 Idealized Force-Displacement Curve (FEMA 356 [21])	18
Figure 2.2 Force-displacement relationship of equivalent SDOF system.....	22
Figure 2.3 Variation of the estimated building period with building height compared with the empirical formulations.....	28
Figure 2.4 Spectral variation of strength factor compared with the code design levels proposed in the specifications of 1975 and 1997.....	29
Figure 3.1 The Methodology used in the Derivation of Reference Fragility Curves	31
Figure 3.2 The variation of η with T for a) low-rise building sub-classes b) mid-rise building sub-classes.....	33
Figure 3.3 General characteristics of ground motion data set in terms of a) location b) surface wave magnitude c) closest distance to fault d) local site conditions e) peak ground acceleration f) effective peak acceleration g) V/A ratio h) effective duration i) energy index	40
Figure 3.4 Dataset classification according to PGV values	45
Figure 3.5 Response Statistics (maximum displacement vs. PGV) for sub-class..	46
Figure 3.6 The illustration of softening index for typical values.....	48
Figure 3.7 Reference Fragility Curves for sub-classes (a) LR-BR (b) MR-BR.....	52
Figure 3.8 Reference Fragility Curves for sub-classes (a) LR-INF (b) MR-INF ..	53

Figure 3.9 Comparison of Reference Fragility Curves for Bare or Infilled RC Frames	54
Figure 3.10 Comparison of Reference Fragility Curves for low-rise or mid-rise RC frames	55
Figure 4.1 The variation of MAXDR with PGV a) LR-INF b) MR-INF	58
Figure 4.2 The influence of a_p on fragility curves for sub-classes	59
Figure 4.3 Mesh type (uniform) sampling for sub-class a) LR-INF b) MR-INF ...	61
Figure 4.4 LHS technique with rank correlation for building subclasses	63
Figure 4.5 The influence of different sampling techniques on fragility curves for subclasses a) LR-INF b) MR-INF	64
Figure 4.6 Comparison of fragility curves using with different sample sizes ($n_s=30, 75, 150$) a) LR-INF b) MR-INF	65
Figure 4.7 Influence of different limit state definitions on fragility curves	67
Figure 4.8 a) Low-cycle fatigue model b) Energy-based hysteresis model	71
Figure 4.9 Sample experimental behavior along with estimated values of α and β . a) Specimen SO3 from Saatcioglu and Ozcebe [42], b) specimen ES3 from Erberik and Sucuoglu [38]	72
Figure 4.10 The influence of degrading hysteresis behavior in the generation of fragility curves for subclasses a) LR-INF and b) MR-INF	73
Figure 5.1 Schematic representation of the comparative procedure	75
Figure 5.2 The epicentral locations of the 1999 earthquakes together with the coordinate center of the database buildings	76
Figure 5.3 Comparison of PGV-based attenuation relationship by Campbell with the recorded PGV values during a) 17 August 1999, b) 12 November 1999 earthquakes	77
Figure 5.4 Logic tree for estimating damage state probabilities of low-rise and mid-rise RC frame buildings in Düzce after 17 August and 12 November earthquakes	80
Figure 5.5 Comparison of estimated damage distributions after August and November earthquakes with the observed damage for a) low-rise b) mid-rise RC buildings	81

CHAPTER 1

INTRODUCTION

1.1 GENERAL

Turkey has suffered from severe earthquakes during the last ten years and these earthquakes caused extensive property damage, many deaths and injuries. Due to the high population and urbanization in earthquake-prone areas, it is possible that such catastrophic events will take place again in future. Furthermore, it is not easy to cope with the devastating results of the earthquakes for a developing country like Turkey. Hence it is quite imperative to quantify the earthquake risk and to take preventive measures to mitigate losses.

Earthquake hazard determination and seismic vulnerability assessment are the components for developing strategies against the earthquake risk. Determination of vulnerability of existing engineering structures requires the assessment of seismic performances of the building stock when subjected to a variety of potential earthquakes.

Fragility assessment is the tool to evaluate the seismic performance of an individual building or building stock. It is necessary to take into account the country-specific characteristics while generating the fragility curves for building structures. Construction practice differs to a large extent among countries and these differences directly influence the fragility of the building under consideration.

This study deals with the generation of fragility curves for low-rise and mid-rise reinforced concrete frame buildings, which constitute approximately 75% of the total urban building stock in Turkey and which are generally occupied for residential purposes. These buildings, which suffered extensive damage after recent earthquakes, are not designed according to the current code regulations and the supervision in the construction phase is not adequate. Hence the buildings possess many deficiencies like the irregularities in plan and elevation, weak column-strong beam connections, poor concrete quality, inadequate detailing of reinforcement in hinging zones, etc. In this study, the test bed, which represents the characteristics of the aforementioned frame buildings, is selected as Düzce damage database. The fragility curves for low-rise and mid-rise reinforced concrete structures in Turkey are proposed as an end product. This enables the assessment of seismic performance and the estimation of seismic damage and loss for the considered building forms in a broad range of hazard intensity.

1.2 LITERATURE SURVEY

Fragility curves are functions which give the probability of reaching or exceeding a specific limit state at different levels of seismic hazard. As such, fragility information is a tool for the measure of the performance of the structure in question within a probabilistic platform due to the inherent uncertainty and randomness in hazard, soil properties and structural performance of the system.

Fragility curves can be derived for one specific system or a component, or for a class of systems and components. Fragility information gives a general idea about the potential of a structural system to be damaged by an earthquake. Besides, it does not provide information about seismic hazard level at the site of the structure. Fragility information should be integrated with seismic hazard to estimate seismic risk at an acceptable level of certainty.

In the generation of fragility curves, there is not a definite method or strategy due to the uncertainty involved in each step of gathering data from ground motion, analysis method, material used and attainment of the limit states. Each fragility curve generation approach has both advantages and disadvantages; depending on the class of structures considered the required level of accuracy and the main goal for which the fragility curves are generated.

There are several methods to generate the fragility curves. The first approach is using expert opinion for the derivation of fragility curves. In this approach, the probability function is developed by the opinions of multiple experts and professionals on damage expected from ground motions. The advantage of this approach is that it is less costly and takes less time. However, it depends on the personal judgments and the opinion of the expert is far from the scientific basis which makes the data arguable. It is preferable when the fragility curves are to be developed for a wide range of damage states and structural systems. One of the systematic studies using expert opinion approach is conducted by Applied Technology Council in a report Seismic Safety Commission of the State of California, ATC-13 [1]. In that study, the experts developed estimates about damage states of the structures subjected to a given hazard parameter, Mercalli Magnitude Intensity. The fragility curves were generated for 40 different structural types with the opinions of 58 experts. The second major study is HAZUS [2], Earthquake Loss Estimation Methodology which was conducted by National Institute of Building Sciences (NIBS) in 1997 and funded by FEMA. In HAZUS [2], the seismic intensity parameters used were spectral acceleration (for non-structural damage) and spectral displacement (for structural damage) instead of MMI that was used in ATC-13.

The second method to construct the fragility curve is to collect damage data in the field after earthquakes in different sites. The advantage of the field data method is that it is useful for characterizing the structural performance of collection of similar structures. However, damage state definition which is based on visual

examination at every location of the work is a challenge with this method. Moreover, advanced statistical methods should be applied to get the parameters of the fragility curve. An example of the fragility curves using field damage data method is the work of Shinozuka et al. [3]. Fragility curves were generated for 1998 of Caltrans' expressway bridges in Los Angeles by collection of the damage data after Northridge earthquake. A two parameter log-normal distribution function was calibrated for the fragility curves and two procedures were considered to determine the parameters for different damage states. Peak ground acceleration (PGA) was used to represent the intensity of the ground motion. The parameters of the distribution are the median and the log-standard deviation. In the first procedure, fragility curves were constructed for four different damage states with estimation of different median and log-standard deviation for each damage state and group of bridges. In second procedure, a different median and a single log standard deviation were estimated for each damage state and group of bridges.

The third method to construct the fragility curve is using experimental data. In this method, the structural type and earthquake intensities can be controlled as required. The shortcoming of the method is using large-scale and realistic experimental models which make the method an expensive and a time-consuming process. Moreover, the available damage data is limited by the amount of experiments that can be carried out. An example of this approach is the study of Chong and Soong [4] where fragility curves were developed for free-standing rigid block sliding on a shaking table against the raised floor surface with five randomly chosen earthquake time histories. For this study, it was aimed to examine the vulnerability of non-structural components in buildings. Horizontal and vertical accelerations were applied in this experiment and acceleration measurements were taken by the use of accelerometers at different locations of shaking table, the raised floor and the rigid block. Horizontal peak ground acceleration values range from 0.3 g to 0.7 g whereas four different scale factors were considered for vertical peak ground acceleration in terms of horizontal peak ground acceleration. Fragility curves were developed for eight different relative displacement failure thresholds between 0.1 inch and 3 inches.

The fourth approach is the use of analytical models to generate the fragility curves. In principal, this approach is similar to the experimental method except that damage data is obtained by numerical analysis. The structural systems or components are analyzed with different ground motion records at different levels of intensity. Analytical methods can be used to generate fragility curves in the absence of field data or experimental data. The most significant advantage of this method is the ease and efficiency of applying the analyses for different structural configurations and ground motions. It is possible to simulate more realistic structural models with the advances in computational structural engineering. However, the results depend on the structural models and ground motion used in the analyses. The method can be easily used with the specific type of buildings. There are two common procedures for generating the seismic excitations in the fragility studies: time-history analysis and the simplified capacity spectrum method.

Time-history analysis is considered to be the most detailed analysis method and used to pretend the response of a structure to a given ground motion excitation. One of the recent studies about the fragility curves is the study of Wen et al. [5] in order to establish the vulnerability function framework for Consequence Based Engineering Paradigm. In this study, the vulnerability of the system was evaluated by different methods: probabilistic displacement demand analysis, limit state probability analysis and fragility curve analysis. The fragility curves are generated for a masonry building in Memphis. In the fragility analysis, spectral acceleration was selected as earthquake hazard parameter whereas the response of the structure was represented by the wall-drift ratio. The ground motions were generated according to the regional seismicity and uniform hazard response spectra.

Another group of researchers, Singhal and Kiremidjian [6] generated fragility curves for low, mid and high-rise buildings. In this study, artificial time histories were simulated by ARMA models. In the analyses, spectral acceleration was used for earthquake hazard parameter. Besides, Park and Ang damage index was used

for response parameter. Different damage states of a concrete building were identified based on the Park-Ang global damage indices of the structure. The statistics of the Park and Ang damage index were obtained at each spectral acceleration value and used to derive the parameters of the lognormal distribution function at that ground motion level. Fragility curves for low and mid-rise buildings are illustrated in Figure 1.1.

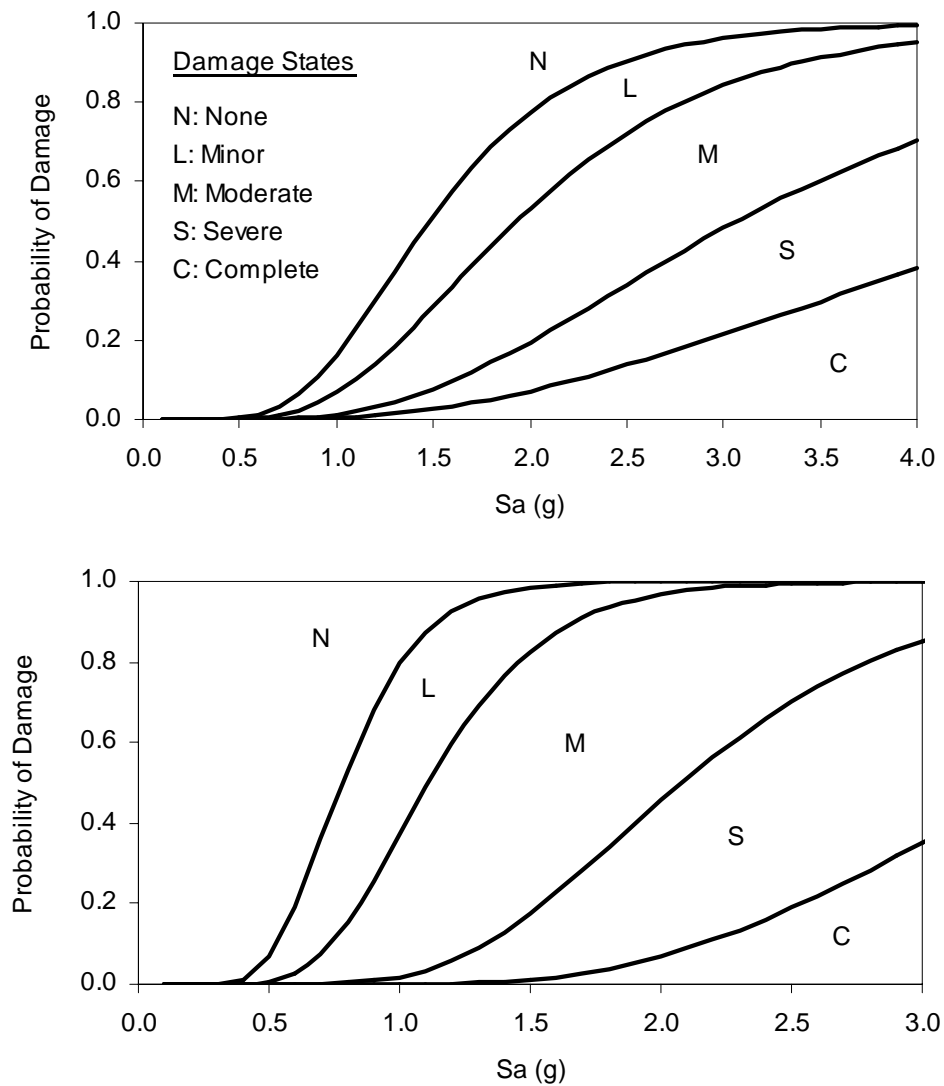


Figure 1.1 Fragility Curves of RC Frames (Singhal and Kremidjian [6]);
a) Low-rise, b) Mid-rise

Recently, researchers have preferred to use spectral analysis because of the fact that time-history analysis is time-consuming and complicated in some cases. Capacity Spectrum Method (CSM) is commonly used analysis type for generating fragility curves. The CSM is a simplified method that estimates the response of a structure from spectrum demand and spectral capacity curves (Barron and Reinhorn [7]). The ground motion parameter is obtained from the spectrum demand curve which is derived from elastic acceleration response spectra of the ground motion record. Basically, the CSM is based on the assumption that the expected median response is determined by the intersection of the spectral capacity and demand curves. The intersection point is called the expected response point. The advantage of the CSM is that it is simple and easy to use in the analysis. The method does not require any time-consuming time history analyses. However, it is based on several assumptions and the results obtained by the CSM should be handled with care. The best example for this procedure is HAZUS Earthquake Loss Estimation Methodology [2]. In Figure 1.2, HAZUS fragility curves of unreinforced masonry with low-code design level (URM-L) and reinforced concrete moment frames (C1M-M) are illustrated respectively. Structural fragility parameter is represented by spectral displacement. Four different damage states are defined in HAZUS: Slight, Moderate, Extensive or Complete.

Another example of fragility curves generated by spectral analysis is the study of Barron and Corvera [8]. In the study, the CSM was applied to a four story structure with RC frames and shear walls. Moreover, the influence of different parameters such as yield strength level, initial period and post yield stiffness ratio were examined while determining the nonlinear response of the considered structure.

In terms of the structural modeling in the analytical method of generating fragility curves, two types of structural systems are employed: Single Degree of Freedom (SDOF) and Multi-Degree of Freedom (MDOF). Simple SDOF models are generally easy to analyze because of having few parameters in the analyses which leads to the completion of the study in a short period of time. However, the

accuracy of the analyses is restricted because of the inherent differences in dynamic behaviors of MDOF and SDOF systems. SDOF modeling procedure is used by many researchers such as Jeong and Elnashai [9]. In the study, the SDOF parameters are represented by stiffness, strength and ductility. The parameters are determined by pushover analysis of the structural system.

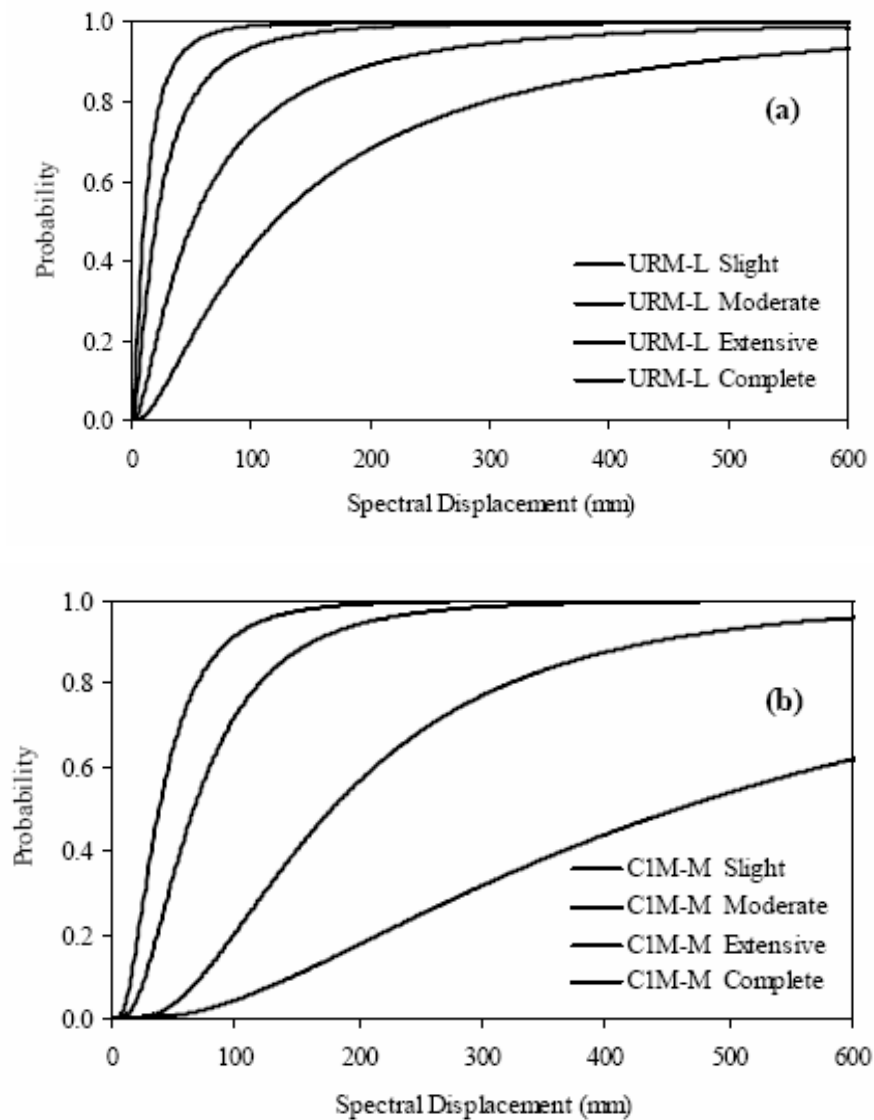


Figure 1.2 HAZUS Fragility Curves; a) Low-rise Unreinforced Masonry Buildings (URM-L), b) Mid-rise Concrete Moment Frame (C1M-M) (HAZUS [2])

Beside ordinary structures, the fragility of special reinforced concrete frame buildings is also conducted just like in the work of Erberik and Elnashai [10]. That study focused on the derivation of fragility curves of flat-slab systems. In Figure 1.3, fragility curves derived for mid-rise reinforced concrete flat-slab systems are presented.

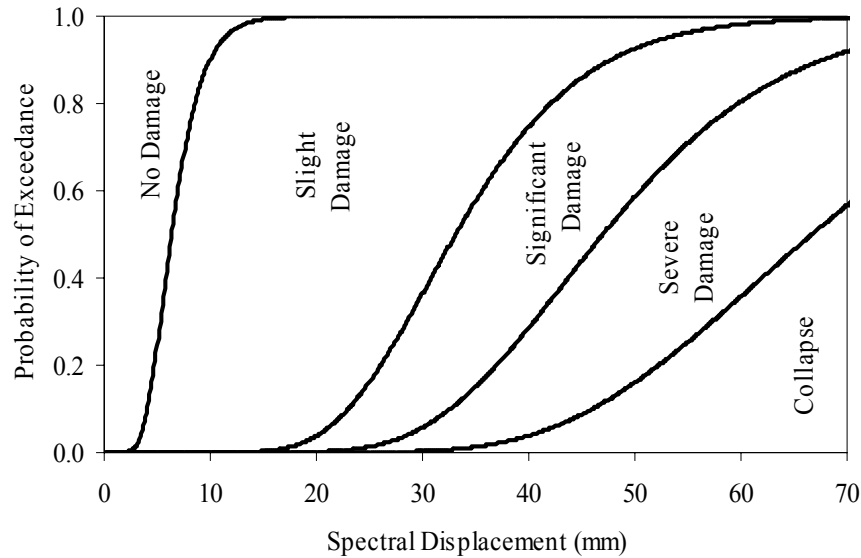


Figure 1.3 Fragility curves of mid-rise RC flat-slab structures (Erberik and Elnashai [10])

There are also fragility studies conducted by Turkish researchers. In the study of Akkar et al. [11], 32 sample buildings representing the characteristics of two to five story reinforced concrete buildings in Turkey were analyzed. Structural response was idealized by SDOF systems. Peak ground velocity is selected as the measure of seismic intensity. The equivalent SDOF system seismic deformation demand is represented by 82 ground motion records. Fragility curves for different number of stories were derived. Kırçıl and Polat [12] and Ay [13] conducted fragility curve studies for low-rise and mid-rise reinforced concrete buildings in Turkey by using planar MDOF models. In the former study, three, five and seven

story RC buildings were designed according to early version of the Turkish Seismic Code [16]. Incremental dynamic analyses were performed to determine the yielding and collapse capacity of sample buildings. As a result of the fragility study, fragility curves were generated in terms of spectral acceleration, peak ground acceleration and elastic spectral displacement. In the latter study, three, five, seven and nine story buildings were evaluated by forming two dimensional analytical models of the buildings. Frame structures were categorized as poor, typical and superior according to the observations after the major earthquakes and specific characteristics of the construction practice in Turkey. The analytical models of three, five, seven and nine story buildings were subjected to time history analyses and the results are obtained in terms of maximum interstory drift ratio. Hence, the probability of exceedance for each ground motion intensity was calculated and the fragility curves were constructed by plotting the calculated exceeding probabilities vs. PGV. In Figure 1.4, fragility curves for MRF3-P (3-story RC moment resisting frame structures with poor construction quality) and MRF9-P (9-story RC moment resisting frame structures with poor construction quality) are presented.

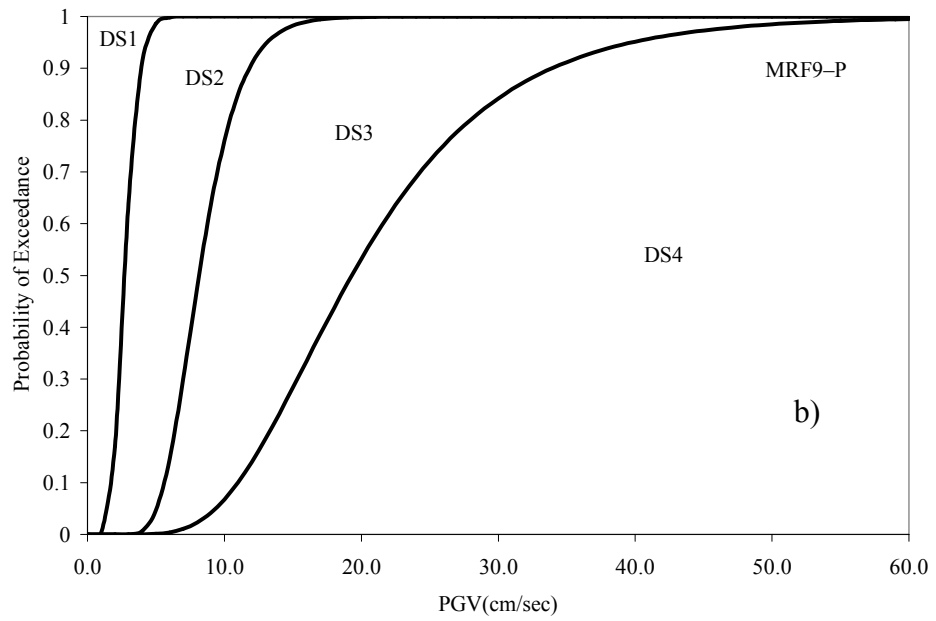
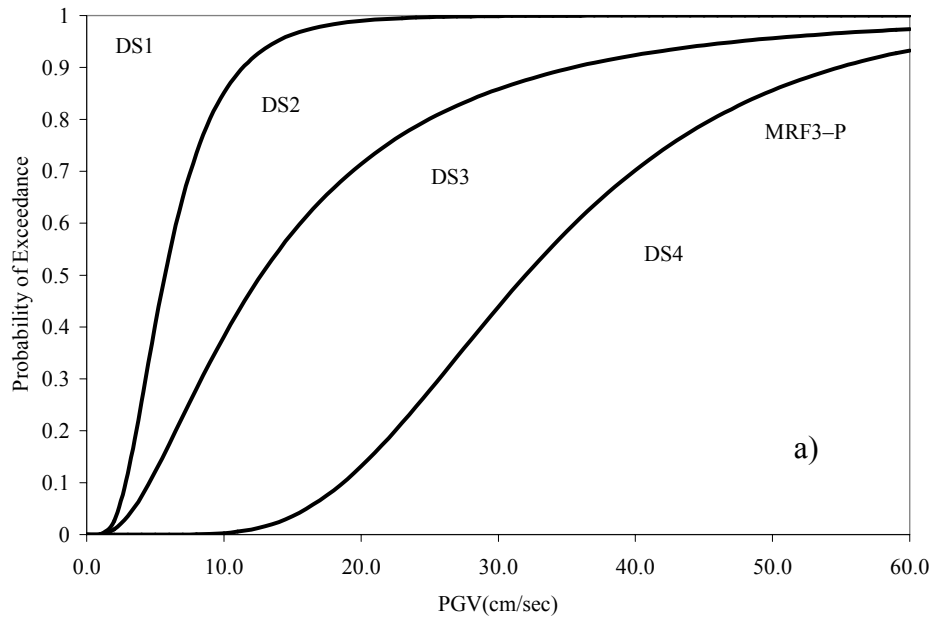


Figure 1.4 Fragility curves of building subclass a) MRF3-P, b) MRF9-P (Ay [13])

1.3 OBJECTIVE AND SCOPE

One of the main objectives of this study is to generate fragility curves for low-rise and mid-rise reinforced concrete buildings in Turkey using actual building data from Düzce damage database. The inventory used in the study is extracted from 500 buildings in Düzce which were exposed to two major earthquakes in 1999. According to the observations made on these buildings, majority of the buildings have not been designed properly. During the selection of structural system, seismic behavior has not been taken into consideration. Furthermore, the supervision in the construction stage is not appropriate as it has been encountered that the concrete quality was poor and detailing was inadequate.

Country-specific characteristics of the building stock play a significant role while generating the fragility curves. The reason is that the construction practice differs from region to region and this issue is usually ignored and fragility curves that have been generated for different earthquake-prone parts of the world according to the other countries characteristics are employed in the earthquake hazard and damage estimation studies in Turkey. However, local characteristics of the buildings influence the fragility curve behavior directly. Determination of the fragility curves for low-rise and mid-rise buildings by considering the country-specific characteristics is the aim of the study.

The building database is divided into two main sub-classes according to the number of stories. A set of fragility curves which are referred as reference fragility curves are generated by using the building database characteristics. Time-history analysis is used to obtain the response statistics of the selected buildings. The parametric study that is conducted to evaluate the effect of different parameters on the final fragility curves is the other objective of the study. Hence, the influence of the post elastic stiffness ratio, simulation and sampling techniques, limit state definition and degrading behavior on the final fragility curves is investigated.

This thesis is composed of six chapters. In Chapter 1, general information about the study and general fragility assessment information is given.

Chapter 2 describes the general characteristics of the Düzce building database. The subclass definition of the selected database according to the height and absence of infill walls is given. Furthermore, Single Degree of Freedom (SDOF) parameters obtained by the idealization from the planar building models are presented.

Chapter 3 includes the generation of the reference fragility curves in terms of classification and characterization of the ground motion dataset, limit state definition, and derivation of the reference fragility curves.

A parametric study is conducted to investigate the influence of post-elastic stiffness ratio, simulation and sampling techniques, sample size, limit state definition and degrading behavior on the final fragility curves in Chapter 4.

Chapter 5 presents the damage estimation study in order to compare the estimated damage with the actual damage distribution.

Finally, Chapter 6 is devoted to summary and conclusion of the study. Recommendations based on the results and conclusions of the study are also given in this chapter.

CHAPTER 2

DÜZCE DAMAGE DATABASE

2.1 OBJECTIVE AND SCOPE

The selected database in this study is composed of 28 reinforced concrete (RC) buildings in Düzce. These buildings were selected as representative among approximately 500 residential RC buildings that were examined after Kocaeli (17 August 1999) and Düzce (12 November 1999) earthquakes. The database under concern has been used before by other researchers; Akkar et al.[11], Yakut et al. [14]; Aydoğan [15]

Number of stories of selected buildings ranges from two to six. The building database is divided into two categories according to the number of stories: buildings with two and three stories are considered as low-rise (LR) and buildings with four to six stories are named as mid-rise (MR). There are 14 buildings in each category (total 28 buildings). The buildings' other properties as listed in Table 2.1 are the construction year, total building height (in meters), the concrete strength (f_c) values (in MPa) obtained by using the Schmidt Hammer method and finally the observed damage after the 1999 earthquakes that affected the region. Building damages were classified in four grades; namely none, light, moderate and severe, or collapsed. A building with light damage can be occupied with minor repairs after the earthquake whereas a moderately damaged building requires structural repairs. If there is severe damage, then such a building is considered as a failure from structural point of view.

The comparison between the construction years of the buildings in the database and the release dates of the national seismic design codes may provide valuable information about the validity of these codes in terms of usage. In Turkey, the first seismic design code was published in 1940 [17], after the devastating Erzincan Earthquake in 1939. Although there had been some efforts to update this immature code in 1942, 1947, 1953, 1961 and 1968, these were not adequate to ensure the seismic safety of building structures until the release of “The Specifications for Structures to be Built in Disaster Areas” in 1975 [16]. However economical and physical losses continued to increase with the occurrence of each earthquake even afterwards. The latest seismic design code which was in use during the investigation of Düzce database buildings was published in 1997 [18] and it is now replaced by the new version in 2007 [19]. The 1997 code included major revisions when compared to the previous specifications and it was more compatible with the well-recognized international codes. As observed from Table 2.1, most of the buildings (68 % of the total) were built during 1975-1997 period and seven buildings (25 % of the total) constructed in the period before 1975.

The quality of concrete of the selected buildings is another issue, with observed f_c values of even 9 MPa due to core samples taken from the buildings. The average f_c value of the buildings in the database is 15.3 MPa with a coefficient of variation (COV) 0.26. In Turkish construction practice, it is common to encounter privately constructed residential RC buildings with an ordinary concrete strength less than 20 MPa and this is also reflected in the database. There seems not to be a consistent trend between the concrete strength and the observed damage.

Table 2.1 General properties of the selected buildings from Düzce damage database.

Building ID	Construction year	No. of stories	Building class	Building height (m)	f_c (MPa)	Observed damage
B01	1985	6	MR	16.3	15	Moderate
B02	1985	6	MR	16.1	14	Moderate
B03	1978	5	MR	14.4	17	Severe
B04	1991	5	MR	14.4	20	None
B05	1985	5	MR	13.8	20	Light
B06	1997	5	MR	14.3	20	None
B07	1985	3	LR	8.3	20	Moderate
B08	1989	4	MR	13.5	20	Moderate
B09	1977	4	MR	11.4	17	Moderate
B10	1975	5	MR	14.6	22	None/Light
B11	1962	2	LR	6.3	14	None
B12	1975	3	LR	8.3	9	Light
B13	1975	3	LR	8.9	14	Moderate
B14	1993	4	MR	11.6	17	Light
B15	1999	3	LR	8.9	13	Light
B16	1982	4	MR	11.6	22	Moderate
B17	1980	3	LR	8.4	9	Light
B18	1970	2	LR	6.3	17	Light
B19	1972	2	LR	5.6	9	Light
B20	1995	3	LR	8.3	14	Light
B21	1990	2	LR	6.1	17	Light
B22	1982	3	LR	8.1	10	Moderate
B23	1985	2	LR	5.8	14	None
B24	1973	3	LR	9.7	17	None
B25	1994	4	MR	12.3	14	Light
B26	1992	5	MR	14.7	13	Moderate
B27	1984	4	MR	12.5	10	Moderate
B28	1981	3	LR	9.6	10	Moderate

2.2 STATISTICAL CHARACTERISTICS OF DUZCE DAMAGE DATABASE

Two different analytical approaches can be considered for the estimation of the seismic vulnerability of specific building stock. In the first approach, each building in the stock is examined individually and the vulnerability of the building stock is obtained by combining the fragility information associated with each building. Very detailed models and analysis procedures are employed; hence the results will be highly accurate. On the other hand, this approach is generally impractical and

economically unfeasible. The second approach is to conduct the fragility studies by using the global response statistics of simplified (or equivalent) analytical models. Hence it becomes possible to represent the building population by a few number of structural parameters. The advantage of this approach is that it is simple and economically feasible. In addition, nontechnical decision makers prefer such simple and rapid estimates of anticipated losses to develop the proper judgment to execute their mitigation plans. However obtained results will be crude and the limitations of models or methods should be clearly understood.

In this study, fragility functions of low-rise and mid-rise RC structures are generated by simplified analytical models as mentioned in second approach. The details are given in the next section. Furthermore, buildings are classified as "bare frame" and "infilled frame" according to the absence and presence of the infill walls in order to investigate the effect of masonry infill walls on seismic response. As a result, the building stock is divided into 4 different subclasses: low-rise bare frame (LR-BR), low-rise infilled frame (LR-INF), mid-rise bare frame (MR-BR), mid-rise infilled frame (MR-INF).

2.2.1 SDOF IDEALIZATION FROM PLANAR BUILDING MODELS

Instead of complex Multi-Degree-of-Freedom (MDOF) analytical models, each building in the database is represented by a simple equivalent Single-Degree-of-Freedom (SDOF) model with three structural parameters: period (T), strength ratio (η) and the post-elastic stiffness as a fraction of the elastic stiffness (a_p). First step to obtain the SDOF structural parameters is to use the pushover curves obtained from nonlinear static analyses in two orthogonal directions by using the analysis platform SAP2000 [20]. Hence, there exist 56 ($28*2$) pushover curves and the corresponding SDOF parameters are obtained for each building model and each orthogonal direction.

Idealization of the pushover curves are conducted by applying the procedure in FEMA 356 [21]. According to the procedure, the effective lateral stiffness, K_e , and

effective yield strength, V_y , of the building shall be obtained after the idealization of nonlinear force-displacement relationship between base shear and top displacement as in Figure 2.1. Line segments on the idealized curve are located using an iterative graphical procedure that approximately balances the area above and below the curve. The effective lateral stiffness, K_e , is taken as the secant stiffness calculated at a base shear force equal to 60% of the effective yield strength of the structure. The post-elastic stiffness ratio, α_p , is determined by a line segment that passes through the actual curve at the calculated target displacement. The effective yield strength should not be taken as greater than the maximum base shear force at any point along the actual curve.

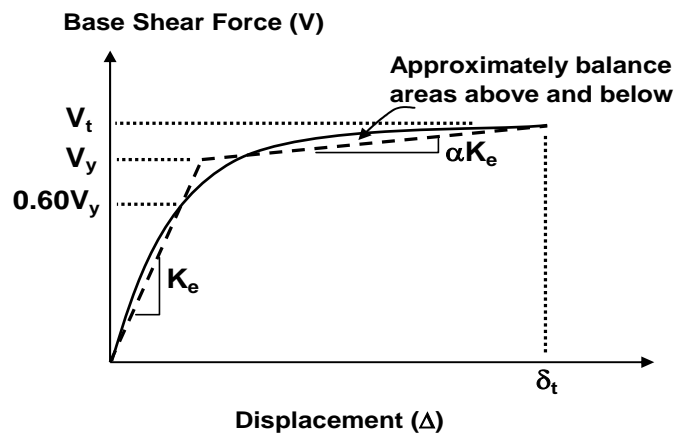


Figure 2.1 Idealized Force-Displacement Curve (FEMA 356 [21])

In this study, ATC-40 [22] procedure is employed in order to obtain equivalent Single-Degree-of-Freedom (SDOF) parameters. Accordingly, a Multi-Degree-of-Freedom system (MDOF) is represented by a SDOF system with effective mass M^* and effective period T_{eff} . After bilinear idealization, the pushover curve of the MDOF analytical model is plotted in the spectral acceleration (S_a) vs. spectral displacement (S_d) domain of the equivalent SDOF system, which is also known as

ADRS (Acceleration Displacement Response Spectra) format, by using Equations 2.1 and 2.2.

$$S_a = \frac{V}{\alpha_1 W} \quad (2.1)$$

$$S_d = \frac{\Delta_{\text{roof}}}{PF_1 \times \phi_{\text{roof},1}} \quad (2.2)$$

where V is the base shear force, W is the weight of the structure, α_1 is the modal mass coefficient for the first fundamental mode, Δ_{roof} is the roof displacement, PF_1 is the modal participation factor for the first fundamental mode and $\phi_{\text{roof},1}$ is the amplitude of the first mode at the level of roof. The parameters α_1 and PF_1 can be further defined as:

$$\alpha_1 = \frac{\left[\sum_{i=1}^N \frac{(w_i \phi_{i,1})}{g} \right]^2}{\left[\sum_{i=1}^N \frac{(w_i)}{g} \right] \left[\sum_{i=1}^N \frac{(w_i \phi_{i,1}^2)}{g} \right]} \quad (2.3)$$

and

$$PF_1 = \frac{\left[\sum_{i=1}^N \frac{(w_i \phi_{i,1})}{g} \right]}{\left[\sum_{i=1}^N \frac{(w_i \phi_{i,1}^2)}{g} \right]} \quad (2.4)$$

where w_i is the weight assigned to level i , $\phi_{i,1}$ is the amplitude of the first mode at level i , N is the level which is the uppermost in the main portion of the structure and g is the gravitational acceleration. The parameters α and PF for each building sub-class is shown on Table 2.2 -2.3.

Table 2.2 PF and α values for for building sub-classes :LR-BR and MR-BR

Building ID	Building Subclass	X-direction		Y-direction	
		PF	α	PF	α
B01	MR-BR	1.288	0.800	1.279	0.804
B02	MR-BR	1.291	0.820	1.280	0.809
B03	MR-BR	1.270	0.862	1.270	0.861
B04	MR-BR	1.270	0.851	1.280	0.834
B05	MR-BR	1.280	0.832	1.290	0.825
B06	MR-BR	1.289	0.843	1.281	0.853
B07	LR-BR	1.280	0.817	1.270	0.836
B08	MR-BR	1.302	0.804	1.289	0.835
B09	MR-BR	1.270	0.819	1.280	0.746
B10	MR-BR	1.290	0.820	1.310	0.809
B11	LR-BR	1.130	0.972	1.130	0.971
B12	LR-BR	1.265	0.819	1.274	0.809
B13	LR-BR	1.214	0.930	1.220	0.917
B14	MR-BR	1.320	0.778	1.280	0.816
B15	LR-BR	1.250	0.817	1.240	0.829
B16	MR-BR	1.295	0.801	1.296	0.800
B17	LR-BR	1.240	0.848	1.260	0.821
B18	LR-BR	1.160	0.955	1.170	0.945
B19	LR-BR	1.190	0.917	1.200	0.900
B20	LR-BR	1.210	0.912	1.220	0.911
B21	LR-BR	1.180	0.933	1.200	0.897
B22	LR-BR	1.285	0.864	1.292	0.854
B23	LR-BR	1.184	0.927	1.184	0.927
B24	LR-BR	1.230	0.904	1.220	0.921
B25	MR-BR	1.250	0.862	1.250	0.863
B26	MR-BR	1.270	0.842	1.280	0.829
B27	MR-BR	1.240	0.913	1.280	0.857
B28	LR-BR	1.190	0.943	1.200	0.938

Table 2.3 PF and α values for for building sub-classes :LR-INF and MR-INF

Building ID	Building Subclass	X-direction		Y-direction	
		PF	α	PF	α
B01	MR-INF	1.298	0.772	1.288	0.787
B02	MR-INF	1.294	0.819	1.308	0.820
B03	MR-INF	1.270	0.872	1.280	0.859
B04	MR-INF	1.270	0.851	1.280	0.849
B05	MR-INF	1.280	0.831	1.280	0.837
B06	MR-INF	1.285	0.848	1.279	0.867
B07	LR-INF	1.280	0.830	1.270	0.851
B08	MR-INF	1.288	0.828	1.285	0.842
B09	MR-INF	1.300	0.851	1.310	0.730
B10	MR-INF	1.300	0.807	1.320	0.823
B11	LR-INF	1.130	0.971	1.140	0.968
B12	LR-INF	1.271	0.808	1.279	0.816
B13	LR-INF	1.211	0.936	1.186	0.953
B14	MR-INF	1.310	0.800	1.280	0.828
B15	LR-INF	1.260	0.803	1.240	0.814
B16	MR-INF	1.299	0.774	1.306	0.783
B17	LR-INF	1.250	0.803	1.260	0.846
B18	LR-INF	1.160	0.954	1.170	0.946
B19	LR-INF	1.180	0.933	1.200	0.910
B20	LR-INF	1.210	0.915	1.210	0.915
B21	LR-INF	1.180	0.934	1.190	0.915
B22	LR-INF	1.281	0.872	1.284	0.873
B23	LR-INF	1.167	0.949	1.186	0.925
B24	LR-INF	1.220	0.920	1.210	0.935
B25	MR-INF	1.270	0.826	1.260	0.873
B26	MR-INF	1.270	0.841	1.280	0.834
B27	MR-INF	1.230	0.916	1.270	0.867
B28	LR-INF	1.190	0.941	1.180	0.951

After converting the pushover curve to a capacity curve in ADRS format, the parameters that define SDOF system are obtained through Equations 2.5 - 2.7.

$$M^* = \alpha_1 M \quad (2.5)$$

$$K^* = \frac{4\pi^2}{T_{\text{eff}}^2} M^* \quad (2.6)$$

$$F_y = V_y = S_{a,y} W^* \quad (2.7)$$

In the above equations, M^* and K^* are the effective mass and stiffness of SDOF system, T_{eff} is the effective period, F_y is the yield force, V_y is the base shear force at yield and $S_{a,y}$ is the spectral acceleration at yield.

Finally the force-displacement relationship of SDOF system is represented as shown in Figure 2.2, where a_p is the ratio of post elastic stiffness of the idealized capacity curve to the elastic stiffness.

The SDOF parameters effective period (T_{eff}), strength ratio (η), which is the effective weight of the structure and the ratio of yield force to the effective weight of the structure and the ratio of parameter a_p are shown in Figure 2.2. From this point on throughout the text, the abbreviation “T” will be used instead of “ T_{eff} ”

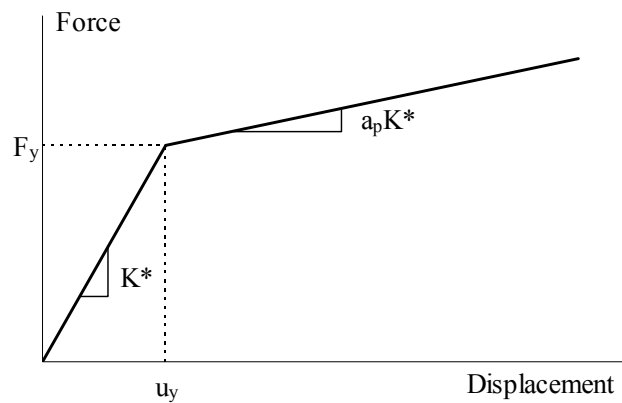


Figure 2.2 Force-displacement relationship of equivalent SDOF system

2.2.2 STATISTICAL OUTCOMES FOR EACH SUBCLASS

The values of SDOF parameters T , η and a_p for each building sub-class obtained by the FEMA and ATC procedures are presented in Tables 2.4-2.7. These parameters can also be represented in terms of the main statistical descriptors, i.e. mean (μ) and standard deviation (σ) and they are summarized in Table 2.8.

Table 2.4 SDOF parameters for the subclass LR-BR

Building ID	Direction	η	T_e	a_p (%)
B07	X	0.318	0.216	0.72
B07	Y	0.299	0.220	0.56
B11	X	0.173	0.384	1.93
B11	Y	0.183	0.390	4.38
B12	X	0.116	0.456	1.12
B12	Y	0.123	0.446	0.89
B13	X	0.197	0.377	1.81
B13	Y	0.203	0.367	1.65
B15	X	0.151	0.502	1.67
B15	Y	0.165	0.510	1.94
B17	X	0.145	0.569	7.84
B17	Y	0.166	0.399	10.02
B18	X	0.381	0.264	1.91
B18	Y	0.360	0.202	0.85
B19	X	0.210	0.363	1.69
B19	Y	0.240	0.310	1.11
B20	X	0.243	0.338	1.54
B20	Y	0.280	0.286	1.20
B21	X	0.389	0.242	1.48
B21	Y	0.460	0.161	0.48
B22	X	0.163	0.363	1.30
B22	Y	0.162	0.353	0.95
B23	X	0.310	0.302	1.70
B23	Y	0.271	0.371	4.73
B24	X	0.201	0.406	2.14
B24	Y	0.143	0.568	3.00
B28	X	0.129	0.549	1.72
B28	Y	0.130	0.508	1.29

Table 2.5 SDOF parameters for the subclass LR-INF

Building ID	Direction	η	T_e	a_p (%)
B07	X	0.435	0.165	0.45
B07	Y	0.350	0.182	0.48
B11	X	0.329	0.244	1.68
B11	Y	0.283	0.208	1.52
B12	X	0.146	0.364	0.75
B12	Y	0.179	0.314	0.51
B13	X	0.227	0.335	1.49
B13	Y	0.268	0.287	1.08
B15	X	0.160	0.472	1.49
B15	Y	0.182	0.436	1.49
B17	X	0.153	0.463	5.27
B17	Y	0.243	0.262	4.44
B18	X	0.438	0.224	1.45
B18	Y	0.393	0.194	0.53
B19	X	0.280	0.251	0.94
B19	Y	0.295	0.240	0.76
B20	X	0.265	0.312	1.36
B20	Y	0.317	0.250	0.93
B21	X	0.420	0.234	1.05
B21	Y	0.559	0.130	0.36
B22	X	0.231	0.253	0.71
B22	Y	0.201	0.276	0.61
B23	X	0.450	0.214	0.98
B23	Y	0.416	0.309	4.03
B24	X	0.271	0.295	1.37
B24	Y	0.245	0.366	1.49
B28	X	0.132	0.515	1.54
B28	Y	0.238	0.265	0.45

Table 2.6 SDOF parameters for the sub-class MR-BR

Building ID	Direction	η	T_e	a_p (%)
B01	X	0.142	0.504	4.94
B01	Y	0.114	0.603	2.00
B02	X	0.088	0.636	1.98
B02	Y	0.093	0.678	1.64
B03	X	0.153	0.502	4.83
B03	Y	0.114	0.451	8.86
B04	X	0.096	0.595	1.60
B04	Y	0.109	0.549	1.12
B05	X	0.105	0.600	1.04
B05	Y	0.118	0.518	1.43
B06	X	0.147	0.453	0.78
B06	Y	0.151	0.426	1.15
B08	X	0.189	0.327	0.88
B08	Y	0.161	0.396	1.45
B09	X	0.076	0.672	3.50
B09	Y	0.099	0.658	2.77
B10	X	0.116	0.509	1.12
B10	Y	0.105	0.568	1.35
B14	X	0.186	0.384	-0.45
B14	Y	0.170	0.456	3.12
B16	X	0.105	0.560	1.77
B16	Y	0.098	0.586	1.22
B25	X	0.139	0.544	1.51
B25	Y	0.191	0.551	8.86
B26	X	0.107	0.500	6.58
B26	Y	0.168	0.428	1.53
B27	X	0.161	0.525	2.68
B27	Y	0.208	0.398	0.87

Table 2.7 SDOF parameters for the sub-class MR-INF

Building ID	Direction	η	T_e	a_p (%)
B01	X	0.183	0.464	5.91
B01	Y	0.154	0.644	2.43
B02	X	0.095	0.587	1.70
B02	Y	0.105	0.608	1.47
B03	X	0.177	0.395	3.07
B03	Y	0.141	0.356	5.45
B04	X	0.099	0.551	1.53
B04	Y	0.163	0.367	0.71
B05	X	0.107	0.568	0.93
B05	Y	0.180	0.340	0.87
B06	X	0.172	0.411	0.70
B06	Y	0.173	0.384	0.99
B08	X	0.298	0.229	0.47
B08	Y	0.184	0.347	1.14
B09	X	0.131	0.382	1.26
B09	Y	0.098	0.644	2.66
B10	X	0.191	0.425	0.86
B10	Y	0.138	0.436	0.87
B14	X	0.221	0.316	-0.14
B14	Y	0.198	0.387	2.26
B16	X	0.135	0.417	1.12
B16	Y	0.127	0.443	0.78
B25	X	0.152	0.454	1.11
B25	Y	0.213	0.510	8.17
B26	X	0.113	0.476	5.85
B26	Y	0.212	0.311	0.89
B27	X	0.172	0.472	2.22
B27	Y	0.245	0.314	0.57

Table 2.8 Main statistical descriptors of each sub-class of buildings after idealization

Parameter	Building Class	Bare Frame		Infilled Frame		All Frames	
		μ	σ	μ	σ	μ	σ
T	Low-Rise	0.372	0.113	0.288	0.095	0.330	0.112
	Mid-Rise	0.521	0.092	0.437	0.107	0.479	0.107
η	Low-Rise	0.225	0.093	0.289	0.109	0.257	0.105
	Mid-Rise	0.133	0.036	0.163	0.049	0.148	0.045
a_p (%)	Low-Rise	2.20	2.15	1.40	1.21	1.80	1.78
	Mid-Rise	2.50	2.32	2.00	1.99	2.25	2.15

It can be stated that the estimated period values with respect to the building height for the sub-classes of buildings confirm well with the empirical period formulations available in the literature. Figure 2.3 shows the comparison of the estimated building periods for bare RC frames in the database (sub-classes LR-BR and MR-BR) with the well-known empirical formulations proposed by Goel and Chopra [23] and Uniform Building Code [24]. The three dashed lines constitute the lower bound (best-fit minus one standard deviation), the best-fit and the upper bound (best-fit plus one standard deviation) of the equation proposed by Goel and Chopra [23]. The solid black line is the logarithmic curve fitted to the database buildings whereas the solid gray line represents the formulation proposed in the Uniform Building Code [24]. The variation of period with building height seems to be in reasonable limits and the best-fit curve of the estimated data matches well with the best-fit curves obtained from the empirical formulations.

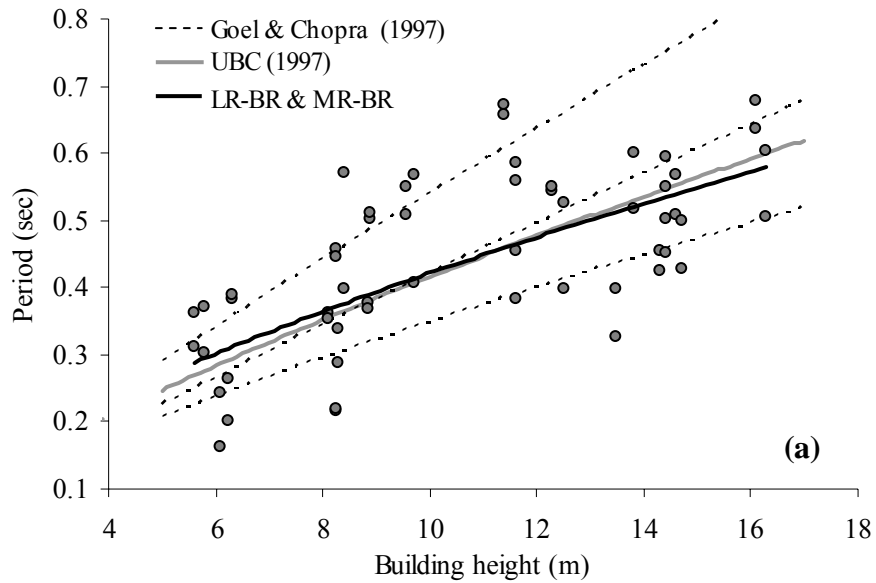


Figure 2.3 Variation of the estimated building period with building height compared with the empirical formulations.

Figure 2.4 presents the spectral variation of strength ratio for all the selected buildings. Regarding the discussion above related to the seismic design codes, the statistical data is classified in three groups according to their construction year of the building: construction before 1975 (Period I), construction between 1975 and 1997 (Period II) and construction after 1997 (Period III). The code-based spectral variations proposed in 1975 [16] and 1997 [18] for local site class of Z2 (soft rock or stiff soil) is also displayed in the same figure. Most of the buildings (especially in the short period range) satisfy the 1975 design level whereas a few can conform to the level dictated by the 1997 Code [18]. This is an expected outcome, since nearly all of the buildings had been built before the release of the 1997 Code [18]. The classification with respect to the construction year does not yield any consistent trend, since there are buildings in each group which satisfy or do not satisfy the code design level.

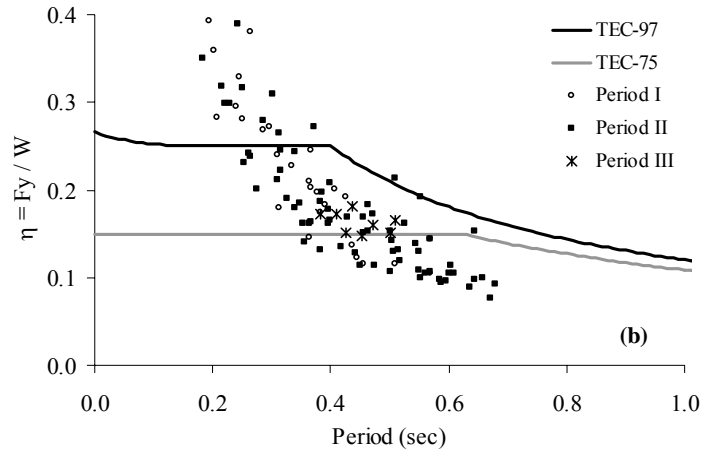


Figure 2.4 Spectral variation of strength factor compared with the code design levels proposed in the specifications of 1975 and 1997

The following observations are based on the statistical outcomes:

- By the introduction of infill walls, the mean periods of low-rise and mid-rise RC structures are decreased by 23% and 16% whereas the mean strength ratios of low-rise and mid-rise are increased by 28% and 23%, respectively. The above trends reveal that increase in stiffness and strength is significant in both low-rise and mid-rise buildings by the addition of infill walls when compared with their bare frame counterparts.
- The mean strength ratio of MR frames is 59% of the mean of LR frames for bare case and the same mean strength ratio of MR frames is 56% of the mean of LR frames for infilled case. Hence the ratio of η_{MR} / η_{LR} is not very sensitive to having bare or infilled frames.
- The dispersion in low-rise buildings is more significant than mid-rise buildings in terms of period and strength.
- The variation in post-elastic stiffness ratio is very high for all building sub-classes.
- Low-rise building models possess higher strength ratios (obvious but worth to mention)

CHAPTER 3

GENERATION OF REFERENCE FRAGILITY CURVES

3.1 METHODOLOGY

There are various methods for the assessment of the fragility of structural systems which differ in expenditure and precision. The type of fragility curve generation method chosen depends on the objective of the assessment but also on the availability of data and technology.

The methodology used in the derivation of fragility curves of low-rise and mid-rise RC frame structures in this study is presented as a flowchart in Figure 3.1. The process begins with the selection of structural configuration. Identification and classification of building sub-classes have been discussed in Chapter 2. Then the building models are idealized as SDOF systems and the related structural parameters are obtained for each building model. Structural variability is taken into account by considering the SDOF structural parameters as random variables. Ground motion records are selected from a wide range of characteristics to take ground motion uncertainty into account. After this step, time history analyses are conducted by using the structural simulations and response statistics are obtained in terms of maximum displacement. Then by using response statistics and limit states which have been determined for each building sub-class in terms of maximum displacement, the probability of exceedance of each limit state under a specific level of seismic intensity (in this study peak ground velocity) is obtained.

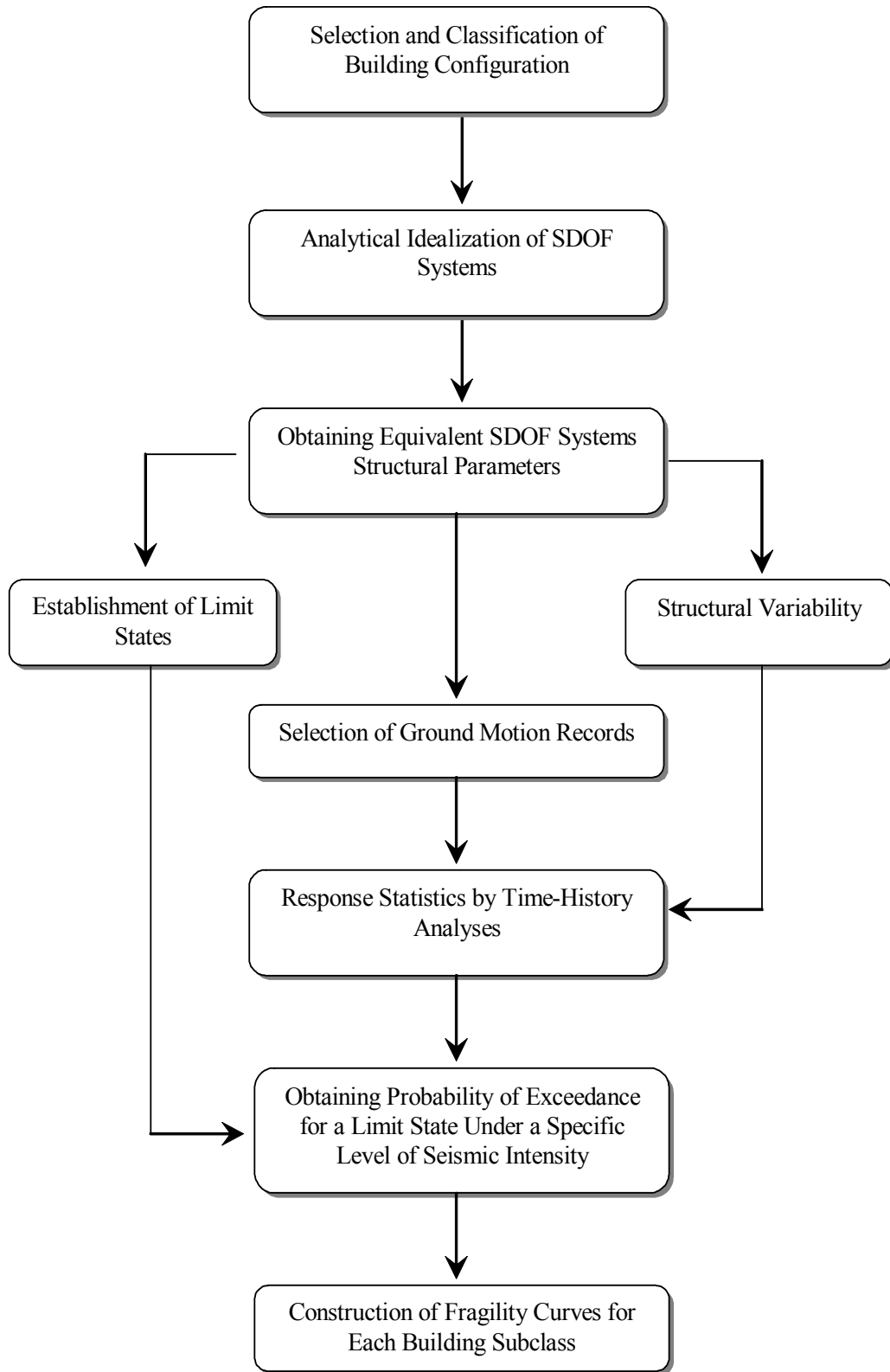


Figure 3.1 The Methodology used in the Derivation of Reference Fragility Curves

Finally, computed probability of exceedance of each limit state is plotted against hazard parameter and a curve is fitted to the scatter data to obtain the final form of the fragility curve for that limit state. The major steps required for the generation of the reference fragility curves for low-rise and mid-rise RC structures from Düzce database are explained below in detail.

3.2 INPUT DATA FOR STRUCTURAL SIMULATIONS

As mentioned in Chapter 2, three structural parameters (period, strength factor, post-elastic stiffness ratio) are obtained from the idealization process for the representation of SDOF systems as structural models. Among the input parameters, period (T) and strength factor (η) are taken as random variables and normal distribution is assumed for these parameters. Post-elastic stiffness ratio (a_p) is considered as a deterministic (constant) parameter and mean value of a_p for each sub-class is used in the analysis. The sample size is 28 considering both orthogonal directions for each building sub-class. The variation of η with T for each sub-class is presented in Figure 3.2 with the corresponding correlation coefficient.

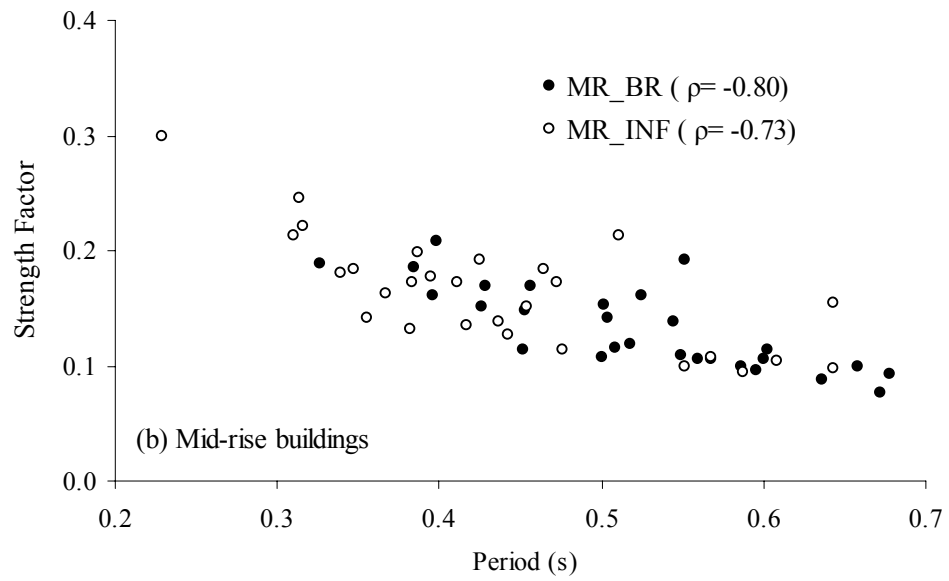
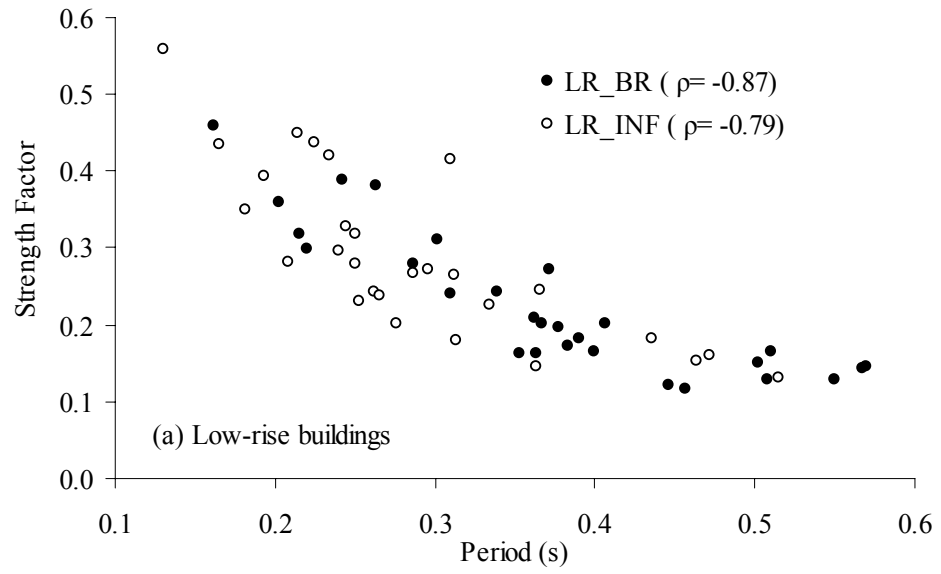


Figure 3.2 The variation of η with T for a) low-rise building sub-classes b) mid-rise building sub-classes

3.3 GROUND MOTION DATA SET

There are 100 records covering a wide range of ground motion characteristics in the dataset from different parts of the world. Peculiar ground motion records due to rupture directivity and extreme site amplification effects are not included in the dataset. Strong motion characteristics of the records are listed in Table 3.1. It contains information about the name, the date and the magnitude of the earthquake, the location and the local site condition of the recording station, distance to fault, scaling factor of the record, peak ground acceleration (PGA), peak ground velocity (PGV), V/A ratio, effective peak acceleration (EPA), energy index (EI) and effective duration (Δt_{eff}).

The magnitude definition considered is the surface wave magnitude (M_s). All the sites are classified as Hard, Medium or Soft considering shear wave velocity (V_s) as a measure. Hence rock sites with $V_s > 760$ m/s are considered as “Hard”, dense soil and soft rock sites with $360 \text{ m/s} < V_s \leq 760$ m/s are assumed as “Medium” and soil sites with $V_s \leq 360$ m/s are classified as “Soft” [25].

V/A ratio (ratio of PGV to PGA) is still a simple parameter to obtain, but it is more enhanced when compared to PGA or PGV alone. It is generally used to emphasize the effect of local soil conditions on ground motion properties. For impulsive type of records, V/A indicates the average duration of the dominant acceleration pulse and for harmonic type of records, it stands for the inverse of the dominant circular frequency [26].

Effective peak acceleration (EPA) is defined as the average of the spectral acceleration (S_a) in the period interval $0.1 < T < 0.5$ seconds, divided by a constant value 2.5, which is accepted as a global acceleration response amplification factor for 5% damped SDOF systems in the acceleration range of earthquake spectra.

Table 3.1 Ground Motion Characteristics

BINS	EARTHQUAKE	LOCATION	COMP	SITE	M _s	D (km)	Scale	PGA (g)	PGV (cm/s)	V/A (s)	EPA (g)	EI	t _{eff} (s)
1	Morgan Hill	Gilroy Array #2 (Hwy 101 & Bolsa Rd)	0	S	6.1	12	1.00	0.157	4.99	0.032	0.099	17.56	18.94
	Vrancea	Bucharest, Building Research Institute	EW	S	6.8	162	1.00	0.054	2.08	0.040	0.036	3.62	8.53
	Manjil	Building & Housing Research Center, Tehran	NS	H	7.3	234	1.00	0.011	1.09	0.098	0.012	3.56	14.63
	Manjil	Building & Housing Research Center, Tehran	EW	H	7.3	234	1.00	0.013	1.24	0.098	0.013	2.92	13.61
	İzmir	Kusadasi Meteorology Station	L	M	6.0	41	1.00	0.067	4.34	0.066	0.059	9.03	10.59
2	Livermore	Fagundes Ranch	270	S	5.8	11	1.00	0.250	9.74	0.040	0.212	9.81	3.22
	Morgan Hill	Gilroy Array #7 (Mantelli Ranch)	90	S	6.1	8	1.00	0.114	5.76	0.052	0.132	11.54	12.10
	Lazio Abruzzo	Cassino-Sant'Elia	EW	M	5.8	23	1.00	0.114	7.90	0.071	0.118	17.83	9.97
	Vrancea	Bucharest, Building Research Institute	NS	S	6.8	162	1.00	0.038	6.45	0.173	0.027	9.61	8.53
	Kocaeli	Kucuk Cekmece	NS	H	7.8	59	1.00	0.173	8.34	0.049	0.146	24.99	30.86
3	Campano-Lucano	Brienza	NS	H	6.9	43	1.00	0.227	11.27	0.051	0.212	30.02	10.23
	Coalinga	Parkfield - Cholame 4W	0	M	6.5	58	1.00	0.131	10.51	0.082	0.133	25.65	13.26
	Loma Prieta	Hayward Muir School	0	S	7.1	45	1.00	0.170	13.63	0.082	0.177	38.00	12.81
	Northridge	Leona Valley, Ritter Ranch	0	S	6.8	41	1.00	0.146	14.88	0.104	0.111	29.49	14.47
	Northridge	Downey County Maint. Bldg.	360	S	6.8	46	1.00	0.223	12.70	0.058	0.201	33.38	17.53
4	Denizli	Directorate of Public Works and Settlement	EW	H	5.1	15	1.00	0.261	15.46	0.060	0.258	23.22	5.91
	Montenegro	Budva, PTT	NS	M	6.3	8	1.00	0.119	19.24	0.164	0.104	34.08	11.02
	Imperial Valley	El Centro Array #1, Borchard Ranch	S40E	S	6.9	23	1.00	0.141	16.43	0.119	0.112	32.19	16.17
	Whittier Narrows	Cedar Hill Nursery, Tarzana	0	M	5.8	41	1.00	0.405	19.16	0.048	0.414	27.71	6.63
	Landers	Amboy	0	H	7.5	73	1.00	0.115	17.86	0.158	0.119	69.01	34.80
5	Alkion	Xilokastro, OTE Building	L	M	6.7	19	1.00	0.289	22.72	0.080	0.263	68.33	15.40
	Kalamata	Kalamata-OTE Building	N10W	H	5.8	10	1.00	0.272	23.55	0.088	0.302	45.64	6.23
	Whittier Narrows	Fremont School, Alhambra	180	M	5.8	14	1.00	0.292	21.72	0.076	0.296	32.01	5.25
	Landers	Amboy	90	H	7.5	73	1.00	0.146	20.07	0.140	0.142	73.86	31.47
	Northridge	Santa Monica, City Hall Grounds	360	S	6.8	27	1.00	0.370	24.91	0.069	0.273	75.96	11.31

Table 3.1 (Continued)

BINS	EARTHQUAKE	LOCATION	COMP	SITE	M _s	D (km)	Scale	PGA (g)	PGV (cm/s)	V/A (s)	EPA (g)	EI	t _{eff} (s)
6	San Fernando	8244 Orion Blvd.	N00W	M	6.5	17	1.00	0.255	29.80	0.119	0.233	98.78	16.58
	Montenegro	Petrovac, Hotel Oliva	EW	H	7.0	25	1.00	0.306	25.31	0.084	0.310	47.24	13.36
	Campano-Lucano	Calitri	EW	H	6.9	16	1.00	0.176	27.46	0.159	0.167	93.21	47.57
	Horasan	Horasan Meteorology Station	EW	H	6.7	33	1.00	0.161	26.02	0.165	0.126	95.54	18.36
	Northridge	Saticoy	90	M	6.8	13	1.00	0.368	28.92	0.080	0.358	98.93	15.63
7	Kalamata	Kalamata-Prefecture	N265	H	5.8	9	1.00	0.215	32.73	0.155	0.216	59.88	5.50
	Kalamata	Kalamata-OTE Building	N80E	H	5.8	10	1.00	0.240	31.51	0.134	0.247	53.07	5.13
	Loma Prieta	Gilroy Array #2	67	S	7.1	12	1.00	0.367	32.92	0.091	0.351	59.20	10.98
	Northridge	Pacoima Kagel Canyon	90	M	6.8	11	1.00	0.301	30.95	0.105	0.265	88.56	10.38
	Loma Prieta	Gilroy Array #1	90	H	7.1	3	1.00	0.442	33.84	0.078	0.547	52.62	3.69
8	Montenegro	Petrovac, Hotel Oliva	NS	H	7.0	25	1.00	0.454	38.82	0.087	0.461	87.07	12.00
	Loma Prieta	Capitola Fire Station	0	S	7.1	16	1.00	0.472	36.15	0.078	0.571	101.92	12.22
	Loma Prieta	Gilroy Array #2	337	S	7.1	12	1.00	0.322	39.09	0.124	0.337	84.52	9.52
	Kobe	Nishi-Akashi	90	S	6.8	11	1.00	0.503	36.60	0.074	0.429	81.60	11.23
	Chi Chi	TCU075, Nantou Tsaotun School	360	S	7.6	3	1.00	0.262	35.38	0.138	0.197	94.22	32.42
9	Loma Prieta	Saratoga	0	M	7.1	4	1.00	0.504	41.35	0.084	0.295	94.42	9.40
	Loma Prieta	Saratoga	90	M	7.1	4	1.00	0.322	43.60	0.138	0.286	87.39	8.27
	Landers	Joshua Tree Fire Station	90	M	7.5	10	1.00	0.284	42.71	0.153	0.211	127.32	28.22
	Northridge	Katherine Rd, Simi Valley	N90E	M	6.8	14	1.00	0.513	44.56	0.088	0.588	77.27	6.76
	Dinar	Dinar Meteorology Station	EW	S	6.1	1	1.00	0.319	40.61	0.130	0.328	130.99	15.54
10	Montenegro	Ulcinj, Hotel Olympic	EW	H	7.0	24	1.00	0.241	47.08	0.199	0.193	99.62	25.99
	Imperial Valley	El Centro Array #5, James Road	S40E	S	6.9	5	1.00	0.550	49.71	0.092	0.415	122.22	8.21
	Cape Mendocino	Petrolia, General Store	0	M	7.1	16	1.00	0.589	48.30	0.084	0.363	96.02	17.90
	Kocaeli	Gebze	NS	H	7.8	15	1.00	0.269	45.59	0.173	0.186	80.09	7.53
	Chi Chi	TCU074, Nantou Nanguang School	360	S	7.6	14	1.00	0.370	46.29	0.128	0.312	116.15	21.19

Table 3.1 (Continued)

BINS	EARTHQUAKE	LOCATION	COMP	SITE	M _s	D (km)	Scale	PGA (g)	PGV (cm/s)	V/A (s)	EPA (g)	EI	t _{eff} (s)
11	Landers	Yermo Fire Station	270	M	7.5	31	1.00	0.245	50.81	0.212	0.177	96.79	19.40
	Northridge	Katherine Rd, Simi Valley	N00E	M	6.8	14	1.00	0.727	51.11	0.072	0.519	87.62	5.93
	Northridge	Castaic Old Ridge Road	360	M	6.8	24	1.00	0.514	52.56	0.104	0.420	118.59	8.69
	Kocaeli	İzmit	EW	H	7.8	8	1.00	0.227	54.28	0.244	0.227	84.25	14.03
	Chi Chi	TCU109	NS	S	7.6	13	1.00	0.155	53.07	0.349	0.140	175.25	31.24
12	Manjil	Abhar	T	S	7.3	98	1.00	0.209	55.44	0.271	0.252	190.86	21.11
	Northridge	W Pico Canyon Blvd, Newhall	N44W	S	6.8	9	1.00	0.355	59.87	0.172	0.253	129.58	14.27
	Loma Prieta	Corralitos	0	S	7.1	3	1.00	0.630	55.20	0.089	0.598	84.82	6.86
	Chi Chi	CHY006	EW	S	7.6	15	1.00	0.364	55.41	0.155	0.307	144.64	24.31
	Düzce	Bolu	NS	S	7.3	6	1.00	0.754	58.25	0.079	0.649	124.25	8.55
13	Kocaeli	Düzce	NS	S	7.8	11	1.00	0.337	60.59	0.183	0.277	126.06	11.99
	Chi Chi	TCU049	NS	S	7.6	4	1.00	0.251	61.19	0.249	0.223	100.38	22.72
	Northridge	Saticoy	180	M	6.8	13	1.00	0.477	61.48	0.131	0.507	155.83	10.61
	Loma Prieta	Hollister - South St. And Pine Dr.	0	S	7.1	17	1.00	0.369	62.78	0.173	0.266	146.10	16.45
	Chi Chi	TCU076	NS	S	7.6	3	1.00	0.416	64.16	0.157	0.337	133.55	28.13
14	Imperial Valley	El Centro Array #6, Huston Road	S40E	S	6.9	4	1.00	0.339	66.47	0.200	0.269	143.17	11.45
	Düzce	Düzce	NS	S	7.3	7	1.00	0.410	65.76	0.164	0.432	142.09	11.14
	Düzce	Bolu	EW	S	7.3	6	1.00	0.822	66.92	0.083	0.492	123.54	9.03
	Kobe	Takarazu	0	S	6.8	1	1.00	0.693	68.28	0.100	0.509	153.72	4.62
	Chi Chi	TCU071	NS	S	7.6	5	1.00	0.655	69.38	0.108	0.601	122.36	23.73
15	Bucharest	Bucharest, Building Research Institute	NS	S	7.1	161	1.00	0.202	73.13	0.370	0.123	142.58	6.85
	Chi Chi	CHY028	EW	S	7.6	7	1.00	0.653	72.78	0.114	0.621	154.35	8.67
	Northridge	Newhall LA County Fire Station	90	S	6.8	11	1.00	0.583	74.84	0.131	0.631	129.90	5.93
	Chi Chi	TCU074, Nantou Nanguang School	90	S	7.6	14	1.00	0.595	74.64	0.128	0.433	202.74	12.61
	Imperial Valley	Meloland Overpass	0	S	6.9	3	1.00	0.314	71.77	0.233	0.213	112.32	8.22

Table 3.1 (Continued)

BINS	EARTHQUAKE	LOCATION	COMP	SITE	M _s	D (km)	Scale	PGA (g)	PGV (cm/s)	V/A (s)	EPA (g)	EI	t _{eff} (s)
16	Northridge	Tarzana Cedar Hill Nursery	360	S	6.8	17	1.00	0.990	77.18	0.080	0.946	164.09	12.63
	Northridge	Sepulveda VA Hospital	360	S	6.8	10	1.00	0.939	76.60	0.083	0.807	146.38	8.19
	Kobe	JMA	EW	M	6.8	1	1.00	0.629	75.04	0.122	0.532	146.83	9.54
	Kocaeli	Yarımca	NS	S	7.8	3	1.00	0.322	79.60	0.252	0.214	158.44	15.76
	Kocaeli	Sakarya	EW	H	7.8	7	1.00	0.407	79.80	0.200	0.293	94.78	15.52
17	Tabas	Tabas	N16W	H	7.3	52	1.00	1.065	80.53	0.077	0.909	212.25	18.04
	Northridge	Rinaldi Receiving Station	N41W	M	6.8	9	1.00	0.480	80.33	0.171	0.500	164.22	8.38
	Northridge	Sepulveda VA Hospital	270	S	6.8	10	1.00	0.753	84.85	0.115	0.489	127.40	7.84
	Kocaeli	Yarımca	EW	S	7.8	3	1.00	0.230	84.70	0.375	0.217	165.41	15.31
	Morgan Hill	Coyote Lake Dam	285	H	6.1	2	1.00	1.298	80.79	0.063	0.672	96.44	3.19
18	Cape Mendocino	Petrolia, General Store	90	M	7.1	16	1.00	0.662	89.45	0.138	0.437	150.92	16.11
	Düzce	Düzce	EW	S	7.3	7	1.00	0.513	86.05	0.171	0.395	173.06	10.91
	Erzincan	Erzincan	EW	S	7.3	2	0.86	0.469	101.83	0.200	0.390	159.47	10.39
	Chi Chi	TCU075, Nantou Tsaotun School	90	S	7.6	3	0.87	0.331	102.02	0.314	0.307	175.10	27.37
	Kobe	Takarazu	90	S	6.8	1	1.00	0.694	85.25	0.125	0.691	140.63	3.69
19	Tabas	Tabas	N74E	H	7.3	52	1.00	0.914	90.23	0.101	0.828	217.21	18.46
	Erzincan	Erzincan	EW	S	7.3	2	1.00	0.469	92.05	0.200	0.390	159.47	10.39
	Northridge	Newhall LA County Fire Station	360	S	6.8	11	1.00	0.589	94.72	0.164	0.582	175.86	5.53
	Kobe	JMA	NS	M	6.8	1	1.00	0.833	90.70	0.111	0.719	178.57	8.33
	Imperial Valley	Meloland Overpass	270	S	6.9	3	1.00	0.296	90.45	0.311	0.223	186.69	6.75
20	Imperial Valley	El Centro Array #5, James Road	S50W	S	6.9	5	1.00	0.367	95.89	0.266	0.394	191.86	9.61
	Imperial Valley	El Centro Array #6, Huston Road	S50W	S	6.9	4	0.87	0.437	113.11	0.264	0.307	210.28	8.24
	Northridge	Slymar, Converter Station	N38W	S	6.8	9	0.90	0.580	107.48	0.189	0.321	226.42	5.22
	Northridge	Tarzana Cedar Hill Nursery	90	S	6.8	17	0.89	1.778	110.16	0.063	1.366	168.24	10.57
	Northridge	Jensen Filter Plant	292	S	6.8	9	1.00	0.593	99.28	0.171	0.448	228.28	5.97

Energy Index (EI) is based on total input energy as a measure of ground motion intensity, or its damage potential with the following expression [27]

$$EI = \frac{1}{T_{\max}} \int_0^{T_{\max}} V_{\text{eq}}(T) dT \quad (3.1)$$

where V_{eq} is the input energy equivalent velocity and it is defined by

$$V_{\text{eq}} = \sqrt{\frac{2E_i(T)}{m}} \quad (3.2)$$

E_i given in Equation 3.2 is the input energy of a linear viscously damped SDOF system and m denotes the mass of the system. T_{\max} in Equation 3.1 is an upper bound for the natural periods of SDOF systems and it is taken as 4 seconds in this study. Previous studies have shown that EI is an effective measure of the damage potential of ground motion records since it takes into account many basic ground motion characteristics.

The duration of ground motion which contributes to the significant part of the vibratory response of SDOF systems is called the effective duration, t_{eff} . There exist various definitions of t_{eff} . The one which is considered in this study belongs to Trifunac and Brady [28]. By definition, it is the time interval where 90 % contribution of the accelerogram intensity takes place. The 90% contribution is selected as the time interval between 5% and 95% of the accelerogram intensity. Accelerogram intensity is described by Equation 3.3.

$$I(t) = \int_0^t f^2(\tau) d\tau \quad (3.3)$$

where $f(t)$ represents the time history of ground displacement, velocity or acceleration. The effective duration is adapted in this study with $f(t)$ representing the ground acceleration variation. Statistical properties of the ground motion set

are presented in Figures 3.3.a-i and Table 3.2.

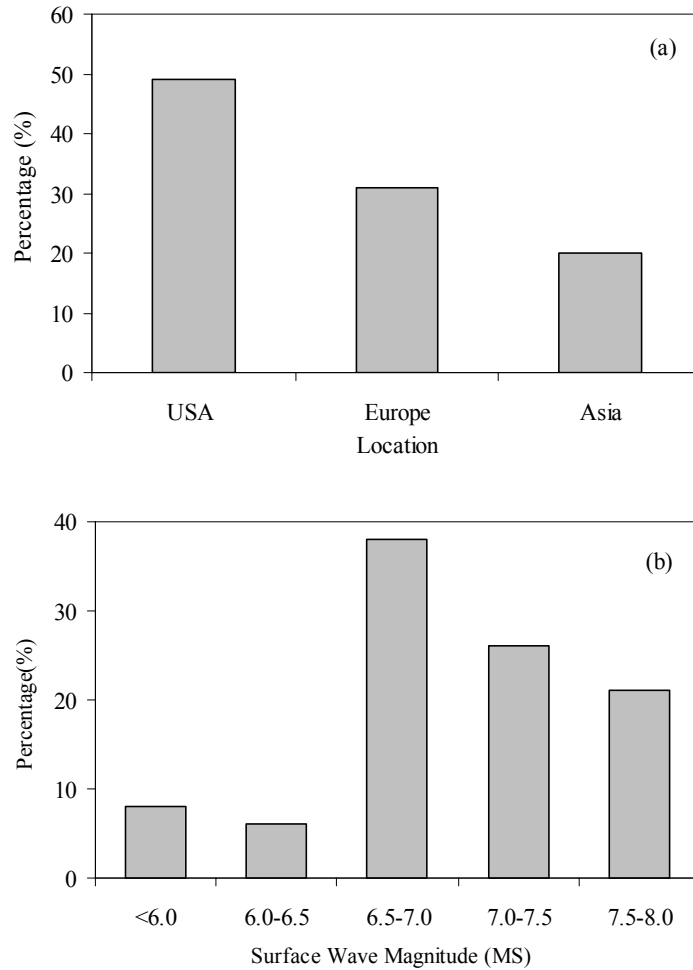


Figure 3.3 General characteristics of ground motion data set in terms of a) location b) surface wave magnitude c) closest distance to fault d) local site conditions e) peak ground acceleration f) effective peak acceleration g) V/A ratio h) effective duration i) energy index

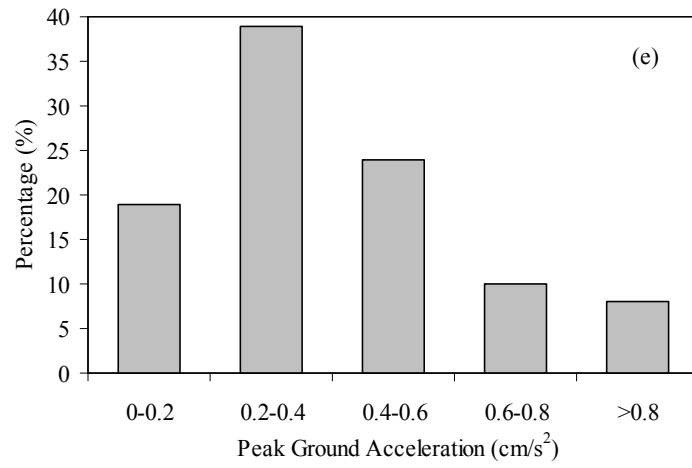
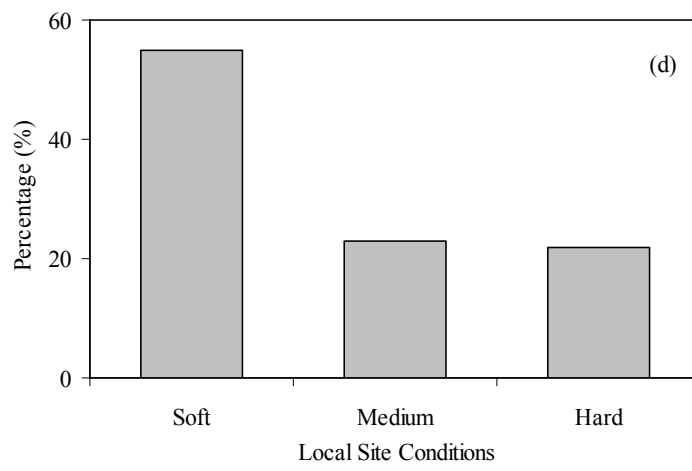
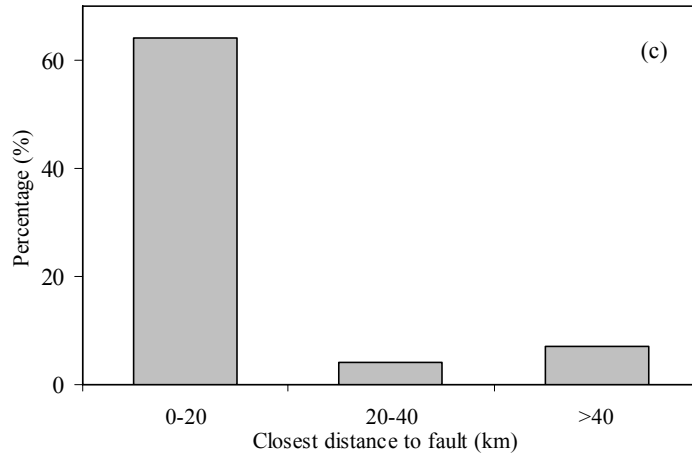


Figure 3.3 (continued)

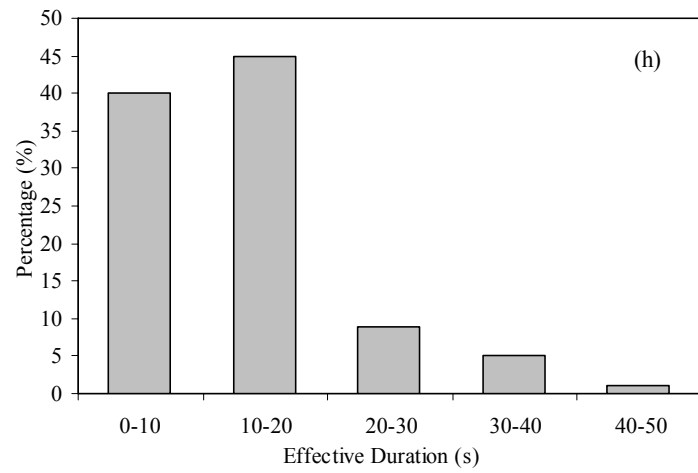
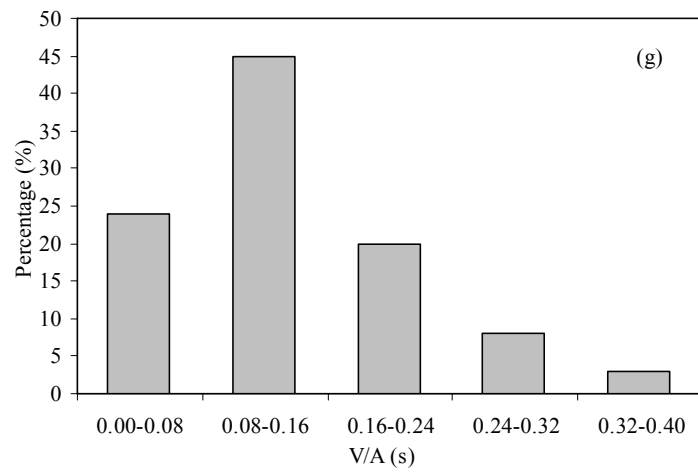
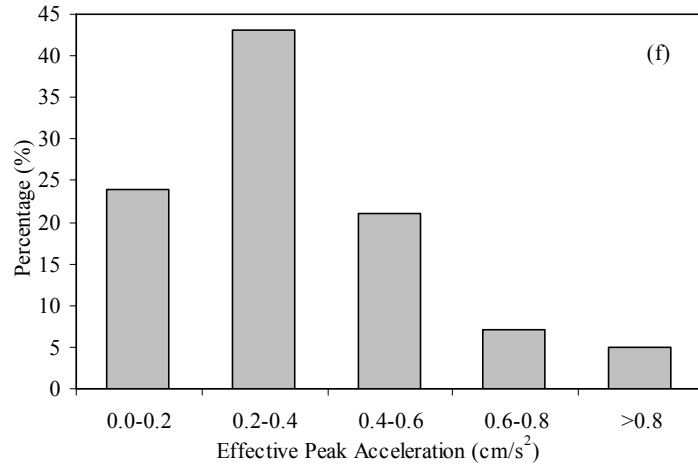


Figure 3.3 (continued)

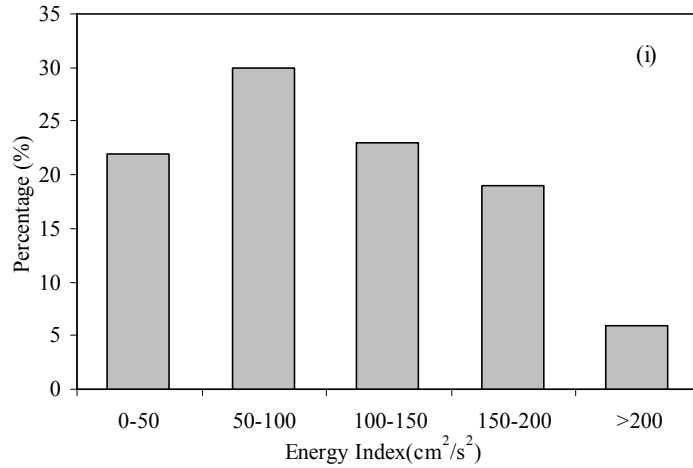


Figure 3.3 (continued)

The general characteristics of the ground motion database can be stated as follows: Nearly half of the records are from USA and most of them have magnitudes larger than 6.5. The closest distance to fault for majority of the records (more than 60%) is smaller than 20 km and generally recorded at soft site conditions. A great percentage of the records have PGA and EPA values in the range 0.2-0.6. The effective duration values are populated in the range 5-20 records and finally the distribution of EI values is nearly uniform in the range 0-200 cm²/s². Briefly it can be stated that ground motion records in the database have a wide range of characteristics which introduces a considerable hazard uncertainty but also able to excite the considered building structure classes in all hazard levels.

Selection of the hazard parameter is of paramount importance since it is difficult to determine a single parameter that represents earthquake ground motions. There are various parameters that have been frequently used in literature such as Peak Ground Acceleration (PGA), Peak Ground Velocity (PGV), Spectral Acceleration (S_a), Spectral Displacement (S_d). Among most commonly used parameters, PGA and PGV are the well-known peak value parameters. It is very easy to obtain them directly from time-history records. In this study, reference hazard parameter is

considered as PGV because it appears to be a more suitable ground motion intensity parameter for describing deformation demands in structures that deform beyond the elastic range. Additionally, PGV is more indicative for defining the correlation between structural damage and ground motion intensity [11]. The selection and classification of the ground motion data is made according to selected reference hazard parameter.

Table 3.2 Statistical Properties of Ground Motion Data Set

	μ	COV
M_s	7.0	0.081
Distance	13.6	1.106
PGA	0.406	0.664
PGV	49.93	0.579
V/A	0.137	0.542
EPA	0.348	0.644
EI	105.20	0.559
Δt_{eff}	13.36	0.595

The dataset classification is made by dividing the ground motion data into 20 bins with PGV intervals of 5 cm/s, each bin including five records. The purpose of such a classification is to observe an even distribution of response as it can also be observed from Figure 3.4.

For most of the records, the original acceleration time trace is employed in the analysis. However only for a few number of records, scaling factors are introduced in order to adjust the PGV values. This is due to the scarcity of ground motion records having high PGV values. It is worth to mention that the change in the amplitudes of the original records due to the employed scale factors is between

10%-15%, or in other words, it is not too large to cause any distortion in the actual characteristics of the corresponding records.

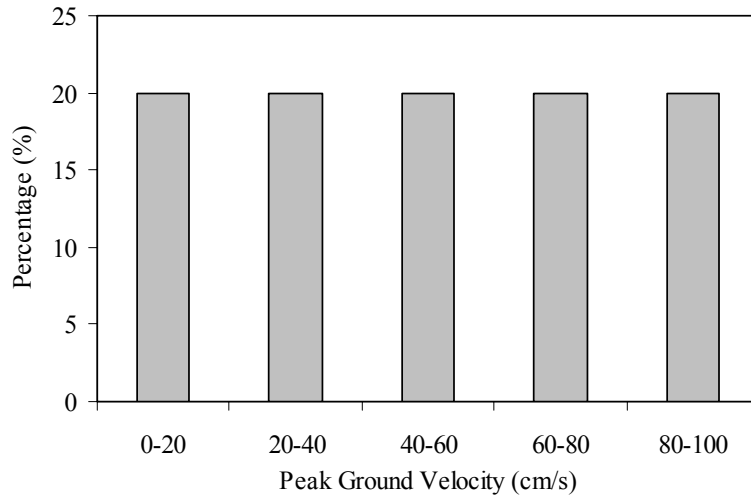


Figure 3.4 Dataset classification according to PGV values

3.4 RESPONSE STATISTICS

The set of 100 ground motion records has been employed for the determination of the maximum displacement response of equivalent SDOF systems. The building sub-classes are represented by SDOF structural parameters (T , η and a_p) as discussed above. Inelastic SDOF time history analyses are employed herein to obtain the response statistics.

A total of 11200 SDOF inelastic time history analyses were conducted for the structural simulations of each building sub-class, in which T and η are considered as random variables. The viscous damping ratio (ξ) is taken as 5 %. The stiffness degrading model [29] is employed in the analyses in order to take into account the inelastic behavior. Maximum response data is monitored for each building at each

ground motion hazard intensity. There are 28 (no of simulations in a sub-class) * 5 (no of records in a ground motion bin) = 140 response data points in a vertical bin. A normal distribution is fitted to calculate the probabilities of exceedance. For the whole range of hazard intensity, 140*20 (no of ground motion bins) = 2800 response data points are calculated for each sub-class. These response points are plotted against mean value of PGV for each bin. The response statistics for each sub-class is illustrated in Figure 3.5 a-d.

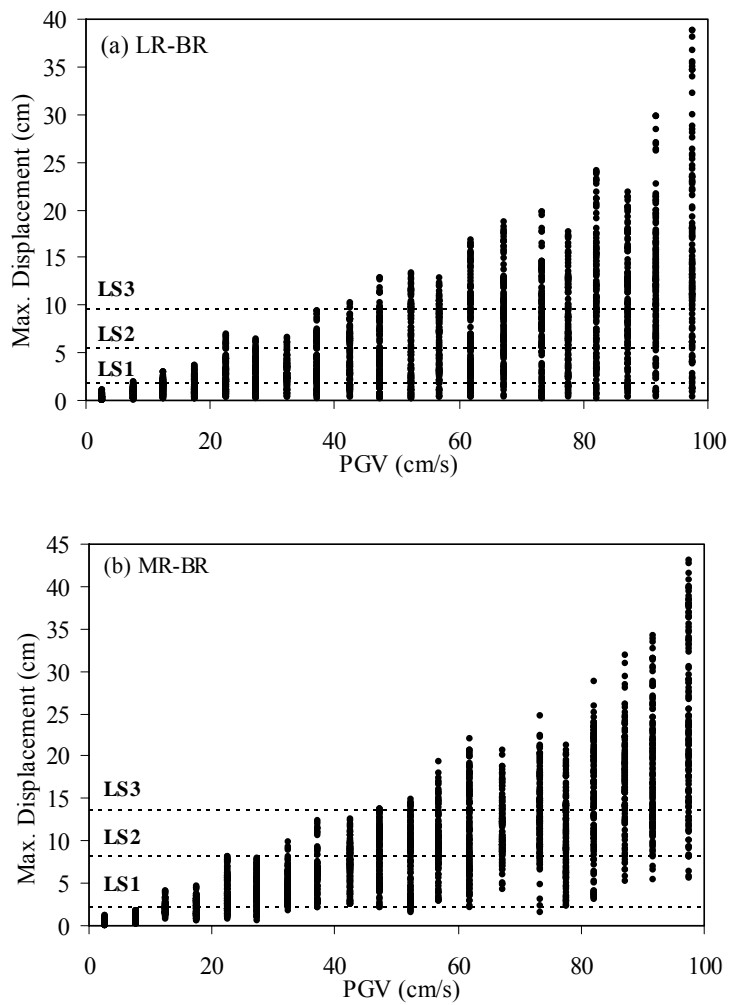


Figure 3.5 Response Statistics (maximum displacement vs. PGV) for sub-class
a) LR_BR b) MR_BR c) LR_INF d) MR_INF

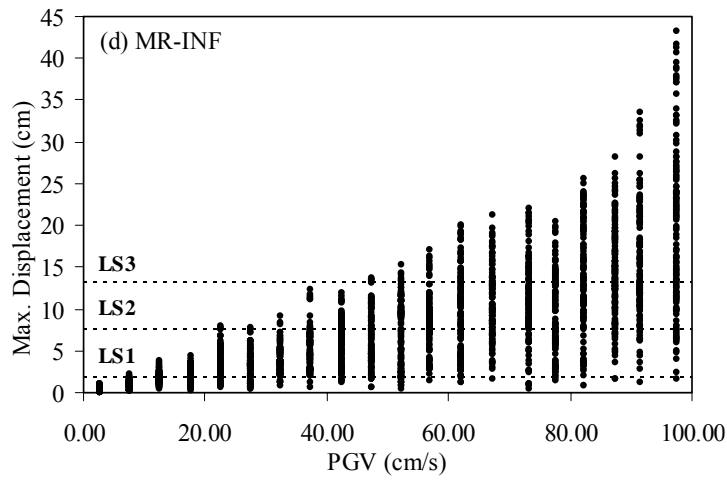
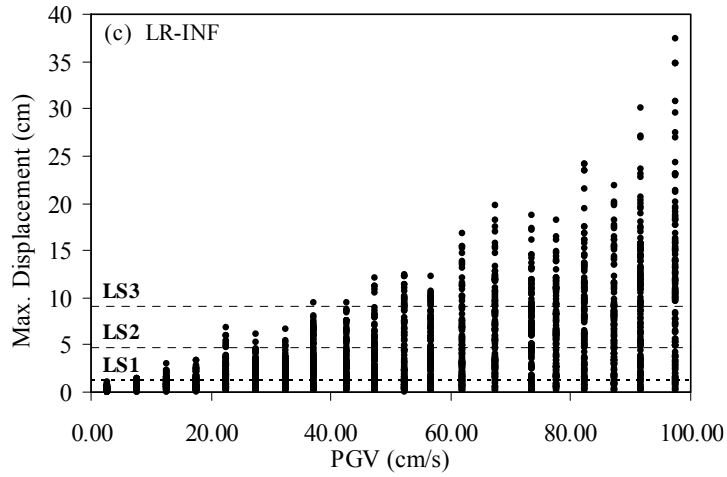


Figure 3.5 (continued)

3.5 LIMIT STATES

Three limit states are defined which are termed as serviceability, damage control and collapse prevention. Since this study focuses on generating the fragility curves for a population of buildings by using simplified models and analyses, it will not be appropriate to define limit states in a detailed manner based on member behaviour, local strains or hinge mechanisms as done for individual buildings. Instead, the limit states are defined in terms of simple global parameters.

Serviceability Limit State (LS1): This limit state is usually governed by the stiffness of the structure; hence it is appropriate to select stiffness-based parameters for the quantification of the performance level.

The definition considered is the softening index SI which was originally proposed by DiPasquale and Cakmak [30]. The index can be defined as:

$$SI = 1 - T_0/T_i \quad (3.4)$$

where T_0 is the initial period of the capacity curve and T_i is the effective (secant) period at some intermediate spectral displacement. The index is equal to zero when $T_0=T_i$ and takes values between 0 and 1 regarding the amount of period elongation due to inelastic action. The upper bound of unity is a theoretical value with the condition that T_i approaches to infinity and physically this value defines the failure state of the structure. The quantification of the Softening Index is illustrated in Figure 3.6 for typical values T_i ($i=1-4$). The accepted value of SI index for LS1 is 0.20 in accordance with previous research [31-32].

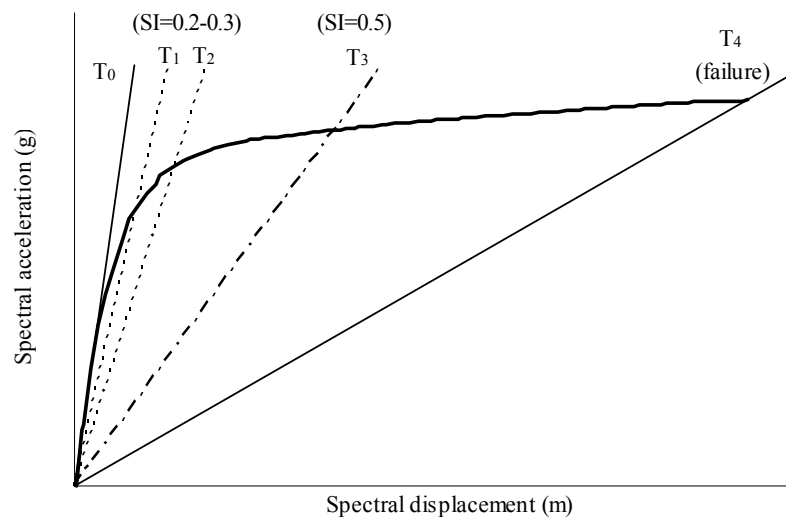


Figure 3.6 The illustration of softening index for typical values

Hence for each structure, the limit state values based on the softening index definition is calculated and the resultant value is used as serviceability limit state value for that structure. The mean values for each sub-class are listed in Table 3.3 in terms of both spectral displacement and drift along with the corresponding coefficient of variations (COV's). Spectral displacement is the parameter required for the construction of fragility curves through SDOF response analyses and the values are obtained from the corresponding capacity spectra of the buildings whereas drift values are also given in Table 3.3 for the sake of comparison with the limit state values in literature and they are obtained from the corresponding pushover curves of the buildings.

Damage Control Limit State (LS2): This limit state is generally governed by strength and deformation. A parameter deducted from the corresponding pushover curve is proposed. This parameter is denoted as Δ_{DC} and it is defined as:

$$\Delta_{DC} = 0.75 \Delta_{CP} \quad (3.5)$$

where Δ_{CP} is the deformation value that represents the Collapse Prevention limit state and taken as 75% of the ultimate deformation obtained from the pushover curve, in accordance with the study of Akkar et al. [11]. The parameter Δ_{DC} is determined for all the buildings and the mean values for each sub-class are listed in Table 3.3 in terms of both spectral displacement and drift along with the corresponding COV's.

Collapse Prevention Limit State (LS3): This limit state is generally governed by deformation. The deformation value that represents the Collapse Prevention limit state is considered as the smaller of the two criteria below:

- The value of the parameter Δ_{CP} , that has been defined as 75% of the ultimate deformation obtained from the pushover curve.
- The deformation value for which the strength drop is more than 20 % compared with the maximum strength value.

Table 3.3 Limit state definitions for sub-classes of buildings

Parameters for Limit State Attainment	Building Sub-classes							
	LR-BR		LR-INF		MR-BR		MR-INF	
	S _d (cm)	Drift (%)	S _d (cm)	Drift (%)	S _d (cm)	Drift (%)	S _d (cm)	Drift (%)
Serviceability Limit State (LS1)								
Mean	1.7	0.27	1.25	0.19	2.1	0.2	1.85	0.18
COV			0.26				0.28	
Damage Control Limit State (LS2)								
Mean	5.4	0.84	4.7	0.78	8.2	0.78	7.5	0.71
COV			0.3				0.31	
Collapse Prevention Limit State (LS3)								
Mean	9.5	1.51	9	1.43	13.5	1.28	13	1.22
COV			0.32				0.34	

The values in Table 3.3 indicate that the mean drift ratio values range between 0.18% - 0.27%, 0.7% - 0.85% and 1.2% - 1.5% for LS1, LS2 and LS3, respectively. When these values are compared with the ones proposed in different guidelines [21-33] and studies [34-35], it is observed that the values are in the same range, but differences exist. The differences are more significant especially when LS3 values are compared. However, these differences are justifiable on grounds of specific structural characteristics of Turkish buildings.

3.6 GENERATION OF FRAGILITY CURVES

In response statistics plots (Figures 3.5 a-d) each vertical bin of scattered demand data corresponds to a hazard level in terms of PGV. In other words, the response statistics obtained from five ground motions in each bin are assumed to be clustered on the vertical line dividing the bin into two halves. A normal distribution is fitted to the demand data and the statistical parameters (mean and

standard deviation) are calculated for each PGV intensity level. The next step is to calculate the probability of exceedance of each limit state for a given intensity level. Then the calculated probability of exceedance values can be plotted against as a function of hazard parameter PGV. As the final step, lognormal cumulative distribution function is fitted to these data points by employing the method of least squares to obtain the final smooth fragility curves. The reference fragility curves for all building sub-classes are presented in Figure 3.7 and 3.8.

The reference fragility curves for all building subclasses are presented once more in Figures 3.9 and 3.10, this time with comparison of presence or absence of infill walls and low-rise or mid-rise construction, respectively. It is observed from the figures that for a specific level of PGV, bare frames (compared to infilled frames) and mid-rise frames (compared to low frames) are generally more vulnerable to seismic action. This observation becomes more significant for LS3 (Collapse Prevention Limit State) in bare-to-infilled frame comparison. The trends obtained from the fragility curves are in accordance with the inherent structural characteristics of Turkish low-to-mid rise RC frame buildings.

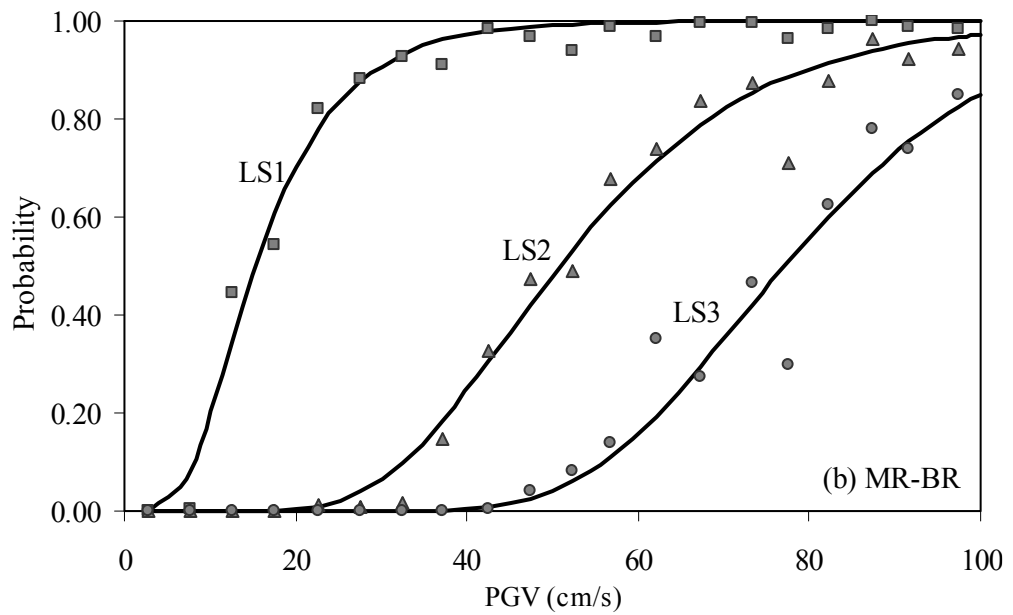
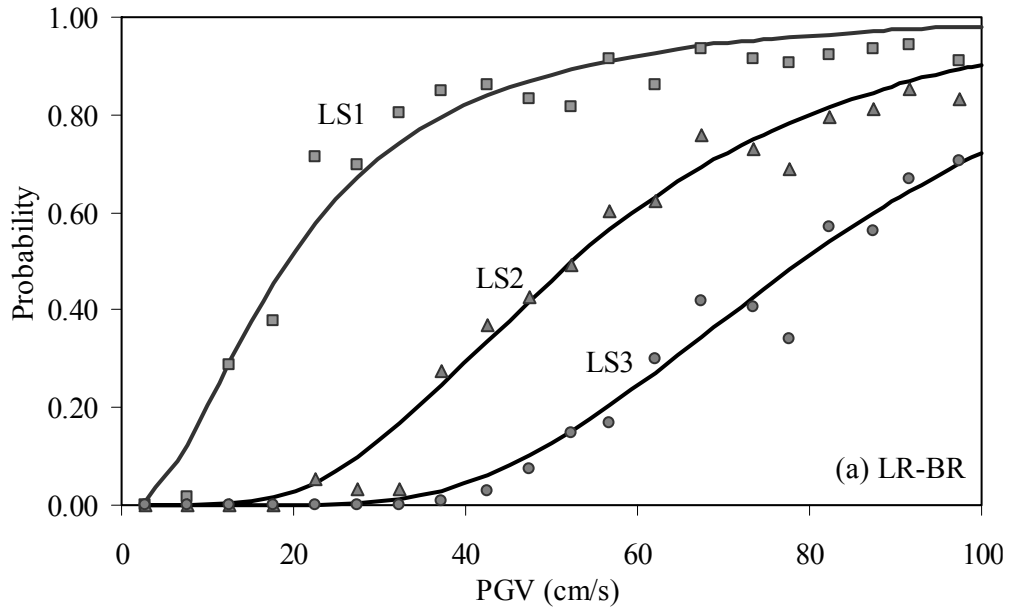


Figure 3.7 Reference Fragility Curves for sub-classes (a) LR-BR (b) MR-BR

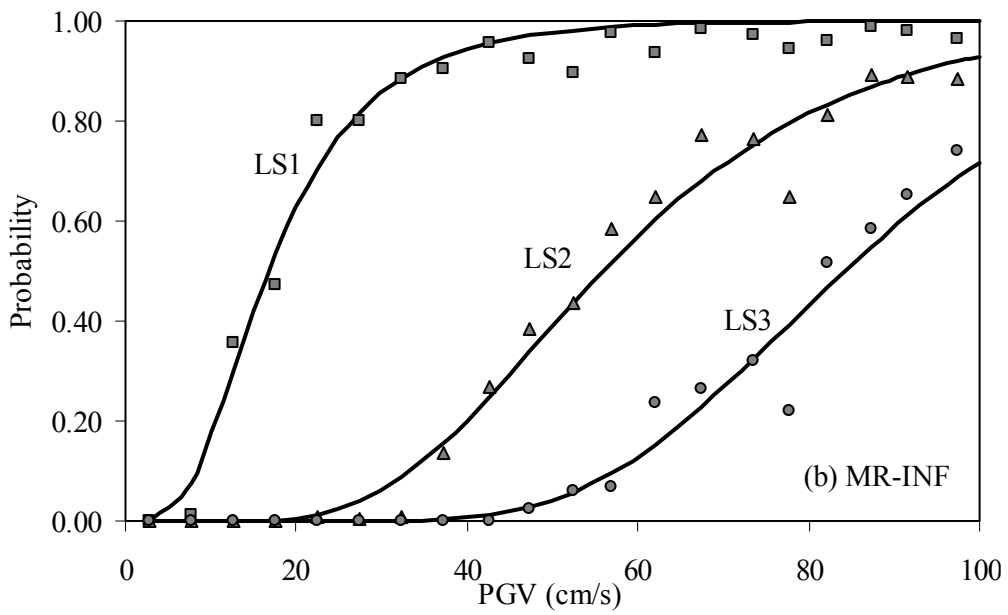
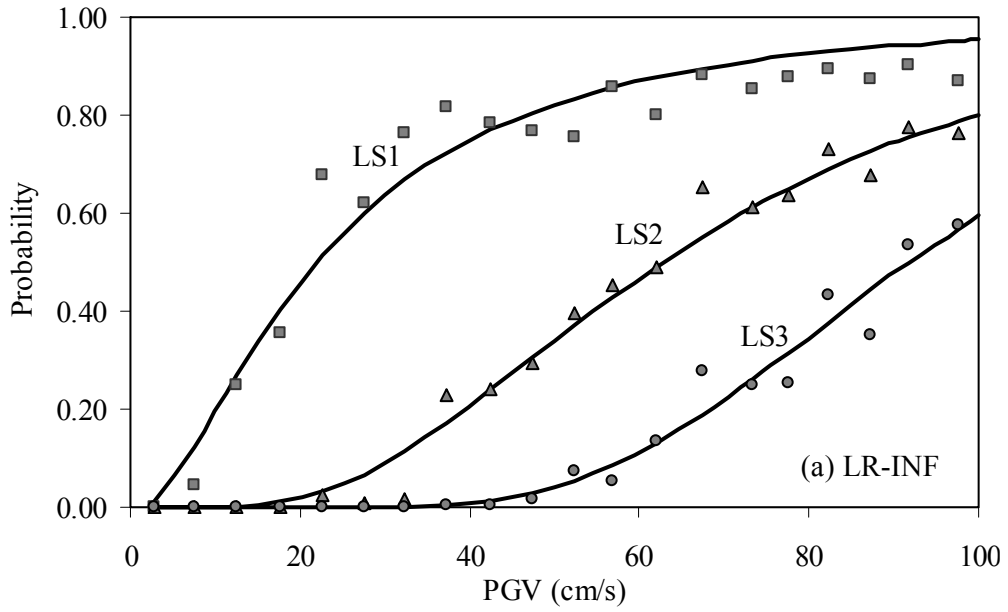


Figure 3.8 Reference Fragility Curves for sub-classes (a) LR-INF (b) MR-INF

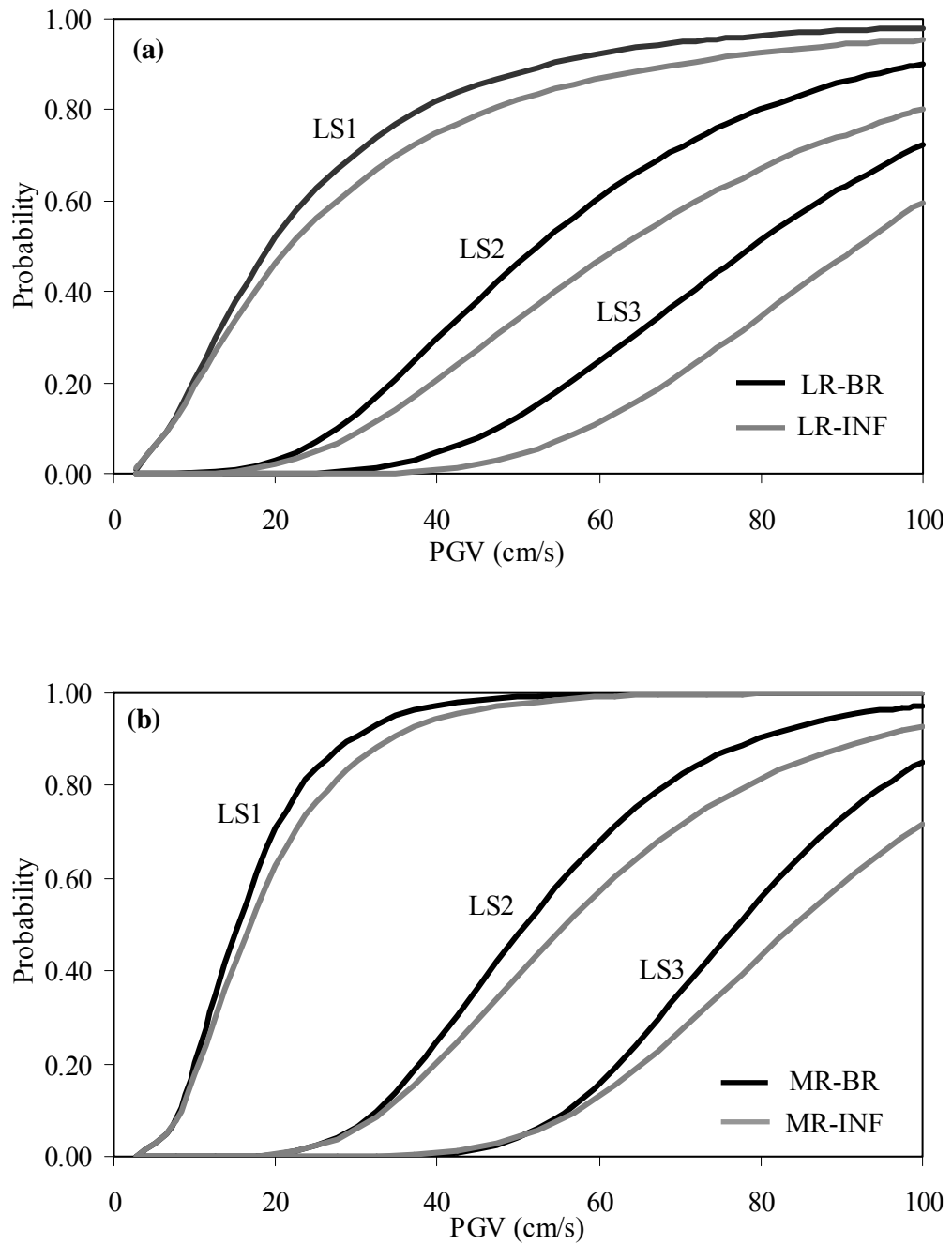


Figure 3.9 Comparison of Reference Fragility Curves for Bare or Infilled RC Frames

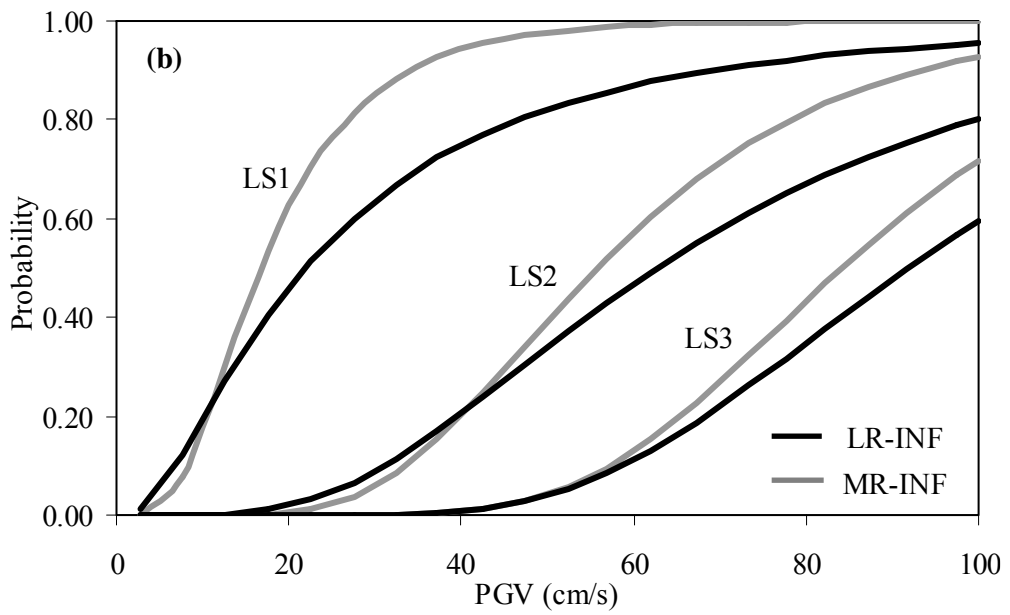
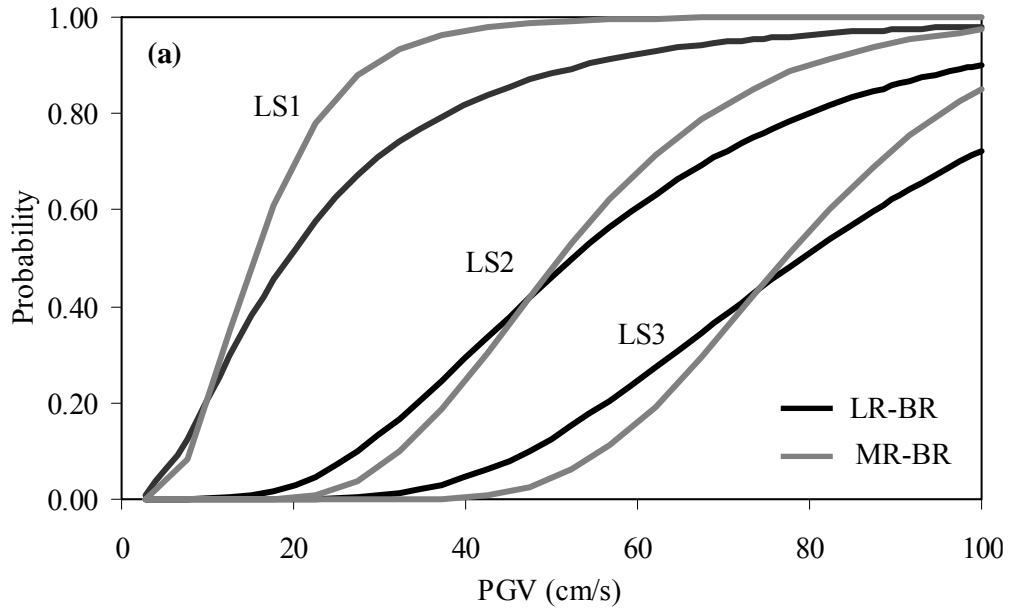


Figure 3.10 Comparison of Reference Fragility Curves for low-rise or mid-rise RC frames

CHAPTER 4

PARAMETRIC STUDY BASED ON FRAGILITY CURVES

4.1 INTRODUCTION

There exist many assumptions and approaches in the development stage of the reference fragility curve set. These assumptions and approaches may or may not affect the final outcomes. In this chapter, a parametric study is carried out to investigate the influence of different parameters and approaches on the final fragility curves by isolating the effect of each parameter (or approach) to be examined. Hence the influence of post elastic stiffness ratio (a_p), simulation and sampling techniques, sample size, limit state definition (deterministic or probabilistic) and degrading behavior on the final fragility curves is examined. The fragility curves obtained in the previous chapter, which were termed as “reference fragility curves”, are also employed in the current phase of the study as a basis for comparison with the fragility curves obtained during the parametric analyses.

In this chapter, parametric analyses are carried out considering only two of the building subclasses: LR-INF and MR-INF since field observations reveal the fact that there exist infill walls in nearly all of the existing RC frame buildings in Düzce database.

4.2 INFLUENCE OF POST-ELASTIC STIFFNESS RATIO

In the generation of reference fragility curves, three SDOF structural parameters (T , η , a_p) are considered as mentioned in Chapter 3. Among these parameters, post-

elastic stiffness ratio (a_p) was taken as a deterministic (constant) parameter by using mean values of a_p for each building sub-class. In this section, the influence of parameter a_p on fragility curve is examined when it is taken as a random variable. Hence, instead of using mean values of parameter a_p for each building sub-class, the values obtained from the bilinearization process for each individual building is used in the structural simulation. For each ground motion in the dataset, it is possible to obtain the maximum displacement ratio (MAXDR) as:

$$\text{MAXDR} = \frac{\text{max. displacement}(\eta_i, T_i, a_{p,i})}{\text{max. displacement}(\eta_i, T_i, a_{p,m})} \quad (4.1)$$

where the numerator stands for the maximum displacement response of idealized SDOF systems considering all the parameters as random variable and the denominator represents the maximum displacement response when parameters η and T are considered as random variable but parameter a_p is taken as constant variable with the mean values of each building subclass. The variation of MAXDR with PGV for subclasses LR-INF and MR-INF is shown in Figure 4.1. The variation is much more significant with an increase in hazard intensity. However for subclasses LR-INF and MR-INF more than 98% of the data is within the ratio limits 1 ± 0.2 . In other words, for the same record, displacement is not very sensitive to parameter a_p in the value range observed for the buildings in the database.

Keeping all the other parameters as the same, the fragility curves are generated again with the same ground motion set and limit state values and then compared with the reference fragility. The comparison is shown in Figure 4.2 for sub-classes LR-INF and MR-INF. The solid black curves represent the reference fragility functions where the parameter a_p is constant and the gray curves represent the new fragility functions where the parameter a_p is variable. It can be clearly stated that the trend observed in Figure 4.1 is also valid for Figure 4.2. There is not much difference between the curves generated for constant a_p and the ones generated for

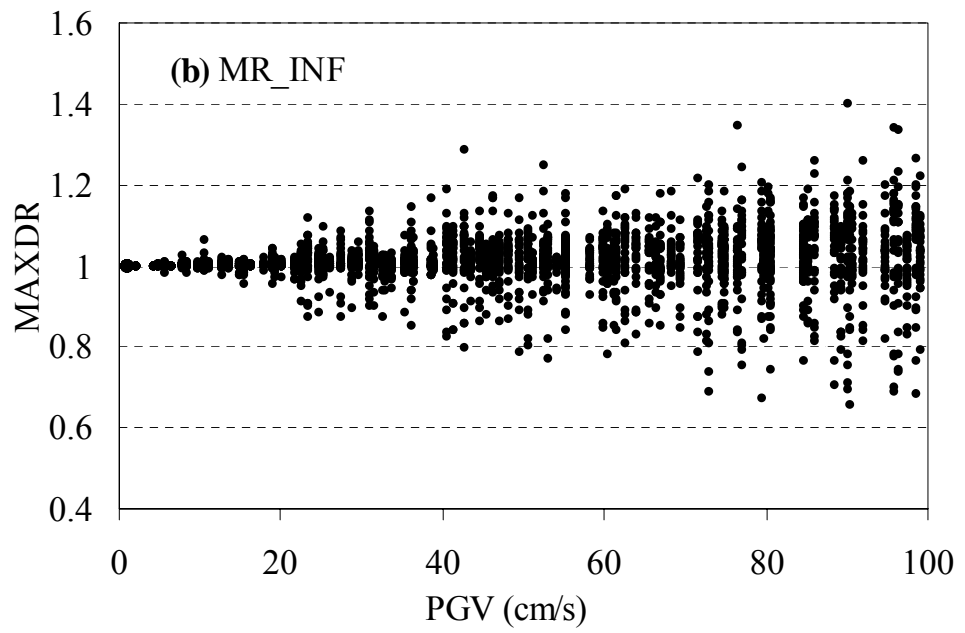
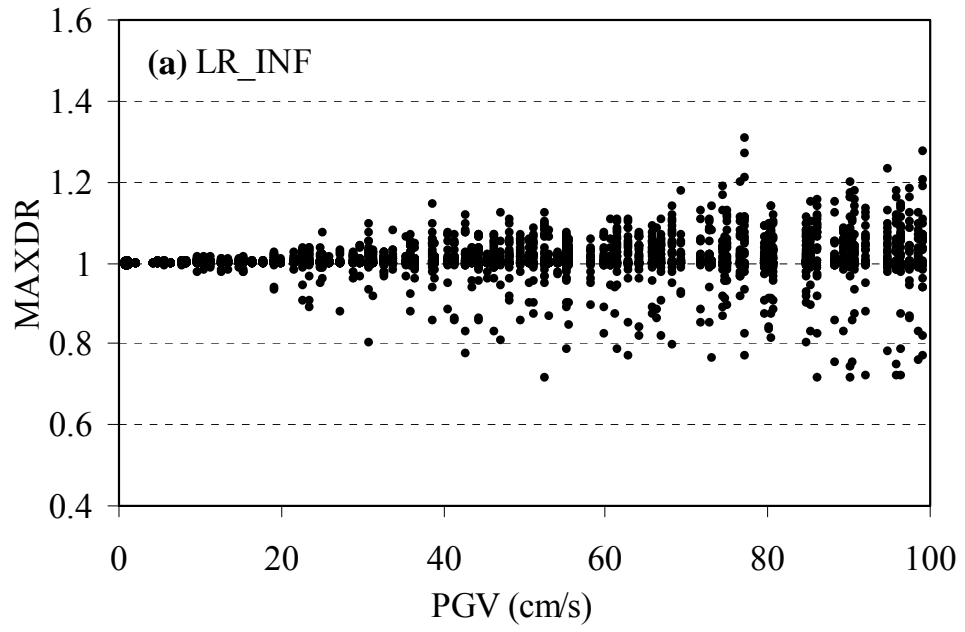


Figure 4.1 The variation of MAXDR with PGV a) LR-INF b) MR-INF

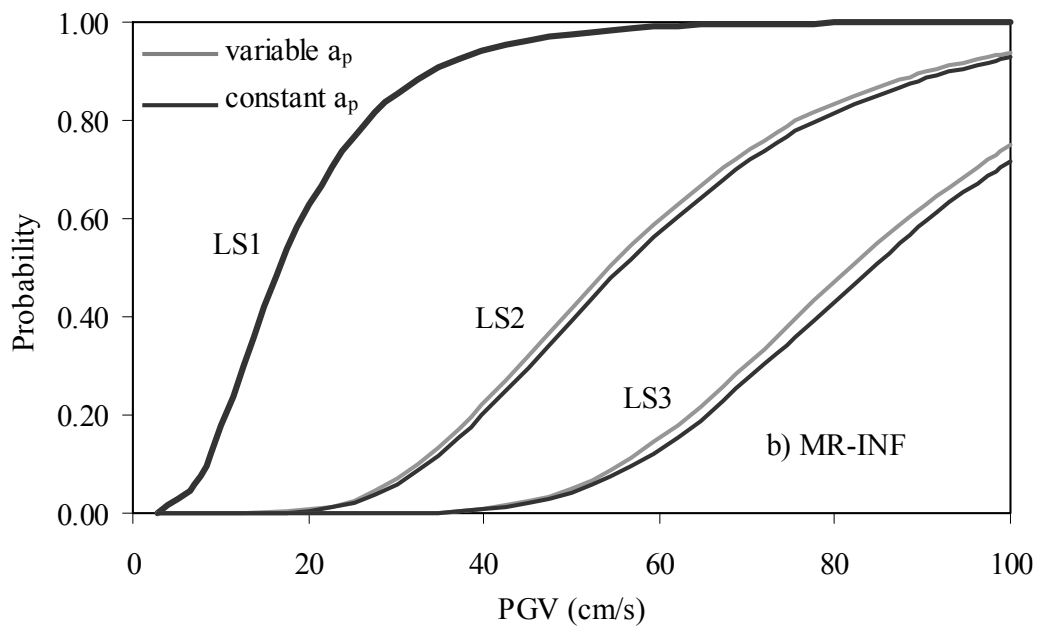
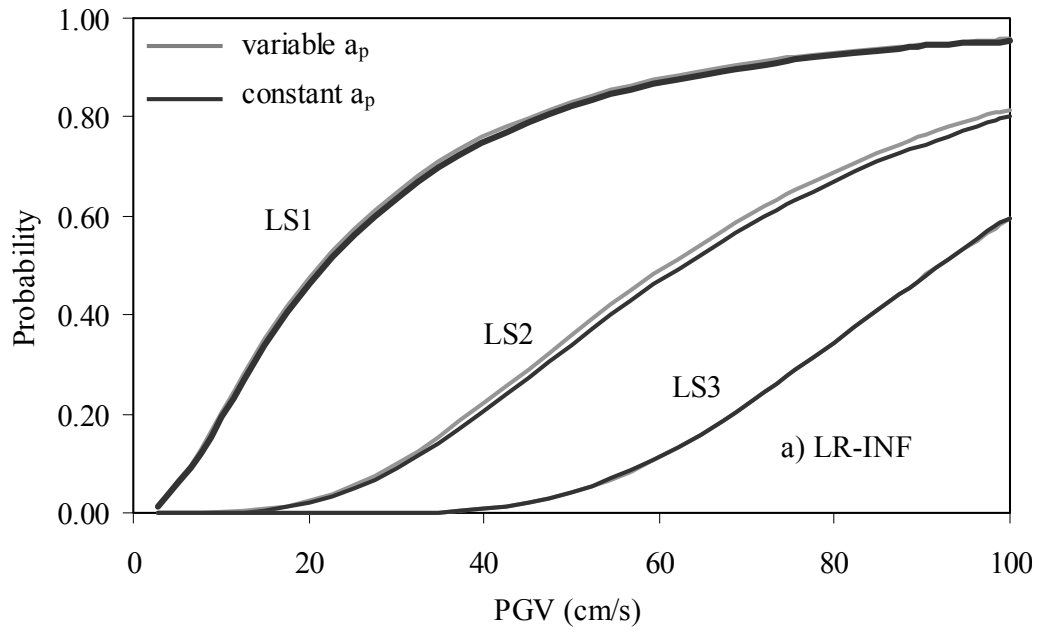


Figure 4.2 The influence of a_p on fragility curves for sub-classes
 a) LR-INF b) MR-INF

variable a_p . The most significant difference takes place in MR infilled RC frame subclass, for the curve representing the probability of exceedence of collapse prevention limit state. But the difference is not more than 8 %. There are minor differences in other curves indicating that it does not matter to include the post-elastic stiffness ratio a_p as a constant or variable parameter. Hence it is concluded that out of three structural parameters, period T and strength ratio η can be taken as variable and post-elastic stiffness a_p can be taken as constant.

It is very important to note that the results obtained are valid for the database used in this study. Hence it may not be possible to obtain similar findings for databases where the statistical distributions of the structural parameters have different characteristics. For instance, for statistical distributions where the parameter a_p contains a significant number of negative values (softening) within the population, the difference between the fragility functions obtained for constant a_p and variable a_p can exhibit a markable variation.

4.3 INFLUENCE OF SAMPLING TECHNIQUES

The most accurate information about the structural characteristics of a building stock can be obtained through field observations. Then this information may be employed in the seismic fragility assessment of the considered stock, as it was done while developing the reference fragility curves. The relationships between two major structural parameters, namely η and T , which were obtained from Düzce field data for sub-classes LR-INF and MR-INF are presented in Figure 4.3 in the form of hollow circles. This data was employed in the generation of reference fragility curves in the companion paper. However, there exist cases where it may not be possible to find field data or the size of data may not be adequate for a realistic statistical evaluation. In such cases, analytical simulation and sampling techniques play an important role in the derivation of final fragility functions.

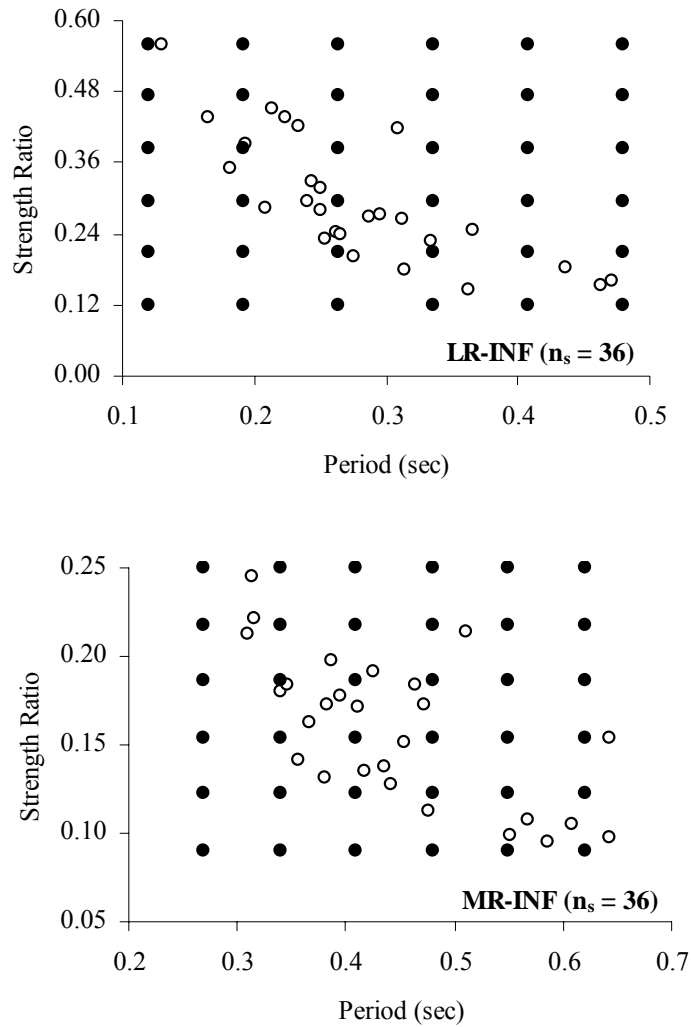


Figure 4.3 Mesh type (uniform) sampling for sub-class a) LR-INF b) MR-INF

In this section, the influence of different simulation techniques on fragility curves is examined. In the first technique, which was used before by other researchers in the generation of fragility curves [11], a range is selected for each random variable (T and η) in each sub-class and the range is divided into a specific number of equal intervals. Hence a rectangular grid of input data is obtained for each sub-class. Examples of such a mesh type generation for sub-classes LR-INF and MR-INF are presented in Figure 4.3 in the form of solid circles. The selected ranges for each

sub-class are divided into five equal intervals, forming a 6x6 (sample size is 36) input data grid.

The second and the more enhanced alternative is to employ sampling techniques for the generation of the structural simulation data. Among these techniques, Latin Hypercube Sampling (LHS) is the most suitable one for structural simulations with small sample size. Developed by McKay et al. [36], it is a technique that provides a constrained sampling scheme instead of random sampling according to the direct Monte Carlo Method, which requires a very large sample size in order to achieve the required accuracy. In the original LHS technique, the correlation between the random variables is not taken into account. However, Figure 3.2 clearly indicates that there is a strong correlation between the random input parameters T and η employed in this study. The coefficient correlation (ρ) is equal to -0.79 and -0.73 for subclasses LR-INF and MR-INF, respectively. The negative sign indicates an inverse correlation between the two parameters (i.e. when T increases, η decreases). Hence a MATLAB code is established that can generate random (T, η) pairs for each sub-class by using LHS technique with rank correlation technique proposed by Iman and Conover [37]. The random pairs generated by this code are illustrated in Figure 4.4 for sub-classes LR-INF and MR-INF.

The influence of different sampling techniques on the final fragility curves is illustrated in Figure 4.5 for building sub-classes LR-INF and MR-INF. The curves are very close to each other, for limit state LS1 and slightly different for limit states LS2 and LS3. Hence it can be concluded that employing different sampling techniques does not affect the fragility functions drastically.

4.4 INFLUENCE OF SAMPLING SIZE

The effect of sample size on the fragility curves is investigated by structural simulations with 30, 75, and 150 pairs of (T, η) data that are generated by LHS technique with rank correlation. In the analyses, all the other parameters are kept constant. The fragility curves of subclasses LR-INF and MR-INF are generated for

each sample size $n_s = 30, 75$ and 100 as depicted in Figure 4.6. From the figures it can be stated that the sample size does not have a significant effect on the final fragility curves.

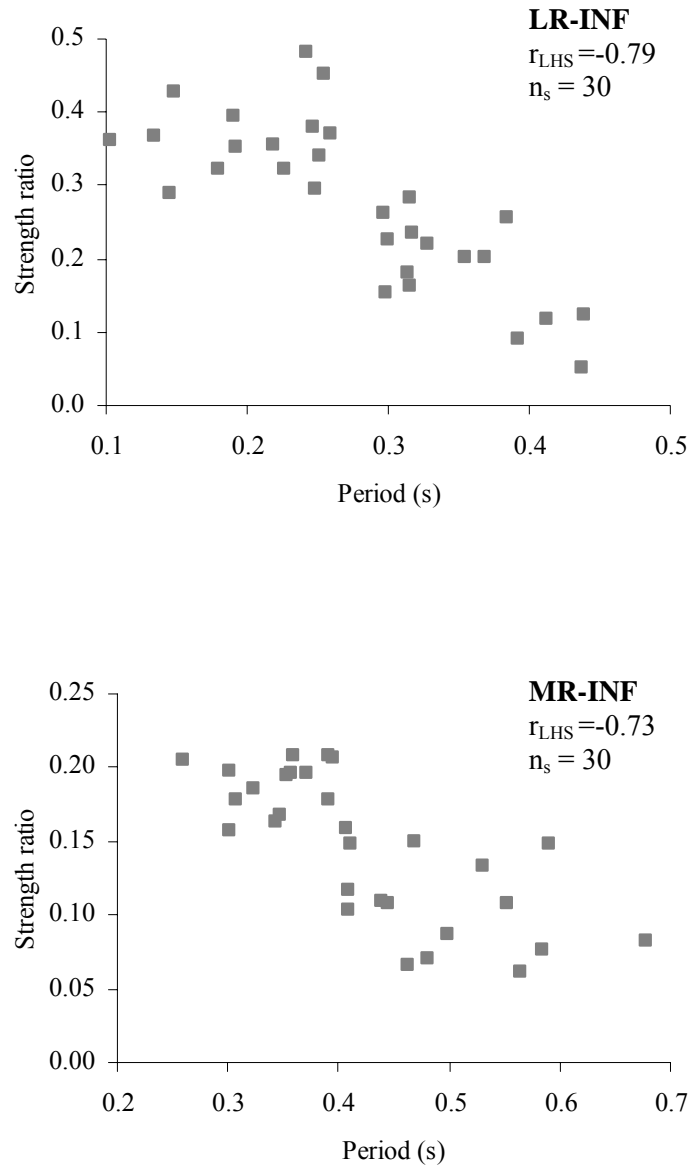


Figure 4.4 LHS technique with rank correlation for building subclasses
a) LR-INF b) MR-INF

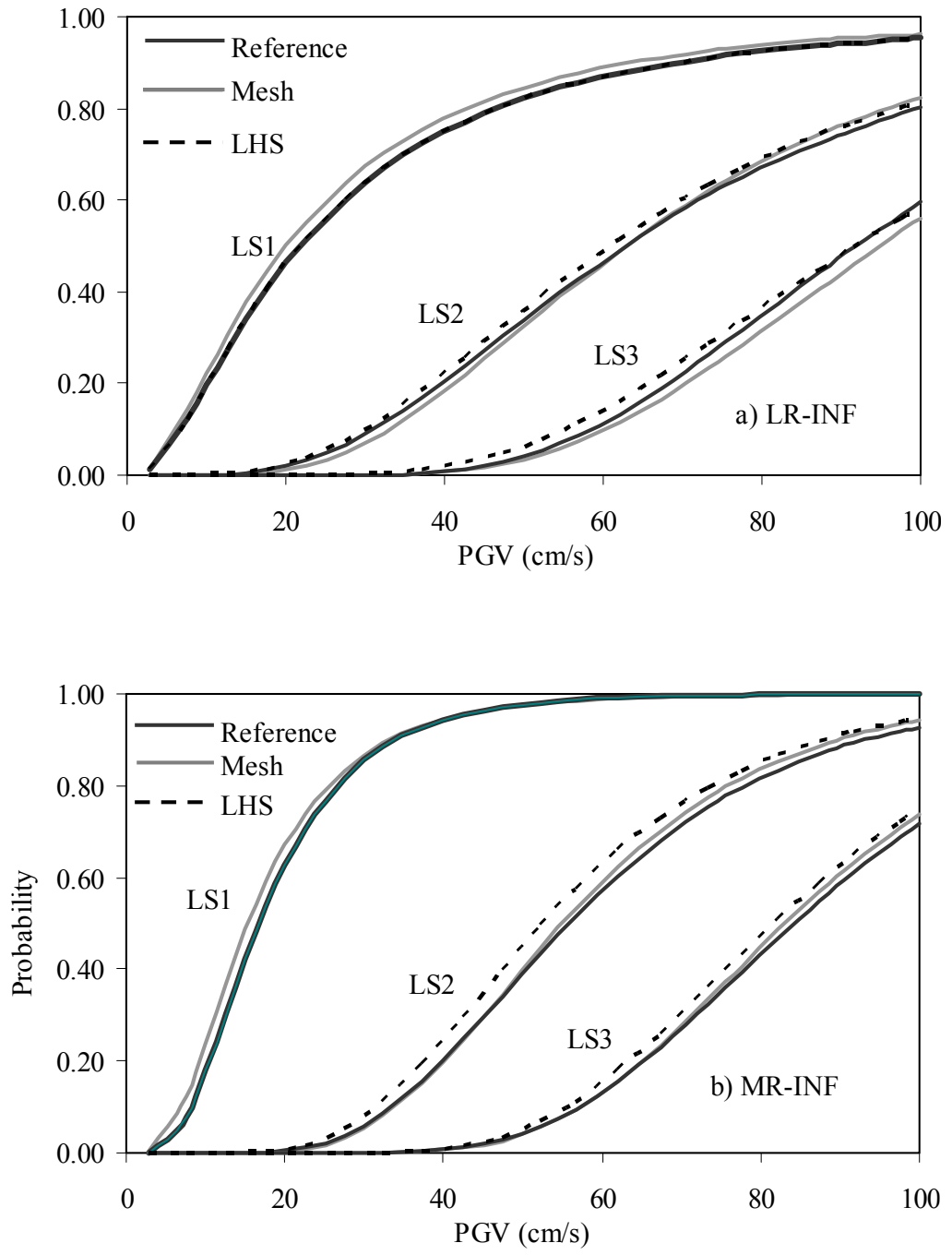


Figure 4.5 The influence of different sampling techniques on fragility curves for subclasses a) LR-INF b) MR-INF

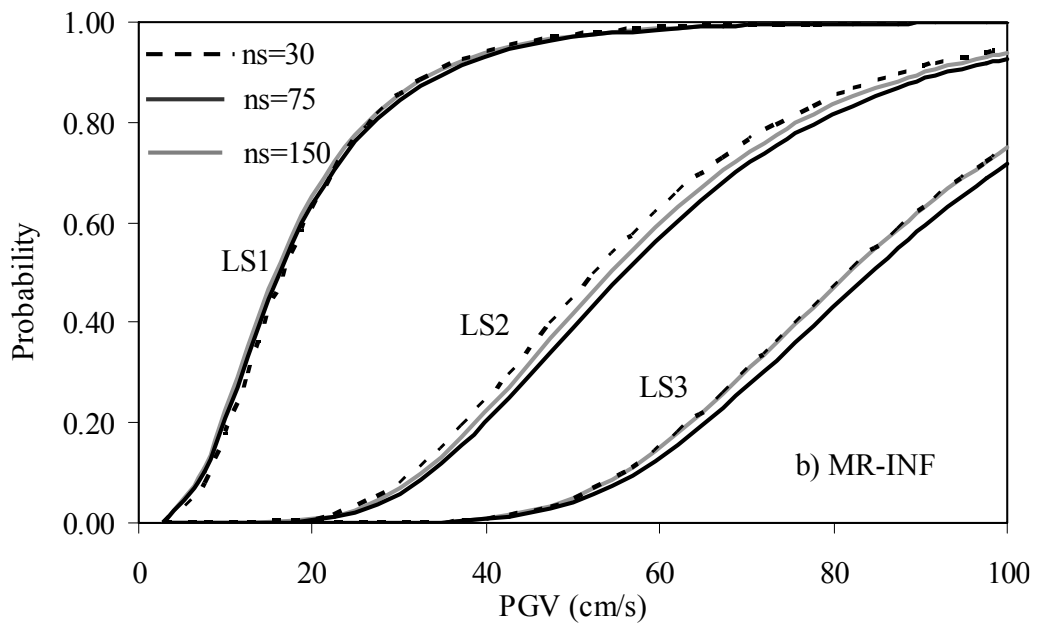
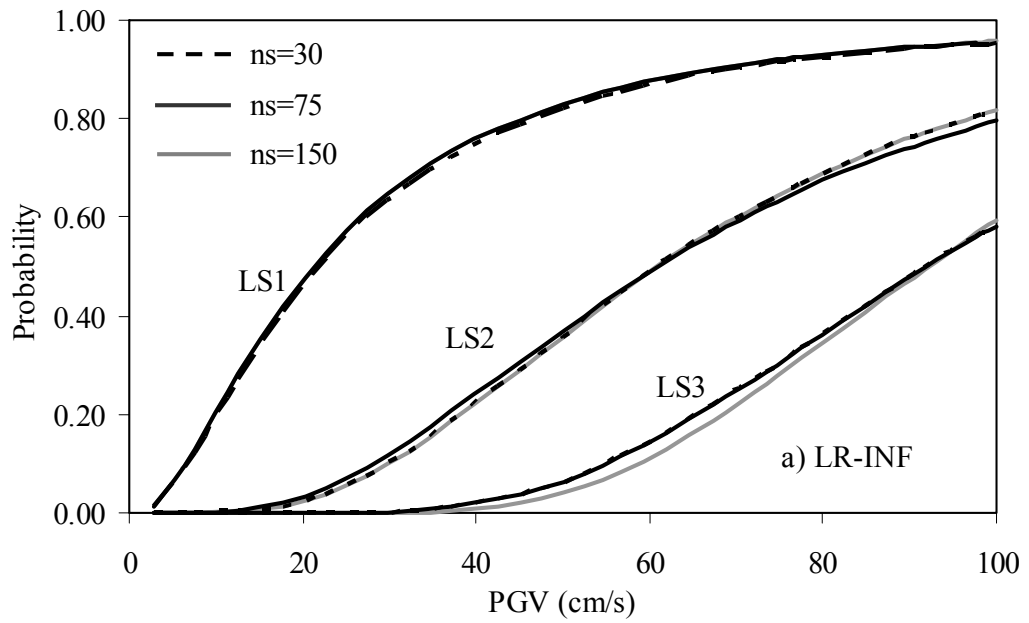


Figure 4.6 Comparison of fragility curves using with different sample sizes ($n_s=30$, 75, 150) a) LR-INF b) MR-INF

4.5 INFLUENCE OF LIMIT STATE DEFINITION

In the reference fragility curve generation, the variability in ground motion and structural characteristics were taken into account and the demand statistics were determined accordingly. The limit states were assumed to be constant (deterministic) parameters. The selected values were simply the mean values obtained from the limit state statistics for that building subclass. However, there is a great deal of uncertainty in the attainment of limit states. In order to investigate the influence of limit state variability on the final fragility curves for low-rise and mid-rise RC frame construction, each limit state is assumed to be normally distributed in the given range of values, for which the mean and the standard deviation (or COV) are calculated from the limit state statistics for that building subclass. The normal distribution assumption is not rejected after the application of Kolmogorov-Smirnov (K-S) goodness-of-fit test on the population of limit state values for each building subclass.

In the generation of fragility curves as opposed to assigning mean values for each limit state and sub-class in the deterministic approach, the statistical descriptors for each limit state are used in the probabilistic approach. Based on the assumed probabilistic approach, a new value is generated for each hazard intensity level with random limit state using normal distribution by LHS method. Each normal probability distribution is divided into 20 non-overlapping intervals on the basis of equal probability of occurrence and 20 different values are randomly selected (i.e. one value per interval is generated) for each hazard intensity level. Final step is to calculate the probability of exceeding the limit state values determined by the LHS method. When compared to reference fragility curves, the differences are significant. Fragility curves become more sensitive to limit state definition especially at low PGV values for MR-INF.

The resulting fragility curves shown in Figure 4.7 reveal the fact that the variability in capacity (limit states) deserves special attention, especially if the

whole range of limit state variability is taken into account. The limit states should be established with special care since they have an impact on the final fragility curves.

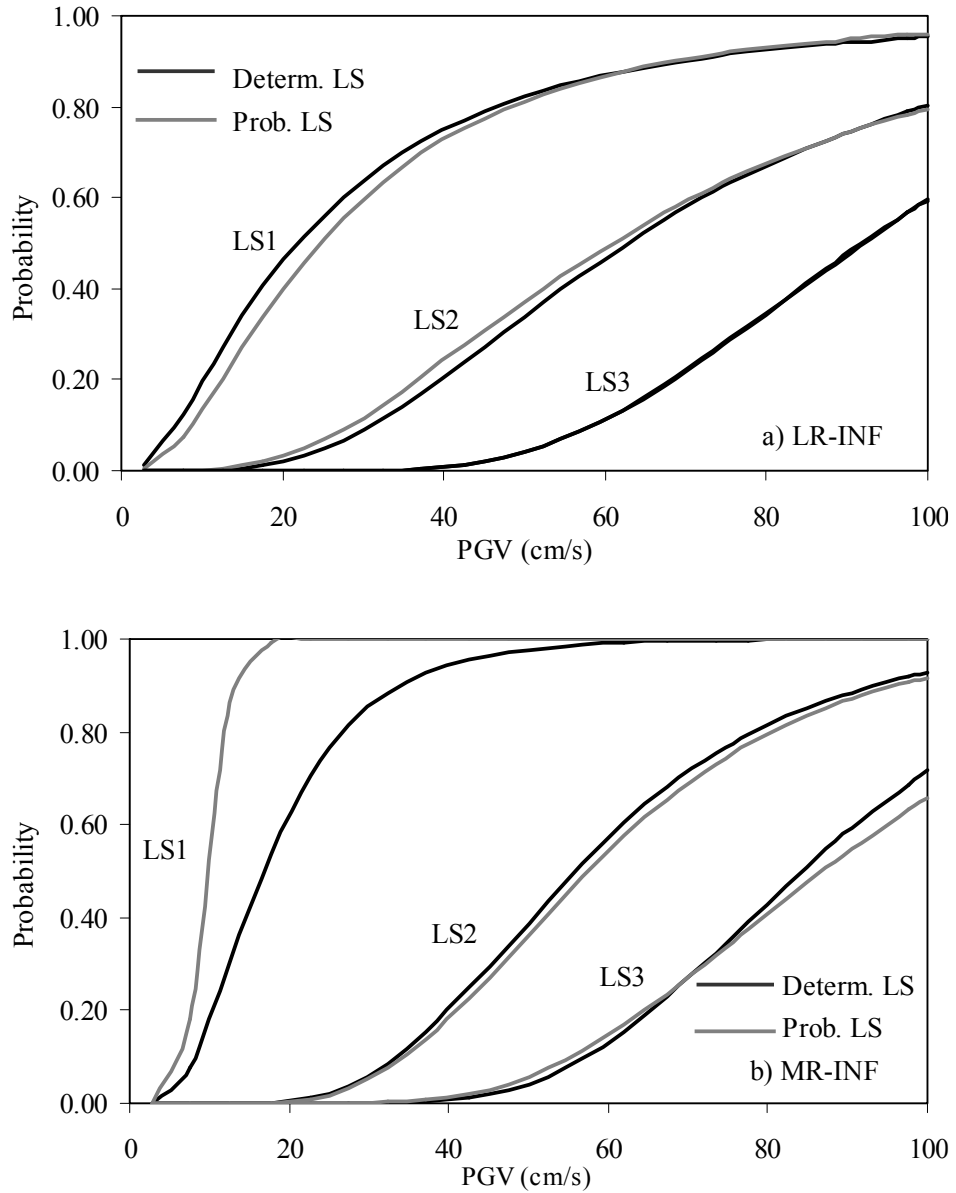


Figure 4.7 Influence of different limit state definitions on fragility curves for subclasses a) LR-INF, b) MR-INF.

4.6 INFLUENCE OF DETERIORATING BEHAVIOUR

In the generation of reference fragility curves, the employed hysteresis model was Clough model. This is a stiffness degrading model with stable hysteresis loops and high energy dissipation capacity [29]. It generally simulates well-detailed, slightly degrading, newly constructed structural systems. However, the structural systems modeled in this study are existing structures with many deficiencies. It is very probable that they will exhibit significant stiffness and strength degradation with reduced energy dissipation capacity. Hence, sensitivity of the fragility curves to degrading structural systems should also be investigated.

A two-parameter low-cycle fatigue model and an energy-based hysteresis model are employed in this study to examine the influence of deterioration in structural properties under repeated excitation cycles for the existing low-rise and mid-rise RC frame structures that are idealized in this study by using equivalent SDOF systems. In low-cycle fatigue model, the relationship between the energy dissipation capacity per cycle (normalized with respect to the first cycle energy dissipation) and the number of constant amplitude cycles is defined in the form of an exponential function [38] as shown in Figure 4.8.a.

$$\bar{E}_{h,n} = \alpha + (1 - \alpha)e^{\beta(1-n)} \quad (4.2)$$

In Equation 4.2, $\bar{E}_{h,n}$ is the normalized dissipated energy at cycle n , α and β are the two low-cycle fatigue parameters. The first parameter α is related to the level of deterioration at large values of n and the second parameter β is related to the rate of deterioration. A system with $\alpha=0$ loses all of its energy dissipation capacity as n approaches to infinity, whereas a system with $\alpha=1$ always retains its energy dissipation capacity (Curve-I in Figure 4.8.a). The second low-cycle fatigue parameter β has a wider range between zero and infinity, and it represents the rate of loss in cyclic energy dissipation capacity. In the limit $\beta=0$ means no degradation whereas $\beta=\infty$ defines a system which loses all of its energy dissipation capacity

after completing the first cycle (Curve-III in Figure 4.8.a). Curve-II in the same figure presents a system with typical fatigue parameters having values between the upper and lower limits.

An energy-based hysteresis model, which takes into account the aforementioned low-cycle fatigue model, is used to simulate the force-deformation response of SDOF deteriorating systems. It is a piece-wise linear hysteresis model that is based primarily on the Clough stiffness degrading model extended with an energy-based memory for simulating strength deterioration. A simple sketch of the model is given in Figure 4.8.b. The details of the energy-based hysteresis model can be found elsewhere [39]. It has been verified that the hysteresis model predicts the observed energy dissipation reasonably well for test specimens under constant and variable amplitude cyclic loading [39-40].

In order to assess the influence of deterioration on the final fragility curves, three different classes for structural systems are proposed. These structural classes are abbreviated as SC1, SC2 and SC3, respectively. SC1 represents class of structures with theoretically non-deteriorating, or in practice slightly deteriorating behavior. This class actually corresponds to new RC building structures that have been designed and constructed according to the current codes and regulations. SC2 represents the structural systems with gradual deterioration in strength with increasing cycle number, plus slight pinching. However the system can still dissipate a considerable amount of energy after a significant number of cycles. SC2 represents the majority of the building stock concerning the RC residential buildings in Turkey. They are generally engineered structures but may violate some fundamental requirements of earthquake resistant design. Finally, SC3 stands for structural systems which experience excessive strength deterioration and pinching in the early stages of load reversals and in turn can not maintain the required energy dissipation capacity. Hence this system class is nothing but the idealization of building structures which have not been designed to resist earthquake loads and have major structural deficiencies that endanger their seismic

safety. Recent earthquakes in Turkey revealed that these types of structures are extremely vulnerable in seismic action. Consequently they suffered heavy damage or even collapsed when subjected to earthquake forces.

In the selection of the appropriate force-deformation relationship and the related model parameters for each class, experimental results of different RC specimens under constant or variable amplitude cyclic loading are employed. The experimental data under concern includes 22 cyclic tests of RC column specimens that belong to four different test programs [38, 41-43]. The details of the experimental database can be found elsewhere [40].

The force-deformation relationship for SC1 is the Clough model since this model represents non-degrading and stable behavior under cyclic loading. The fragility curves generated by using this class of structural systems are simply the reference fragility curves that are already available. For SC2 and SC3, energy-based hysteresis model is employed, for which the fatigue parameters are obtained from a previously conducted study [40]. Accordingly, the fatigue parameters that represent SC2 are taken as $\alpha=0.6$ and $\beta=0.5$, which were obtained after a calibration process using the experimental results of eight different specimens with moderate deterioration under cyclic loading within the database. The observed behavior of one of the specimens is presented in Figure 4.9.a for the sake of demonstration together with the estimated fatigue parameters α and β . The values assigned to the model parameters for SC3 are $\alpha=0.3$ and $\beta=0.7$ in accordance with nine different specimens that exhibited severely degrading behavior under cyclic loading. One of these specimens is shown in Figure 4.9.b. The estimated fatigue parameters for this specimen are also given in the figure.

The generated curves for moderately (SC2) and severely degrading (SC3) structural systems are then compared with the reference fragility curves represented by the non-degrading Clough model (SC1) in Figure 4.10. The reference fragility curves are shown as black lines whereas the ones obtained for

moderately and severely degrading structural systems are shown in gray and dotted lines, respectively. It is obvious that there is a great difference between the three sets of curves. Hence, the degradation characteristics of the structural model seem to have a major influence on the final fragility curves.

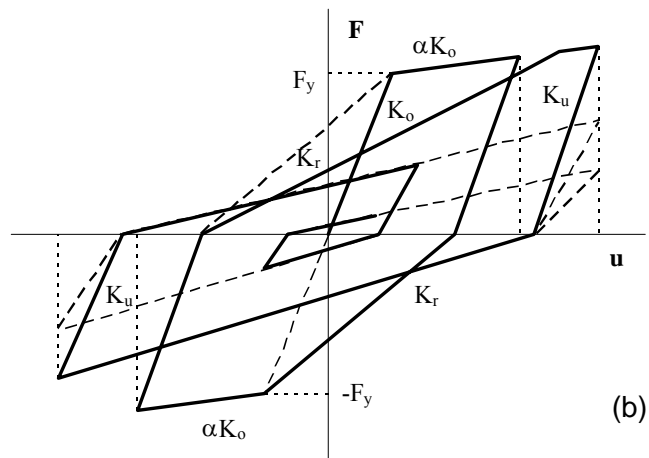
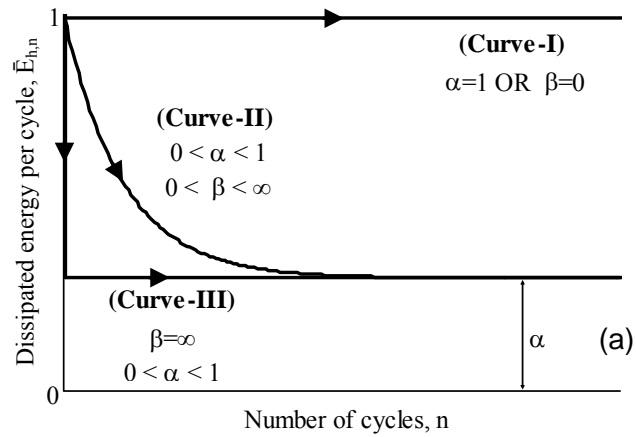


Figure 4.8 a) Low-cycle fatigue model b) Energy-based hysteresis model.

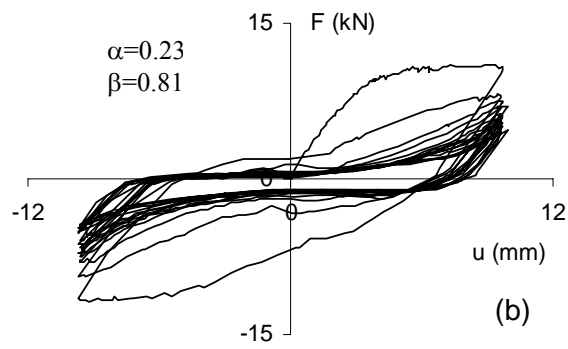
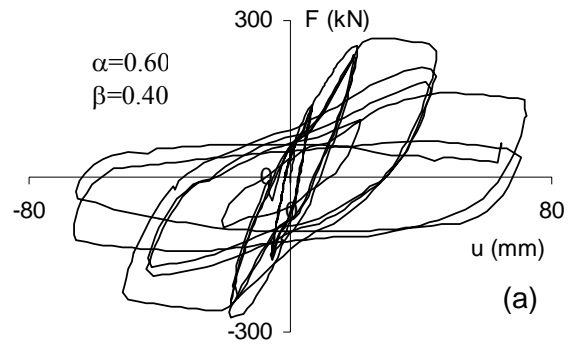


Figure 4.9 Sample experimental behavior along with estimated values of α and β .
 a) Specimen SO3 from Saatcioglu and Ozcebe [42], b) specimen ES3 from Erberik and Sucuoglu [38]

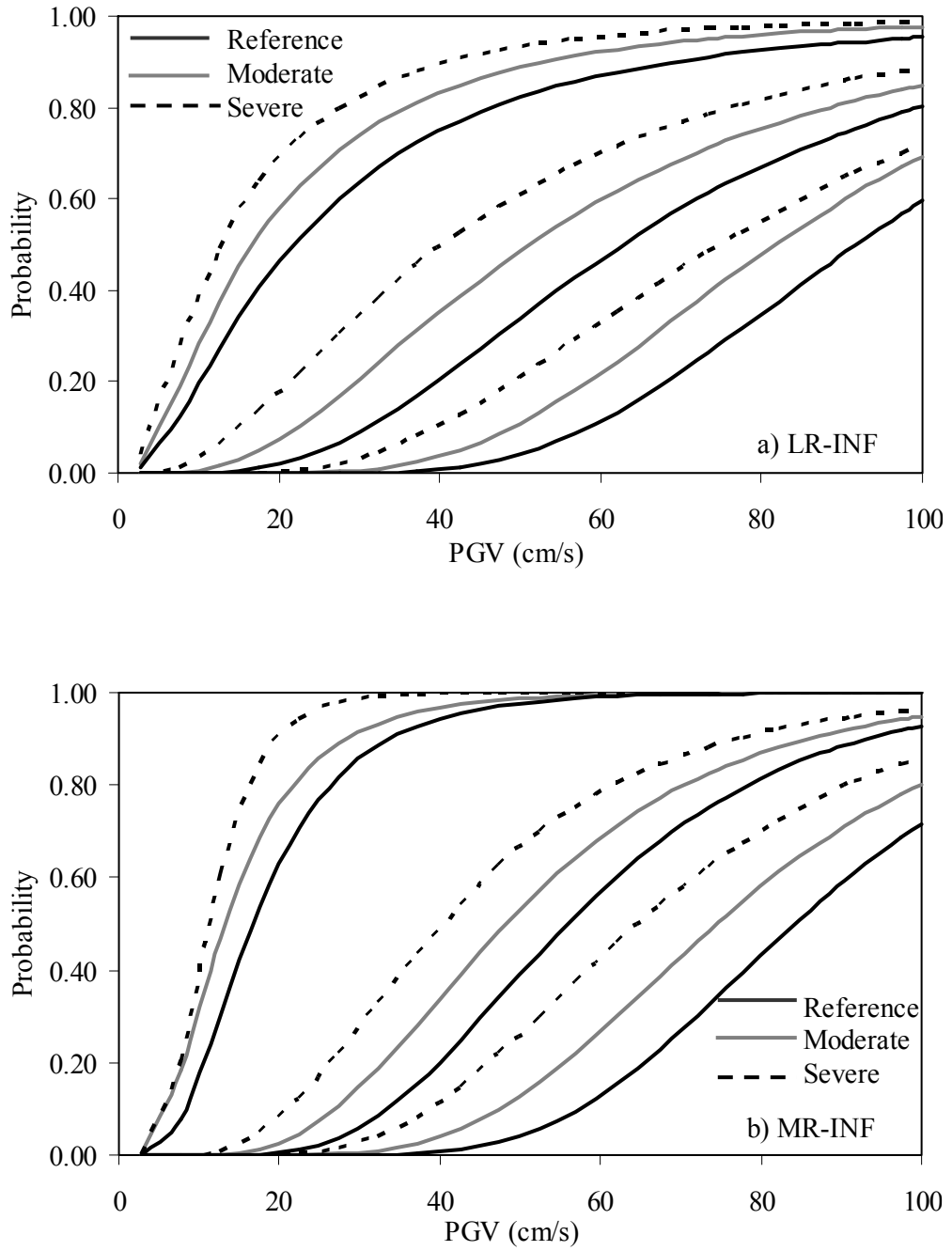


Figure 4.10 The influence of degrading hysteresis behavior in the generation of fragility curves for subclasses a) LR-INF and b) MR-INF.

CHAPTER 5

DAMAGE ESTIMATION STUDY

5.1 GENERAL

Two severe ground motions occurred in Düzce during the 17 August 1999 Kocaeli and 12 November 1999 Düzce earthquakes within a period less than three months. Hence the building structures in Düzce which are subjected to these events provide invaluable field data in terms of observed damage after a series of seismic excitations. In the last part of the study, a comparative approach is used in which the observed damage after the 1999 earthquakes (see Table 2.1) is compared with the estimated damage by employing the fragility curves generated for low-rise and mid-rise RC frame structures. Such an approach is valuable, in the sense that it will give an idea about the validity of the generated fragility curves and if it is possible to obtain estimated damage distribution after two consecutive major earthquakes on comparable grounds with the actual field data. The outline of the procedure is presented below in a few steps. Furthermore a simple sketch of the procedure is given in Figure 5.1.

- Consider two major earthquakes that affected the building population under consideration: Kocaeli earthquake (17 August 1999) and Düzce earthquake (12 November 1999).
- Find the corresponding PGV values at the center of building population by using appropriate attenuation relationships.
- Obtain damage probability values for low-rise and mid-rise RC buildings by using the generated fragility functions and PGV values. The employed

set of fragility curves are the ones generated for the subclasses LR-INF and MR-INF with probabilistic limit states, exhibiting moderately degrading behavior.

- Compare the obtained results with the actual damage distribution.

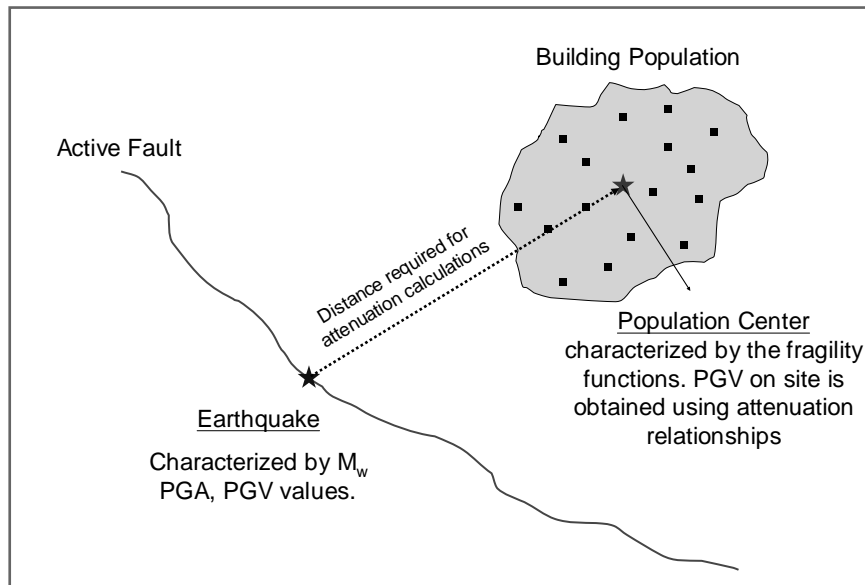


Figure 5.1 Schematic representation of the comparative procedure

Two major earthquakes occurred on the west segment of the North Anatolian Fault on August 17, 1999 and on November 12, 1999 with moment magnitudes $M_w=7.4$ and $M_w=7.1$, respectively. The epicenter of the former earthquake was located at 40.70 N, 29.99E, whereas the epicenter for the latter earthquake was located at 40.79 N, 31.11 E [44]. On 17 August 1999, the fault rupture of 140 km length in the eastward direction propagated almost to Düzce and stopped 12 km away from the city. On 12 November 1999, another 40 km of the same fault was broken further toward the east. The rupture in Düzce earthquake started from the termination of the rupture in Kocaeli earthquake and passed 6 km south of Düzce

[45]. The epicentral coordinates of the 1999 earthquakes are shown in Figure 5.2 together with the coordinate center of the building population considered in Düzce.

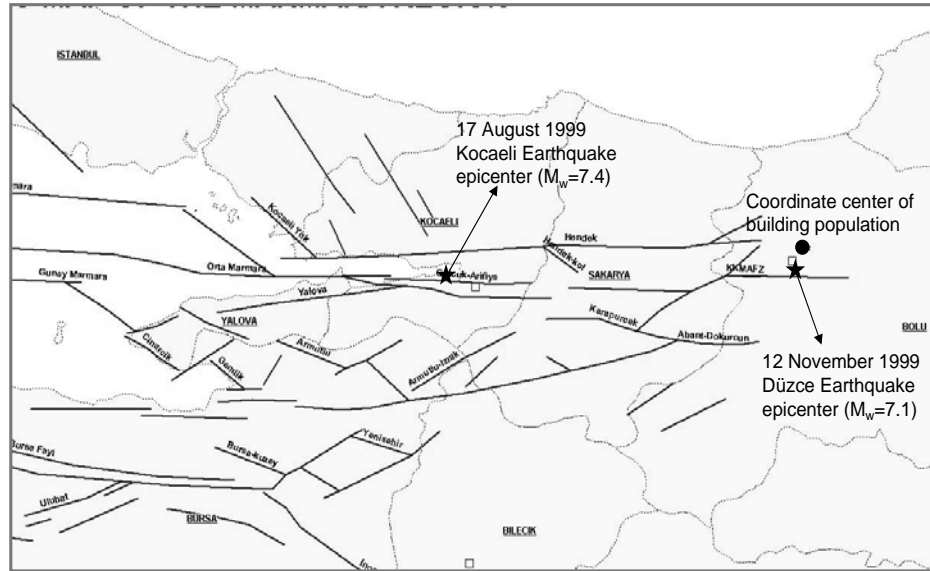


Figure 5.2 The epicentral locations of the 1999 earthquakes together with the coordinate center of the database buildings

In order to obtain the damage state probabilities of the considered buildings, on-site PGV values are required. To obtain the on-site values, PGV-based attenuation relationship recommended by Campbell [46] is employed. This relationship is the modified version of the expression that was originally developed by Campbell and Bozorgnia [47] for horizontal PGA. The PGV-based attenuation function is obtained for two different site categories: soil and rock. Figures 5.3.a and 5.3.b present the empirical attenuation functions for these two site categories together with the recorded PGV vs. distance to fault information from strong motion stations during the 1999 earthquakes [44]. Although it is not appropriate to make a comparison between the estimated PGV variation with respect to fault distance obtained by the empirical equation and the recorded PGV values during the earthquakes due to limited data, it can be stated that the selected PGV-based

attenuation relationship can be employed with an adequate level of confidence to estimate the on-site PGV values in such a simple procedure.

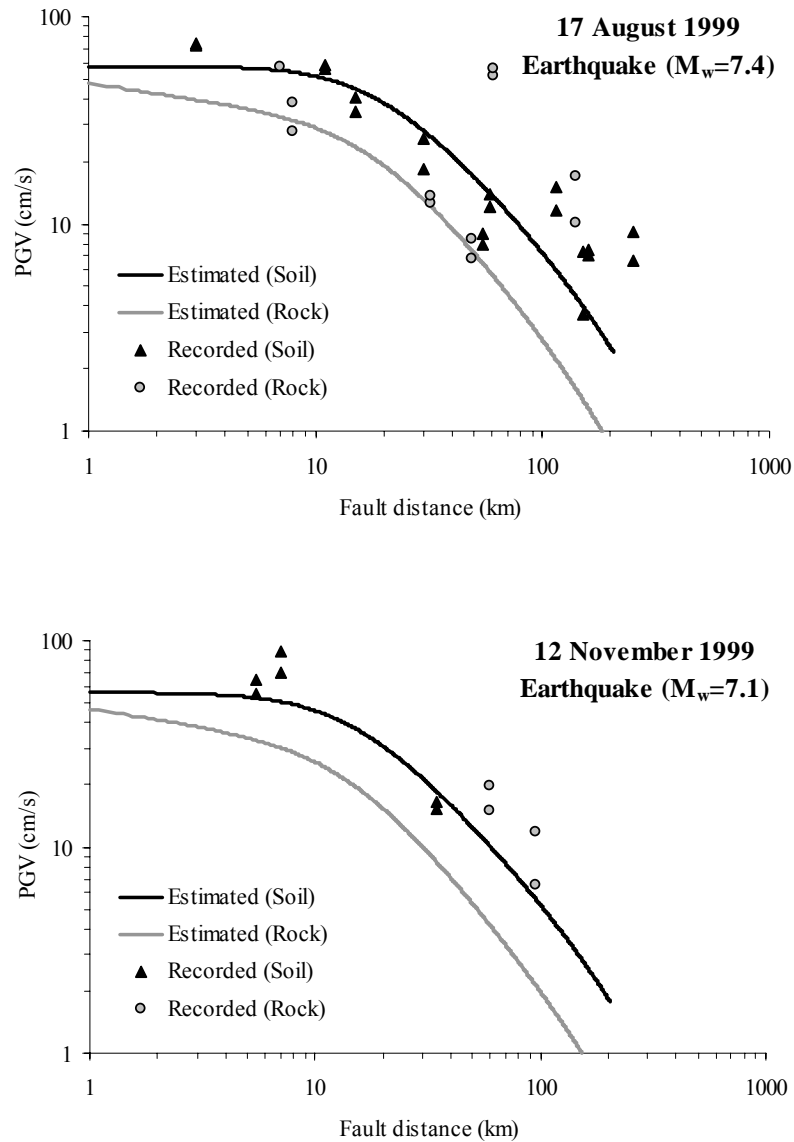


Figure 5.3 Comparison of PGV-based attenuation relationship by Campbell with the recorded PGV values during a) 17 August 1999, b) 12 November 1999 earthquakes.

The site geology of the region where the database buildings are located is known to be soil deposits [48]. Hence the on-site PGV values at the coordinate center of the Düzce building population are obtained from Campbell's empirical equation for soil sites as 23.15 cm/s and 43.5 cm/s for 17 August 1999 earthquake and 12 November Düzce earthquakes, respectively. The values indicate that the buildings are mainly affected by the latter earthquake although they sustained some level of damage during the former one. This result can be attributed to the fact that the epicenter of the latter earthquake is very close to the building site when compared to the epicenter of the former earthquake (see Figure 5.2).

Since the buildings are subjected to two earthquakes in a short period of time and the field observations are carried out afterwards, it is necessary to consider the influence of both earthquakes on the final damage state of the buildings. Assuming that the same set of fragility curves can be used to estimate the damage after both earthquakes, the best way to reflect such a statistically dependent relationship is to employ the Total Probability Theorem [49]. According to this theorem, if the probability of an event A depends on the occurrence of other events E_i , $i=1, 2, \dots, n$, it may be stated that

$$P(A) = P(A|E_1)*P(E_1) + P(A|E_2)*P(E_2) + \dots + P(A|E_n)*P(E_n) \quad (5.1)$$

where $P(A|E_n)$ denotes the conditional probability of event A assuming that event E_n has occurred. The above formulation is adjusted for calculating the conditional damage probabilities of the buildings in the database. The probabilities of being in None, Light, Moderate and Severe damage states after both earthquakes are calculated as:

$$P(DS_2=N) = P(DS_2=N|DS_1=N) P(DS_1=N) \quad (5.2 a)$$

$$P(DS_2=L) = P(DS_2=L|DS_1=N) P(DS_1=N) + P(DS_2=L|DS_1=L) P(DS_1=L) \quad (5.2 b)$$

$$P(DS_2=M) = P(DS_2=M|DS_1=N) P(DS_1=N) + P(DS_2=M|DS_1=L) P(DS_1=L) + P(DS_2=M|DS_1=M) P(DS_1=M) \quad (5.2 c)$$

$$P(DS_2=S) = P(DS_2=S|DS_1=N) P(DS_1=N) + P(DS_2=S|DS_1=L) P(DS_1=L) + P(DS_2=S|DS_1=M) P(DS_1=M) + P(DS_2=S|DS_1=S) P(DS_1=S) \quad (5.2 d)$$

where the capital letters N, L, M and S correspond to the damage states “None”, “Light”, “Moderate” and “Severe”, DS_1 and DS_2 denote the damage states after the August and November earthquakes, respectively.

The logic tree that is constructed in order to estimate damage state probabilities of low-rise and mid-rise RC frame buildings in Düzce after two devastating earthquakes (namely 17 August 1999 Kocaeli and 12 November 1999 Düzce earthquakes) is presented in Figure 5.4. The results are presented in Figures 5.5.a and 5.5.b for LR-INF and MR-INF sub-classes. The figures show the estimated damage distributions both after the August and the November earthquakes, together with the finally observed damage. The probability of having each damage state is presented by the percentage of the building database. Based on the figures, the damage distributions for both low-rise and mid-rise RC buildings are slightly overestimated, especially for none-to-slight levels of damage. However it can be stated that the overall correlation between the observed and the estimated damage is satisfactory for the purposes of crude damage estimation for quick response after an earthquake by employing such a simple comparative procedure.

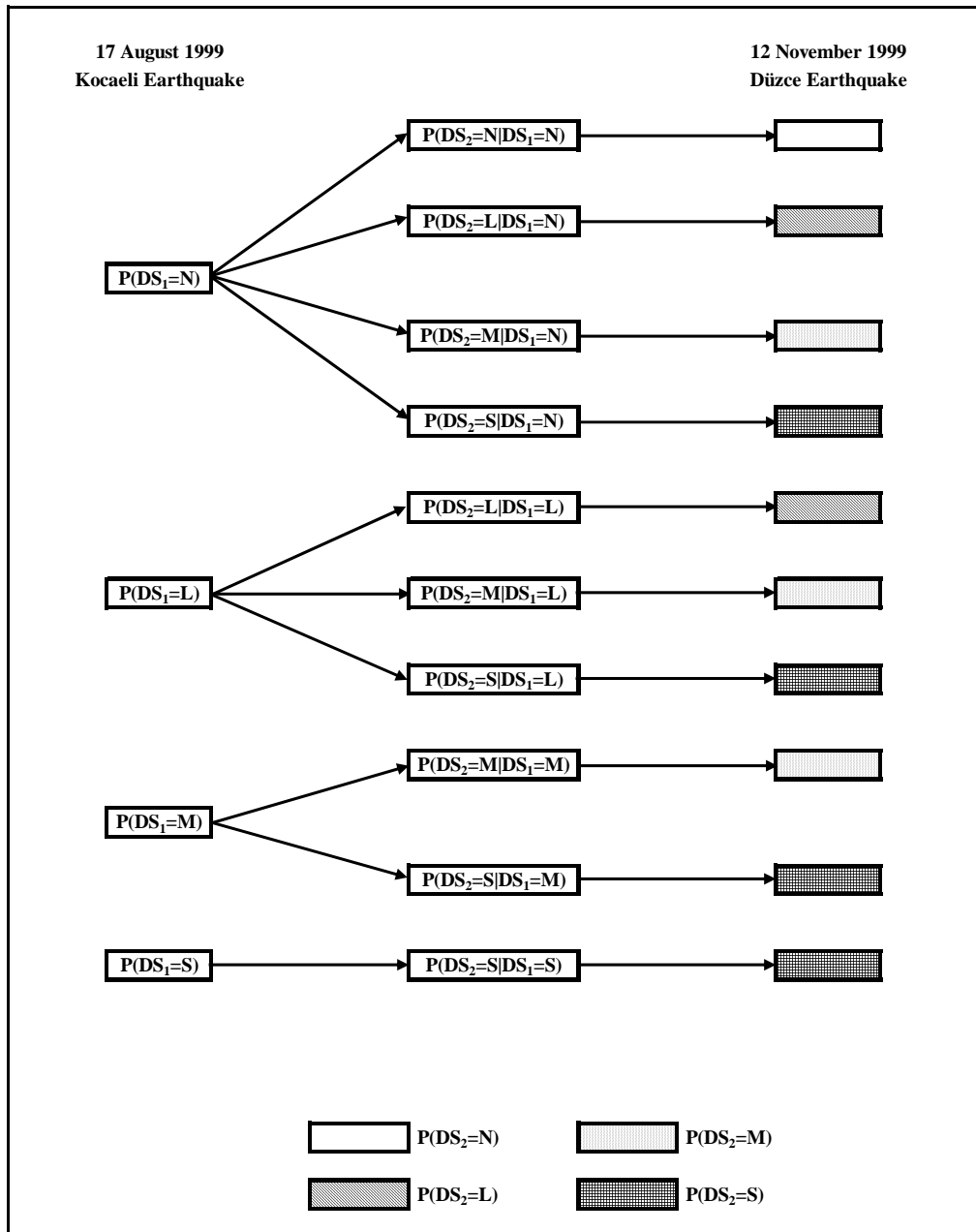


Figure 5.4 Logic tree for estimating damage state probabilities of low-rise and mid-rise RC frame buildings in Düzce after 17 August and 12 November earthquakes

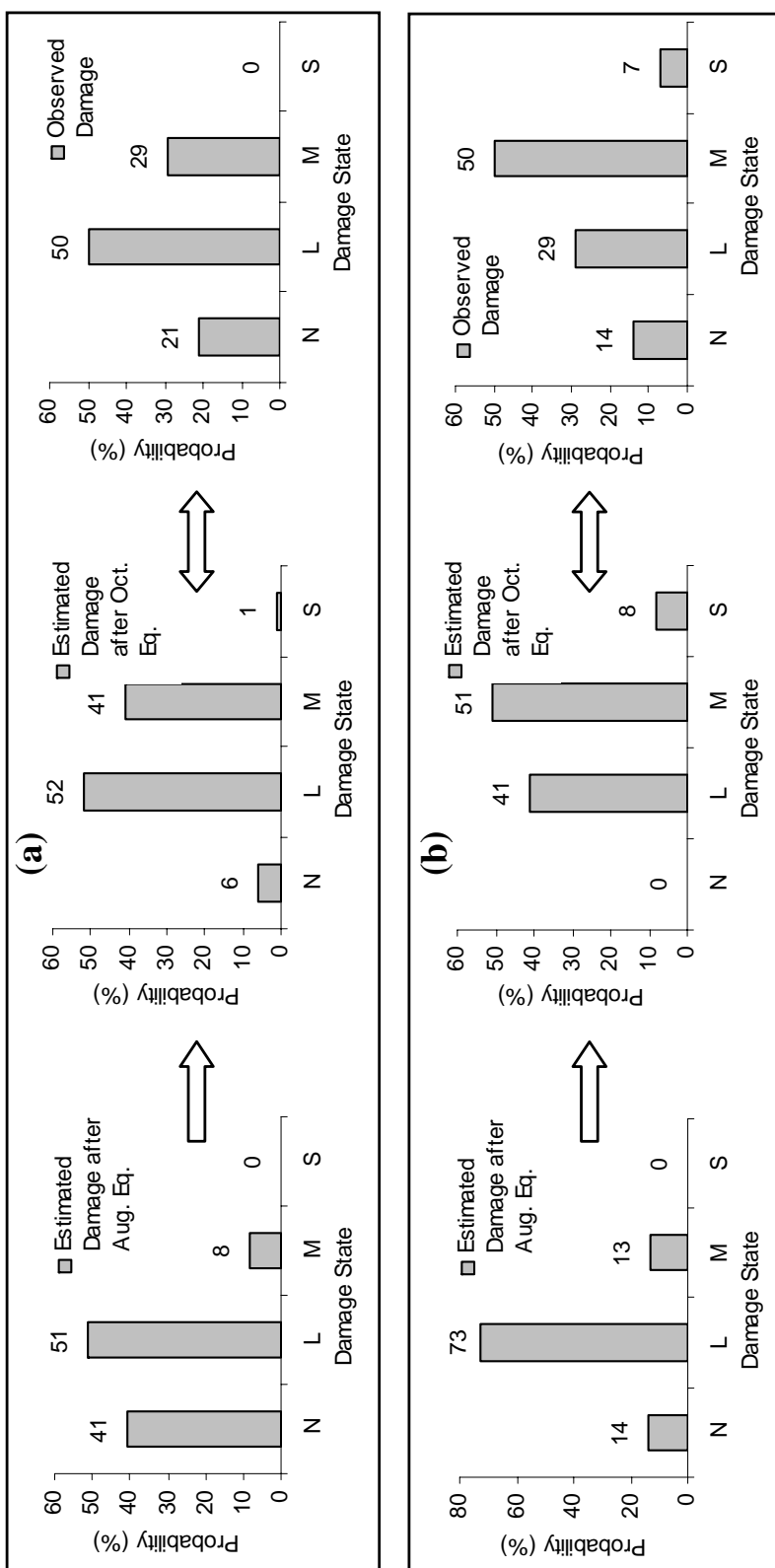


Figure 5.5 Comparison of estimated damage distributions after August and November earthquakes with the observed damage for a) low-rise b) mid-rise RC buildings

CHAPTER 6

SUMMARY AND CONCLUSIONS

6.1 SUMMARY

In this study, it is aimed to conduct the seismic fragility-based assessment of low-rise and mid-rise reinforced concrete frame buildings in Turkey by using Düzce damage database. 28 reinforced concrete buildings were extracted from 500 buildings in Düzce database which are deemed to represent the typical characteristics of low-rise and mid-rise RC buildings in Turkey.

The building stock is divided into two sub-groups according to the number of stories: low-rise and mid-rise. Furthermore, the buildings are classified as “bare frame” and “infilled frame” with respect to the absence or presence of the infill walls. Hence, there are four sub-classes of frame buildings: low-rise bare frame (LR-BR), low-rise infilled frame (LR-INF), mid-rise bare frame (MR-BR), mid-rise infilled frame (MR-INF). Each building is represented by an equivalent single-degree of freedom system with three structural parameters: period (T), strength ratio (η) and post-elastic stiffness ratio (a_p). Among these input parameters, T and η are considered as random variables in the analyses whereas a_p is considered as a deterministic parameter.

Ground motion records are extracted from 100 ground motion sets from different locations around the world. The hazard parameter is selected as Peak Ground Velocity (PGV) and ground motion records are grouped into 20 bins with intervals of 5 cm/s according to the PGV values.

The limit states are defined in terms of simple global parameters and termed as Serviceability, Damage Control and Collapse Prevention. Since limit states play a significant role on the generation of the fragility curve, a comprehensive study is conducted in order to attain well-defined and realistic limit states.

Nonlinear time-history analyses are conducted to obtain the demand statistics. A normal distribution is fitted to the demand data and the statistical parameters for each PGV intensity level. Afterwards, the probability of exceedance of each limit state is calculated for the mean values of PGV at each bin of ground motion records. Hence, the damage vs. hazard relationship is constructed by plotting the calculated probability of exceedance values as a function of the hazard parameter, PGV. A lognormal fit is applied to the damage vs. hazard parameters to obtain the final smooth fragility curves. The fragility curves obtained for the considered building sub-classes are named as reference fragility curves.

Then a parametric study is conducted to examine the influence of different parameters on fragility curves. The procedure for the generation of the reference fragility curves is reapplied by isolating the effect of each parameter. The influence of the post elastic stiffness ratio (a_p), simulation and sampling techniques, sample size, limit state definition (deterministic or probabilistic) and degrading behavior on the final fragility curves is investigated. The fragility curves obtained during parametric analyses are compared with the reference fragility curves.

Finally, the damage estimation study is conducted by considering two major earthquakes (Kocaeli earthquake (17 August 1999) and Düzce earthquake (12 November 1999)) that affected the building structures in Düzce within a short period of time. The observed damage after two major earthquakes is compared with the estimated damage by employing the fragility curves. PGV values at the center of building population are founded by using attenuation relationships.

Damage probability values are obtained from generated fragility curves. Consequently, obtained results are compared with the actual damage distribution.

6.2 CONCLUSIONS

Considering the fact that the results obtained in the generation of reference fragility curves, parametric study and damage estimation study are based on the specific characteristics of the limited structural database used in this study, the following conclusions can be stated:

- By the introduction of infill walls, the mean periods of low-rise and mid-rise RC structures are decreased by 23% and 16% whereas the mean strength ratios of low-rise and mid-rise are increased by 28% and 23%, respectively. The above trends reveal that increase in stiffness and strength is significant in both low-rise and mid-rise buildings by the addition of infill walls when compared with their bare frame counterparts.
- The mean strength ratio of MR frames is 59% of the mean of LR frames for bare case and the same mean strength ratio of MR frames is 56% of the mean of LR frames for infilled case. Hence the ratio of η_{MR} / η_{LR} is not very sensitive to having bare or infilled frames.
- The dispersion in low-rise buildings is more significant than mid-rise buildings in terms of period and strength.
- The variation in post-elastic stiffness ratio is very high for all building sub-classes.
- Reference fragility curves indicate that for a specific level of peak ground velocity, bare frames (compared to infilled frames) and mid-rise frames (when compared to low-rise frames) are generally more vulnerable to seismic action. This observation becomes more significant for ultimate limit state.

- The trends obtained from the reference fragility curves are in accordance with the inherent structural characteristics of Turkish low-to-mid-rise RC frame buildings.
- Among the three main SDOF structural parameters (period, strength factor and post-elastic stiffness ratio), the variability in the post-elastic stiffness ratio does not have a significant effect on the fragility functions.
- Simulation techniques, from the simplest one (mesh-type generation) to the most enhanced one (LHS technique with rank correlation) does not influence the final fragility curves to a great extent.
- Sample size seems not to affect the final fragility functions.
- Uncertainty in the capacity should be taken into account by quantification of the variability in the limit states considered since the sensitivity of the fragility curves to limit state definitions seems to be high.
- Degradation characteristics seem to have a drastic influence on the final fragility curves, especially in the case of severe strength degradation.
- Promising results are obtained regarding the comparison of actual and estimated damage distributions, especially for the low-rise RC buildings. The differences may be attributed to the assumptions present in the fragility curve generation procedure and seismic hazard analysis.
- Final outcome of the study is a set of fragility curves for typical low-rise and mid-rise RC frame buildings in Turkey. Several studies have been conducted recently that deals with the fragility information of RC frame buildings in Turkey. The novelty of this study comes from the fact that there exists no study that focuses on the effect of the ingredients of the fragility curve generation procedure for Turkish RC frame buildings. It is a known fact that ground motion uncertainty has a considerable effect on final fragility curves and it is not considered in this study. However this study shows that uncertainty in capacity and degrading structural characteristics also alter the fragility curves significantly. Hence these parameters should be determined with great attention in order to obtain reliable estimates in terms of earthquake damage and loss.

6.3 RECOMMENDATIONS FOR FUTURE STUDY

Based on the results and conclusions of this study, following recommendations can be derived:

- The building stock is composed of reinforced concrete frame buildings. Fragility analysis can also be conducted for different structural types; such as masonry buildings, steel and pre-cast buildings.
- The hazard parameter is PGV in the generation of the fragility curve. Fragility information can be derived by using alternative hazard parameters like peak ground acceleration (PGA), spectral displacement and spectral acceleration.
- The fragility curves obtained in this study can be compared with the curves generated in other studies concerning Turkish RC frame building construction. It is also possible to compare the generated curves with the ones obtained for other earthquake prone regions around the world in order to assess the differences in local construction practice.

REFERENCES

- [1] Applied Technology Council (ATC), 1985, *Earthquake Damage Evaluation Data for California*, ATC-13, Redwood City, California
- [2] National Institute of Building Sciences (NIBS), 1999, HAZUS Technical Manual (3 volumes), prepared for Federal Emergency Management Agency, Washington, DC.
- [3] Shinozuka M., Feng M., Kim H., Uzawa T. and Ueda T., 1999b, *Statistical Analysis of Bridge Fragility Curves*, Technical Report, Multidisciplinary Center for Earthquake Engineering, Buffalo, New York.
- [4] Chong W.H. and Soong T.T., 2000, *Sliding Fragility of Unrestrained Equipment in Critical Facilities*, Technical Report MCEER 00-0005, Buffalo, New York.
- [5] Wen Y.K., Ellingwood G.T., and Bracci, J., 2003, *Vulnerability Function Framework for Consequence-based Engineering*, Draft Report, Project Title: DS-4, Vulnerability Functions, Mid-America Earthquake Center, University of Illinois at Urbana Champaign.
- [6] Singhal A. and Kiremidjian A.S., 1997, *A Method for Earthquake Motion-Damage Relationships with Application to Reinforced Concrete Frames*, Technical Report, NCEER 97-0008, Buffalo, New York.

- [7] Barron R., and Reinhorn A., 2000, *Spectral Evaluation of Seismic Fragility of Structures*, Technical Report, Multidisciplinary Center for Earthquake Engineering Research, Buffalo, New York.
- [8] Barron – Corvera R, 2000, *Spectral Evaluation of Seismic Fragility of Structures*, PhD Thesis, Development of Civil, Structural and Environmental Engineering, State University of New York at Buffalo, New York.
- [9] Jeong S.H. and Elnashai A.S., 2004, *Parametrized Vulnerability Functions for As-built and Retrofitted Structures*, PEER Report 2004/05, Proceedings of International Workshop on Performance-Based Seismic Design Concepts and Implementation, Bled Slovenia, pp. 185-196.
- [10] Erberik M.A. and Elnashai A.S., 2004, *Fragility Analysis of Flat-slab Structures*, Engineering Structures, Vol.26, pp. 937-948.
- [11] Akkar S., Sucuoğlu H. and Yakut A., 2005, *Displacement-based fragility functions for low and mid-rise ordinary concrete buildings*, Earthquake Spectra, Vol. 21, No. 4, pp. 901–927.
- [12] Kırçıl M.S., and Polat Z., 2006, *Fragility analysis of mid-rise RC frame buildings*, Engineering Structures 28 , pp. 1335-1345.
- [13] Ay B.Ö., 2006, *Fragility Based Assessment of Low-Rise and Mid-Rise Reinforced Concrete Frame Buildings in Turkey*, M.S. Thesis, Middle East Technical University, Ankara.
- [14] Yakut A., Yılmaz N. and Bayılı S., 2003, *Analytical Assessment of Seismic Capacity of RC Frame Buildings*, International Conference in Earthquake Engineering to Mark 40 Years from Catastrophic 1963 Skopje Earthquake

and Successful City Reconstruction-SE 40EEE, CD-ROM, Skopje-Ohrid, Macedonia.

- [15] Aydoğan V., 2003, *Seismic vulnerability assessment of existing reinforced concrete buildings in Turkey*, M.S. Thesis, Middle East Technical University, Ankara.
- [16] Turkish Ministry of Public Works and Settlement, 1975, Specifications for Buildings to be Built in Disaster Areas, Ankara.
- [17] Turkish Ministry of Public Works and Settlement, 1940, Specifications for Buildings to be Built in Disaster Areas, Ankara.
- [18] Turkish Ministry of Public Works and Settlement, 1997, Specifications for Buildings to be Built in Disaster Areas, Ankara.
- [19] Turkish Ministry of Public Works and Settlement, 2007, Specifications for Buildings to be Built in Earthquake-Prone Regions, Ankara.
- [20] Computers and Structures Inc, 2002, SAP 2000, Nonlinear, Version 8.08, Structural Analysis Program, Computers and Structures, Inc., Berkeley, CA.
- [21] ASCE (American Society of Civil Engineers), 2000, *Prestandard and Commentary for the Seismic Rehabilitation of Buildings*, Federal Emergency Management Agency, FEMA 356, Washington, DC.
- [22] Applied Technology Council (ATC), 1996, *Seismic Evaluation and Retrofit for Concrete Buildings*, ATC-40, Redwood City, California

- [23] Goel R.K. and Chopra A.K., 1997, *Period formulas for moment resisting frame buildings*, Journal of Structural Engineering ASCE 123 (11), pp. 1454-1461.
- [24] Uniform Building Code, 1997, International Conference of Building Officials, Whittier, California
- [25] ASCE (American Society of Civil Engineers), 2000, *NEHRP Guidelines for the Seismic Rehabilitation of Buildings*, FEMA 273, Washington D.C.
- [26] Sucuoğlu H. and Nurtuğ A., 1995, *Earthquake ground motion characteristics and seismic energy dissipation*, Earthquake Engineering and Structural Dynamics 24, pp. 1195-1213.
- [27] Sucuoğlu H., Gülkan P., Erberik A., and Akkar S., 1999, *Measures of Ground Motion Intensity in Seismic Design*, Proceedings of the Uğur Ersoy Symposium on Structural Engineering, Ankara.
- [28] Trifunac M.D. and Brady A.G, 1975, *A study on the duration of strong earthquake ground motion*, Bulletin of Seismological Society of America 65, pp. 581-626.
- [29] Clough R.W., Johnston S.B., 1966, *Effect of Stiffness Degradation on Earthquake Ductility Requirements*, Proceedings, Second Japan National Conference On Earthquake Engineering, pp. 227-232.
- [30] DiPasquale E. and Cakmak A.S., 1987, *Detection and assessment of seismic structural damage*, Technical Report NCEER-87-0015, State University of New York, Buffalo, NY.

- [31] Reinhorn A.M., Kunnath S.K. and Mander J.B., 1992, *Seismic design of structures for damage control, Nonlinear Seismic Analysis and Design of Reinforced Concrete Buildings*, edited by Fajfar P. And Krawinkler H., Elsevier: 63-76.
- [32] Park Y.J., Ang A.H.S., and Wen Y.K., 1995, *Seismic damage analysis of RC buildings*, Journal of Structural Engineering ASCE; 111(4), pp. 740-757
- [33] SEAOC, 1995, *Performance Based Seismic Engineering of Buildings*, Vision 2000 Committee, Structural Engineers Association of California, Sacramento, California.
- [34] Ghobarah A, 2004, On Drift Limits Associated with Different Damage Levels. Proceedings of an International Workshop on Performance-Based Seismic Design Concepts and Implementation Bled Slovenia, pp. 321-332.
- [35] Mosalam K.M., Ayala G., White R.N. and Roth C., 1997, *Seismic Fragility of LRC Frames with and without Masonry Infill Walls*, Journal of Earthquake Engineering 1(4), pp. 693-720.
- [36] McKay M.D., Conover W.J. and Beckman R.J., 1979, *A Comparison of Three Methods for Selecting Values of Input Variables in the Analysis of Output from a Computer Code*, Technometrics, Vol.21, pp. 239-245.
- [37] Iman R.L. and Conover W.J., *A Distribution Free Approach to Inducing Rank Correlation Among Input Variables*, 1982, Communications in Statistics, Vol. 11 (3), pp. 311-334.

- [38] Erberik M.A. and Sucuoğlu H., 2004, *Seismic Energy Dissipation in Deteriorating Systems through Low-cycle Fatigue*, Earthquake Eng. and Str. Dyn., Vol. 33, pp. 49-67.
- [39] Sucuoğlu H. and Erberik M.A., 2004, *Energy Based Hysteresis and Damage Models for Deteriorating Systems*, Earthquake Eng. and Str. Dyn., Vol. 33, pp. 69-88
- [40] Sucuoğlu H. and Erberik M.A., *Evaluation of Inelastic Displacements in Deteriorating Systems using an Energy-based Approach*, Proceedings of the International Workshop Bled, Slovenia, PEER Report No.2004/05, pp. 421-433.
- [41] Wight J.K., Sözen M.A., 1973, *Shear strength decay in reinforced concrete columns subjected to large deflection reversals*, Structural Research Series No. 403, Civil Engineering Studies, University of Illinois, Urbana-Champaign, IL.
- [42] Saatçioğlu M., G. Özcebe, 1989, *Response of reinforced concrete columns to simulated seismic loading*, ACI Structural Journal, January - February: 3-12.
- [43] Pujol S., 2002, *Drift capacity of reinforced concrete columns subjected to displacement reversals*, Ph.D. Thesis, Purdue University, IN.
- [44] Earthquake Engineering and Research Center Marmara and Düzce Earthquakes Engineering Report, 2000, Middle East Technical University, Civil Engineering Department, Ankara Turkey.

- [45] Sucuoğlu H. and Yılmaz T., 2001, *Düzce, Turkey; A city hit by two major earthquakes in 1999 within three months*, Seismological Research Letters, Vol. 72 No.6,679-689.
- [46] Campbell K.W., *Empirical Near-Source Attenuation Relationships for Horizontal and Vertical Components of PGA, PGV and Pseudo-Absolute Acceleration Response Spectra*, Seismological Research Letters 1997; 68(1): 154-179.
- [47] Campbell K.W. and Bozorgnia Y., 1994, *Near-Source Attenuation of Peak Horizontal Acceleration from Worldwide Accelerograms Recorded from 1957 to 1993*, Proceedings of the 5th US National Conference on Earthquake Engineering, pp: 283-292, Chicago.
- [48] Lettis W, Bachhuber J, Barka A, Brankman C, Somerville P and Witter R. Chapter 1: Geology and Seismicity, 1999 Kocaeli Turkey Earthquake Reconnaissance Report, Earthquake Spectra, Supplement A to Vol.16, 2000: 1-9.
- [49] Ang AHS and Tang WH., 1975, *Probability Concepts in Engineering Planning and Design*, Vol.1: Basic Principles, John Wiley & Sons,